LONG PERIOD SEISMIC METHODS FOR IDENTIFYING SMALL, UNDERGROUND NUCLEAR EXPLOSIONS

Shelton S. Alexander

Pennsylvania State University

Prepared for:

Air Force Office of Scientific Research
Advanced Research Projects Agency

22 August 1973

Unclassified

Security Classification

AD 766857

DOCUMENT CONTROL DATA - R & D

(Security classification of title, body of abstract and indexing annotation must be entered when the overall report is classified)

1. ORIGINATING ACTIVITY (Corporate author) The Pennsylvania State University Department of Geosciences, Geophysics Section University Park, Pennsylvania 16802	2a. REPORT SECURITY CLASSIFICATION Unclassified 2b. GROUP

3. REPORT TITLE

Long Period Seismic Methods for Identifying Small, Underground Nuclear Explosions

4. DESCRIPTIVE NOTES (Type of report and inclusive dates)

Final Report June 1, 1969 - March 31, 1973

5. AUTHOR(S) (First name, middle initial, last name)

Alexander, Shelton S.

6. REPORT DATE	7a. TOTAL NO. OF PAGES	7b. NO. OF REFS
August 22, 1973	151	22

8a. CONTRACT OR GRANT NO	9a. ORIGINATOR'S REPORT NUMBER(S)
AFOSR-69-1796	
b. PROJECT NO. AO 1722	None
c. 62701D	9b. OTHER REPORT NO(S) (Any other numbers that may be assigned this report) AFOSR - TR - 73 - 1603
d.	

10. DISTRIBUTION STATEMENT

APPROVED FOR PUBLIC RELEASE; DISTRIBUTION UNLIMITED.

11. SUPPLEMENTARY NOTES		12. SPONSORING MILITARY ACTIVITY
TECH, OTHER	Reproduced by NATIONAL TECHNICAL INFORMATION SERVICE US Department of Commerce Springfield, VA. 22151	Air Force Office of Scientific Research/NPG 1400 Wilson Boulevard Arlington, VA 22209

13. ABSTRACT The overall objective of this research has been to develop and test new methods for isolating diagnostic long-period information that can be used to distinguish small underground nuclear explosions from earthquakes.

Major accomplishments.

The major accomplishments of this research include the following: (a) a method for extracting spectra of weak Rayleigh and Love waves by combined use of matched filtering and array summing; (b) mode separation techniques for isolating individual Rayleigh and Love modes frequency by frequency and measuring their excitation; (c) showing that Rayleigh wave spectral shapes, radiation patterns, and energy distribution among modes is consistent from explosion to explosion in given source areas while Love wave excitation seems to depend strongly on near-source geological structure and prevailing regional stresses; (d) a method for combined use of Love and Rayleigh waves to obtain a surface wave magnitude estimate that is nearly independent of fault strike, dip, slip, and at the longer periods (30-50 seconds) depth; (e) showing by relative dispersion measurements and comparison of explosions and collapses at NTS that explosion generated Love waves result from the release of shear energy in the immediate vicinity of the shot point and not through conversion of compressional waves; (f) a method for computing the spectral distribution of energy with time on a seismogram that allows quantitative evaluation of the partitioning of energy among seismic phases to be done routinely and makes it practical to utilize all the information on the seismogram; earthquakes and explosions in Nevada of comparable body wave magnitude show distinctly different energy partitioning both temporally and spectrally when evaluated in this manner and (g) a method for obtaining surface wave dispersion (hence structure) in the vicinity of a given source region by use of array of sources in that region and only a few distant recording stations.

DD FORM 1 NOV 65 1473

Unclassified

Security Classification

166

FINAL REPORT

LONG-PERIOD SEISMIC METHODS FOR IDENTIFYING SMALL, UNDERGROUND NUCLEAR EXPLOSIONS

S. S. Alexander (814-865-2622)

The Pennsylvania State University
Department of Geosciences
Geophysics Section
204 Mineral Sciences Building
University Park, Pennsylvania 16802

Grant No. AFOSR - 69-1796
Mod. No. AFOSR - 69-1796A
Project-Task 8652
Contract Interval: 1 June 1969-31 March 1973
Amount of Contract: $119,642

Prepared

for

AIR FORCE OFFICE OF SCIENTIFIC RESEARCH
~~OFFICE OF AEROSPACE RESEARCH~~
UNITED STATES AIR FORCE
AFOSR (SRPG), ARLINGTON, VIRGINA

WORK SPONSORED BY THE ADVANCED RESEARCH PROJECTS AGENCY

TABLE OF CONTENTS

TABLE OF CONTENTS - continued

LONG-PERIOD SEISMIC METHODS FOR IDENTIFYING SMALL, UNDERGROUND NUCLEAR EXPLOSIONS

Brief Summary

I. Objective

The overall objective of this research has been to develop and test new methods for isolating diagnostic long-period information that can be used to distinguish small underground nuclear explosions from earthquakes.

II. Major Accomplishments

The major accomplishments of this research include the following: (a) a method for extracting spectra of weak Rayleigh and Love Waves by combined use of matched filtering and array summing; (b) mode separation techniques for isolating individual Rayleigh and Love modes frequency by frequency and measuring their excitation; (c) showing that Rayleigh wave spectral shapes, radiation patterns, and energy distribution among modes is consistent from explosion to explosion in given source areas while Love wave excitation seems to depend strongly on near-source geologic structure and prevailing regional stresses; (d) a method for combined use of Love and Rayleigh waves to obtain a surface wave magnitude estimate that is nearly independent of fault strike, dip, slip, and at the longer periods (30-50 seconds) depth; (e) showing by relative dispersion measurements and comparisons of explosions and collapses at NTS that explosion generated Love waves result from the release of shear energy in the immediate vicinity of the shot point and not through conversion of compressional waves; (f) a new method for computing the spectral distribution of energy with time on a seismogram that allows quantitative evaluation of the partitioning

of energy among seismic phases to be done routinely and makes it practical to utilize all the information on the seismogram; earthquakes and explosions in Nevada of comparable body wave magnitude show distinctly different energy partitioning both temporally and spectrally when evaluated in this manner; (g) a method for obtaining surface wave dispersion (hence structure) in the vicinity of a given source region by use of an array of sources in that region and only a few distant recording stations; (h) a method for experimentally determining Rayleigh wave ellipticity dispersion at a single, three-component station thereby allowing an estimate of the crust and upper mantle structure under the receiver to be made; (i) a method for obtaining accurate relative locations of events using only observed arrival times of P-waves and/or matched-filtered surface waves at a common set of receiving stations; and (j) implementing these methods with IBM 360/67 computer programs which permit routine application of these techniques to large amounts of data.

These developments are relevant to all three of the major problem areas in the VELA Uniform program — detection, location, and identification of underground nuclear explosions, because they constitute effective new methods for utilizing long-period information in each of these problem areas.

This grant has supported wholly or in part three completed Ph.D. theses and three that are nearing completion. In addition some of the basic techniques developed have led to more thorough testing on larger data sets by other organizations. Publications based on the work summarized above are:

Alexander, S. S., 1969, Analysis Techniques for Isolating Seismic Source Parameters Using Long-Period Surface and Body Waves, Presented at meeting on Geophysical Theory and Computers, U.M.C., in Copenhagen.

Alexander, S. S., 1969, Improved Surface Wave Magnitude and Source Mechanism Measurements from Combined Use of Love and Rayleigh Waves, Presented at I.U.G.G. in Madrid, paper in preparation for B.S.S.A.

Alexander, S. S., 1969, Spectral Excitation of Surface Waves by Nuclear Explosions and Near-Source Structure. Trans. Am. Geophys. U., vol. 50, no. 11, p. 646.

Alexander, S. S., 1970, Energy Partitioning Among Phases for Earthquakes and Explosions. Trans. Am. Geophys. U., vol. 51, no. 11, p. 778.

Alexander, S. S., 1970, The Use of Higher Mode Rayleigh and Love Waves to Obtain Source Mechanism Parameters. Trans. Am. Geophys. U., vol. 51, no. 4, p. 354.

Alexander, S. S., 1971, Spectral Propagation of Seismic Signals, Report ARPA-T10-71-13-2 on ARPA Seismic Coupling Conference, pp. 91-107.

Alexander, S. S., 1972, New Computational Techniques for Determining Seis- Source Parameters, Paper Presented at the 9th Symposium on Geophysical Theory and Computers, Calgary, Canda.

Alexander, S. S., and Taylor, R. W., 1968, Spectral Estimates for Weak Teleseismic Surface Waves. Trans. Am. Geophys. U., vol. 49, no. 4, p. 718.

Alexander, S. S., and Taylor, R. W., 1969, Source Parameters and Crustal Structures in Active Seismic Areas from Relative Event Analysis. Trans. Am. Geophys. U., vol. 50, no. 4, p. 240.

Alexander, S. S., R. R. Michlik, and P. Glover, 1972, A Variable Sampling Rate (VRS) Technique for Digitizing Analog Records Efficiently and Economically, Presented at Spring A.G.U. Meeting.

Alexander, S. S., L. S. Turnbull, Jr., and R. J. Greenfield, 1973, Non-Linear Least Squares Determination of Seismic Source Parameters Using Frequency Dependent Radiation Patterns of Rayleigh and Love Waves, Trans. Am. Geophys. U., vol. 54, no. 4, p. 367.

Newton, C. A., 1973, An Investigation of Rayleigh Wave Ellipticity with Applications to Earth Structure, Ph.D. Thesis, The Penna. State Univ., University Park, Pa. 16802.

Newton, C. A., and Alexander, S. S., 1969, Rayleigh Wave Ellipticities and Inferred Structure, Presented at B.S.S.A. Meeting in St. Louis, Mo.

Newton, C. A., and Alexander, S. S., 1973, An Equivalent Flat-Earth Transformation for Computing Rayleigh Modes in a Spherical Earth, Trans. Am. Geophys. U., vol. 54, no. 4, pp. 374.

Spence, W. J., 1973, Crustal and Upper Mantle P-Wave Velocity Heterogeneity and the Problem of Earthquake Location, Ph.D. Thesis, The Penna. State Univ., University Park, Pa. 16802.

Spence, W. J., and Alexander, S. S., 1968, A Method for Determining the Relative Location of Seismic Events: Earthquake Notes, vol. 39, no. 3-4, p. 13.

Taylor, R. W., 1972, Remote Determinations of Earth Structure from Relative Event Analysis with Applications to the Mid-Atlantic Ridge, Ph.D. Thesis, The Penna. State Univ., University Park, Pa. 16802.

Taylor, R. W. and Alexander, S. S., 1973, Differential Surface Wave Analysis as a Means for the Seismic Investigation of Inaccessible Areas, submitted to Geophys. Journal.

Taylor, R. W., and Alexander, S. S., 1973, Rayleigh Wave Dispersion and Amplitude Measurements for a Section of the Mid-Atlantic Ridge, submitted to Geophysics. Journal.

INTRODUCTION

This report describes research conducted on the problem of utilizing long-period information to improve our capability of identifying small, underground nuclear explosions. The results appear here in rather condensed form with more complete details given in the Appendices or referenced publications.

RESULTS

The results summarized above are discussed in the main body of this report under several main categories: surface wave detection and analysis, source parameters, crustal structure, relative location of events, and computational programs.

Surface Wave Detection and Analysis

1. Detecting and separating Love and Rayleigh waves for small events. The single channel and array matched filter methods developed originally by Alexander and Rabenstine (1967a, 1967b) for lowering the detection threshhold for Rayleigh waves and increasing their signal-to-noise ratio were adapted for use on the I.B.M. 360/67 and extended to include spectral shaping of natural reference filters for optimum S/N gain, calculations of synthetic matched filters from dispersion and attenuation observations, and adjustments for natural reference filters to correct for epicentral distance differences. Our results indicate that for continental-sized arrays the frequency dependent differential attenuation along the various source to receiver paths should be included to obtain a better S/N in the array sum. A first approximation to this correction can be obtained by empirically equalizing all the reference event spectra to a single shape and applying the same station equalizations to the spectra of the individual seismograms being analyzed. However, if the reference event is an earthquake, frequency-dependent radiation patterns (source mechanism) may be

responsible for a large fraction of observed variations in spectral shapes for different azimuths. Consequently, this correction should be made with due caution and preferably established by examining a large explosion signal or averaging several sets of corrections from sizeable earthquakes in the source region of interest.

Because Love wave excitation is potentially as useful for identification of small events as Rayleigh waves, we set out to apply the same matched filter methods for detecting weak Love waves. The problems involved in actually obtaining pure Love-wave reference filters by combining the horizontal components in such a way that Rayleigh waves are eliminated soon became apparent. Simple rotation of horizontal components usually does not succeed because lateral refraction gives rise to frequency dependent propagation directions at each station. Moreover, Love waves of a given frequency may be propagating in a different direction than Rayleigh waves of the same frequency when they reach a particular station, so that Rayleigh particle motion is not orthogonal to Love wave particle motion. We were able to devise a method which will effect the desired separation, however. Briefly it consists of determining the direction of propagation of Rayleigh waves with frequency either from three components at a single station using ellipticity constraints or from an array (e.g. LASA) of vertical components, then for each frequency rotating the horizontal components to obtain a component normal to the Rayleigh direction, and finally synthesizing the pure Love signal for use as a reference filter. These spectral rotation operators can then be applied to seismograms containing weak signals from the same source region. In effect this operation amounts to a Rayleigh wave rejection filter which retains almost all of the Love

wave energy. An alternative approach is to use the Rayleigh directions and measured ellipticities to subtract the Rayleigh wave contribution from the horizontal components. Once these operations have been applied then the modified seismograms and Love wave reference filters can be used in exactly the same manner as in the Rayleigh wave matched filter procedure.

Another approach for separating Love and Rayleigh fundamental modes, applicable only to arrays, was also devised. First, high resolution frequency-wave number filtering is applied to the array of vertical components. At each frequency this gives estimates of the signal power, propagation direction, and propagation velocity for the Rayleigh waves. Then the same procedure is applied to each set of corresponding unrotated horizontal components. For each set containing appreciable Love and Rayleigh energy two peaks appear, one giving the Love wave power (scaled by the square of the appropriate direction cosine), the velocity and direction of propagation and the other giving the analogous horizontal component Rayleigh wave estimates. Simply summing the partial powers for each set gives the total Love and Rayleigh power at each frequency. The identification and separation of Love waves by this method is unambiguous because the horizontal Rayleigh wave f-k peaks match one-to-one those obtained from the vertical components. The remaining peaks, therefore, represent the Love wave contributions. This method is particularly useful when the propagation directions for Love and Rayleigh waves are different since the Love and Rayleigh f-k peaks are moved farther apart, whereas when the directions coincide, the phase velocity differences may not be sufficient to effect total separation. However, if the Rayleigh-wave ellipticities are known, then the Rayleigh contribution can be subtracted from the horizontal f-k

spectra to leave only the Love wave; or the horizontals can be rotated 90° to the Rayleigh direction and a transverse f-k spectrum computed. The threshhold for using this modified f-k approach remains to be established. However, it clearly is useful for providing the parameters needed in the previous methods for obtaining reference Love wave filters and the rotation operators for preprocessing of the small events.

The success of all of these separation methods depends critically upon knowing the instrument response (both amplitude and phase) of all three components of each station. Consequently, considerable care must be exercised in applying these techniques on a routine basis.

2. Spectra of weak surface wave signals

Theoretical analysis predicts and limited experimental evidence on larger events confirms that, in addition to substantial differences in total surface wave energy for explosions and earthquakes of comparable P-wave magnitude, the overall spectral shapes of explosions and earthquakes may differ substantially. At the larger magnitudes at least, earthquakes signals are generally enriched in long-period energy compared to explosions. However, theoretical calculations (Von Seggern, 1969) show that earthquake spectra can match the explosions shapes or even exhibit greater high frequency excitation for certain fault orientations and source-to-receiver azimuths. We also documented this effect experimentally.

Figure 1 compares (for the stations and distances indicated) the shapes and positions of Rayleigh wave spectral peaks for LONGSHOT and the 22 November 1965 Rat Island earthquake of comparable body wave magnitude. The stations are on a single azimuth from the source. There

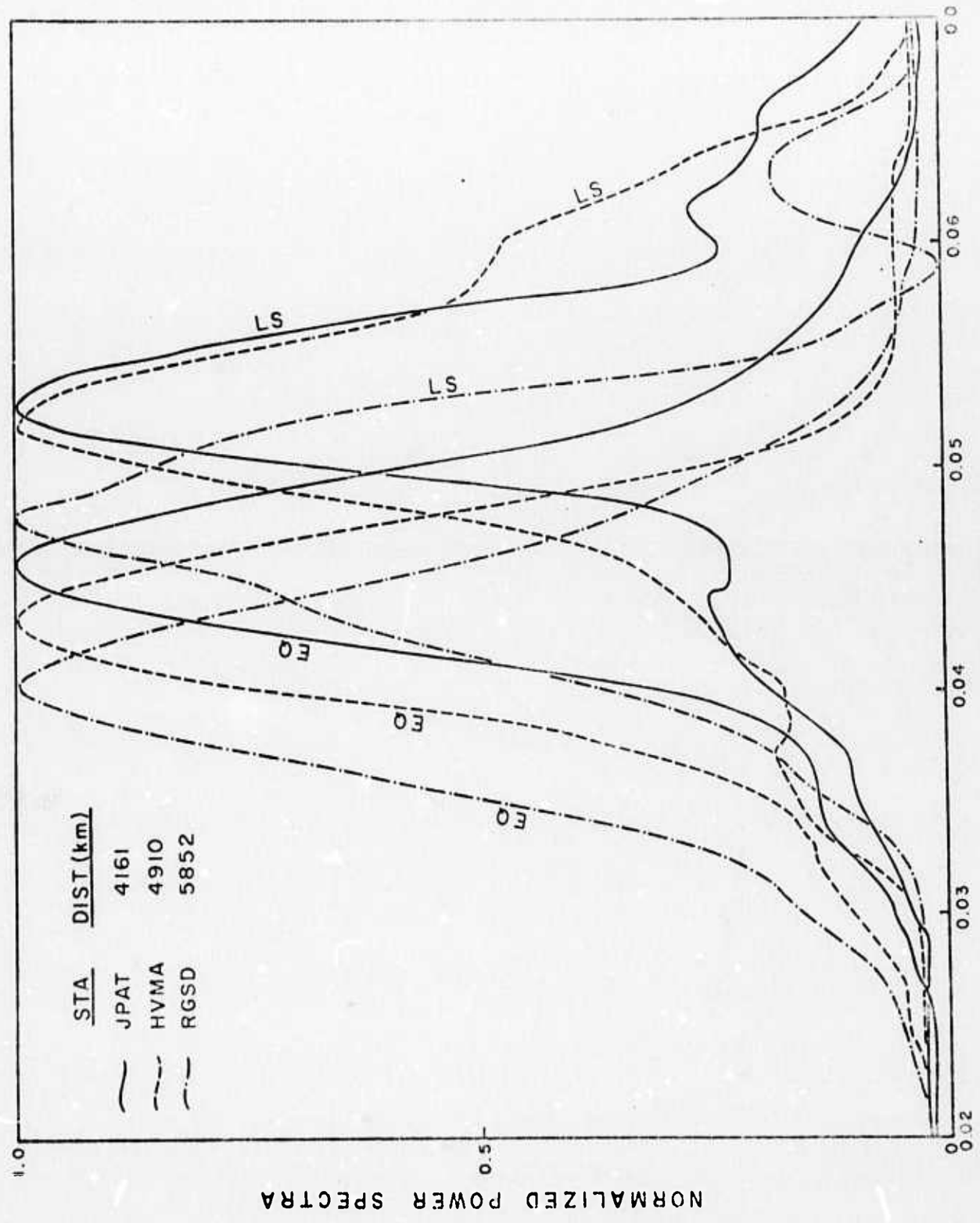

Figure 1. LONGSHOT & 22 Nov. 1966 EQ

appears to be a systematic shift in spectral peak to lower frequency as the distance increases for both the earthquake and the explosion. Frequency dependent attenuation with distance along the inter-station transmission paths may be responsible for the observed shift, since the shift is in the proper sense. Regardless of the physical explanation this example points out the importance of comparing events only using stations in common for the events of interest (i.e. in the cases plotted here, each station, taken individually, has distinctly different spectra for the two events as does the average of the common set; however, had we compared the LONGSHOT spectrum observed at RGSD with the earthquake spectrum obtained at JPAT the shapes would be quite similar). The ratio of the earthquake peak power to the LONGSHOT peak power is approximately 750 for all stations (i.e. an amplitude ratio of about 25).

Figure 2 shows that the 22 November 1965 Rat Island earthquake exhibits a frequency dependent radiation pattern while the LONGSHOT explosion with the same M_b does not (at least for two azimuths differing by about 25 degrees). The reasoning is that for two stations (RGDS and RKON) located at about the same epicentral distance but differing azimuth the LONGSHOT spectrum peaks at the same frequency at both stations with a very similar shape at the longer periods while the earthquake peaks at about .04 Hz at RGSD and at .045 Hz at RKON with a significantly different shape even at the lower frequencies. This similarity for LONGSHOT shows that path effects are comparable for both azimuths, especially so for periods of 20 seconds and above. Therefore the observed azimuthal difference in the earthquake's spectrum must be due to the source mechanism. This suggests (as does theory) that frequency dependent radiation patterns are

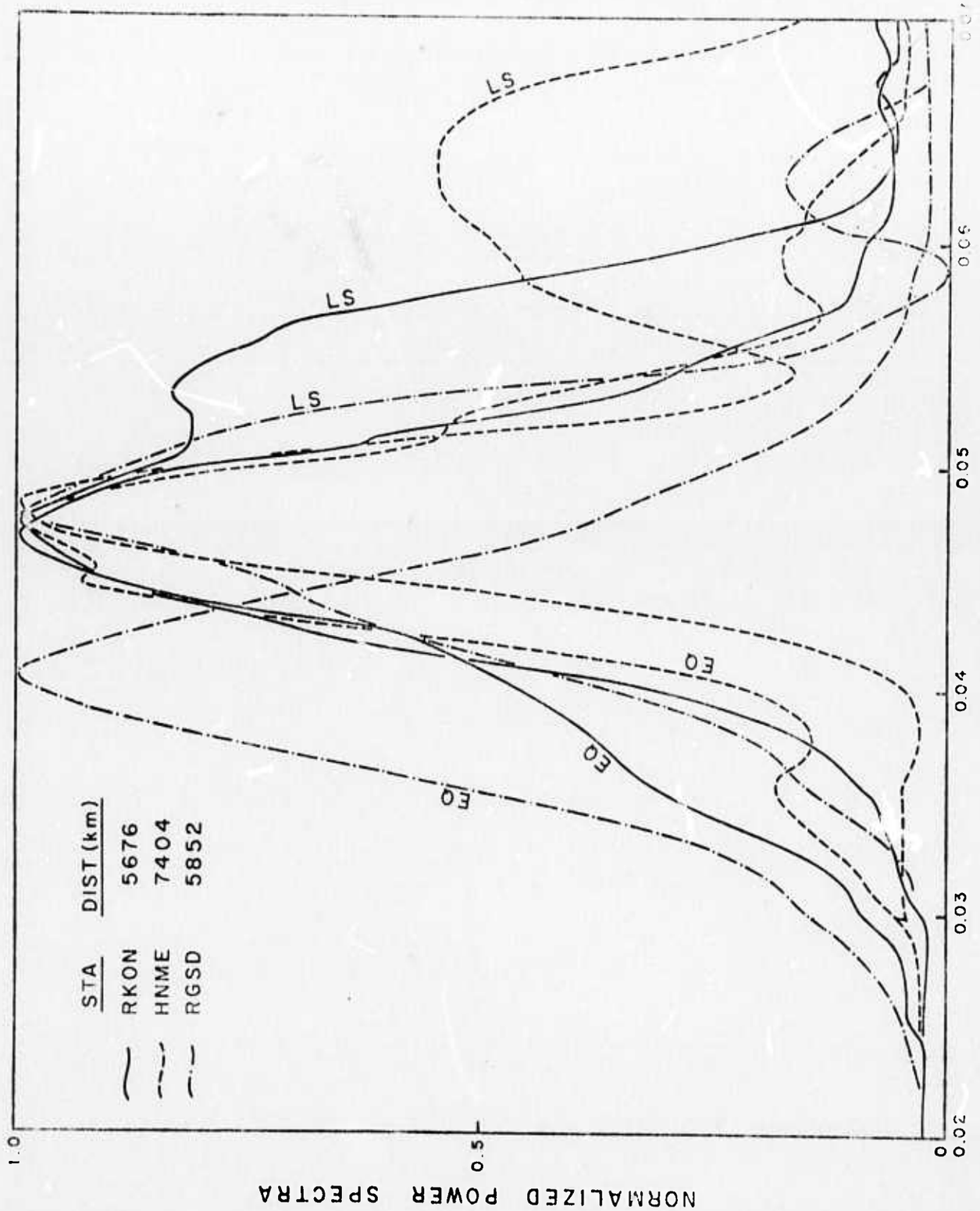

Figure 2. LONGSHOT 8 22 Nov. 1966 EQ

indicative of earthquakes and may be used in conjunction with M_s vs M_b criteria in identifying events provided the transmission path can be ruled out as the cause of different observed spectral shapes along different azimuths.

Attenuation along the path and site response definitely distort the observed Rayleigh wave spectral shape and level as is evident in Figure 1. These effects can be largely eliminated, however, if we compare only events occurring in the same source region at a common network of receivers because the transmission paths are in common for all events propagating to the same set of stations. This approach (regionalization) avoids the uncertainty involved in making corrections for these effects and allows direct comparison of source differences.

Figure 3 shows normalized spectra of Rayleigh and Love waves for three NTS explosions recorded at PGBC. The corresponding Rayleigh wave seismograms are shown in Figure 4. It is clear that the Rayleigh waves from these explosions have almost identical spectral shapes while the Love waves are more variable reflecting differences in the excitation of SH energy from event to event. The RKON Rayleigh wave signals (hence spectra) are also similar for these small events as seen in Figure 4. There are numerous other examples in the recent literature further suggesting that explosion generated Rayleigh wave spectral shapes are invariant over a significant range in body-wave magnitude. A report by Alexander and Lambert (1972) summarizes these findings and presents spectra of additional sets of explosions and earthquakes further confirming the points made in this section.

In spite of the above and other complications, spectral information

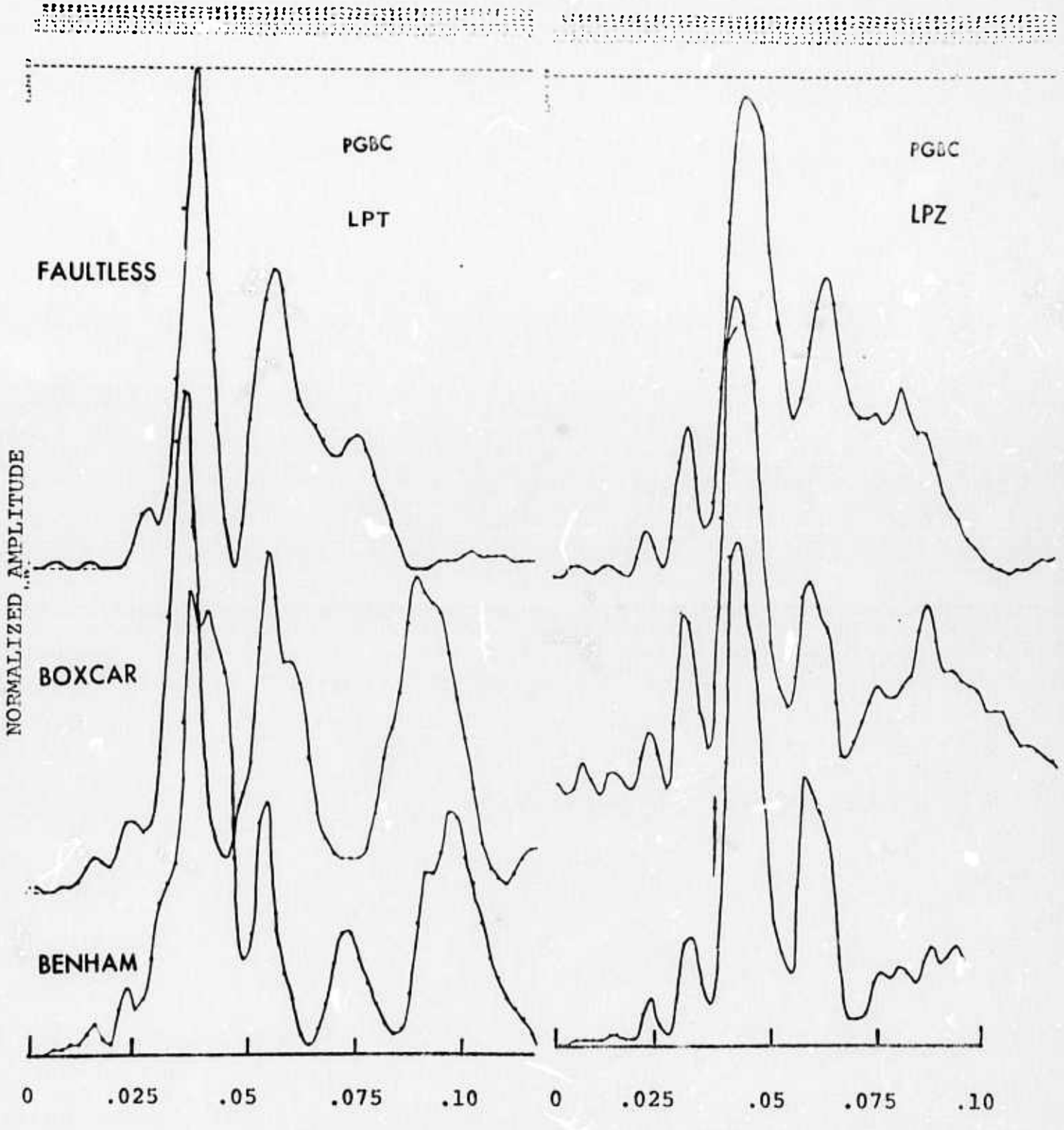
PGBC
LPT
PGBC
LPZ
FAULTLESS
BOXCAR
BENHAM
NORMALIZED AMPLITUDE
0
.025
.05
.075
.10
0
.025
.05
.075
.10
f(hz)

Figure 3.

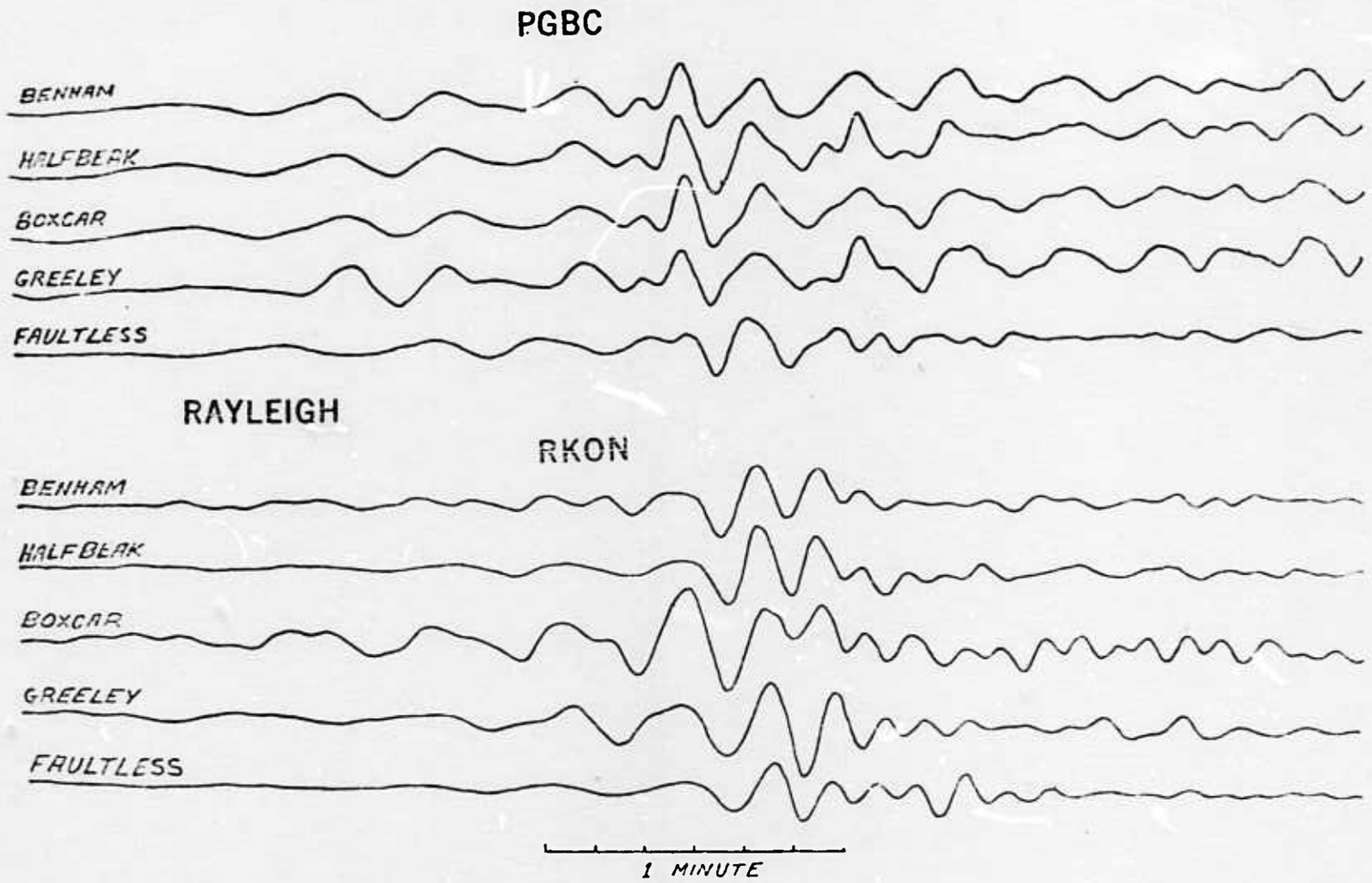

Figure 4. Rayleigh-Wave Signals at PG-BC and RK-ON.

is important to obtain as part of the characterization (regionalization) of the seismic events that are expected to occur in given areas of interest. We extended the matched filter methods discussed earlier to permit improved estimates of spectra to be obtained.

Briefly the procedure used is as follows: (a) compute the power spectrum of a velocity window T_1 containing the weak signal for each station; (b) subtract from each such spectrum a noise power estimate obtained from a long portion of the seismogram preceding the signal window. This gives the conventional spectral estimate at each station; (c) sum these individual noise-corrected spectra over an array; (d) extract from each matched filtered seismogram a time window T_2 about the expected signal peak and compute its power spectrum. This spectrum contains the desired signal power (smoothed) but with $\frac{T_2}{T_1}$ less noise power than the result at step (a) above; (e) subtract a noise power estimate obtained from a long noise sample preceding the signal window; (f) sum these individual noise-corrected matched filter spectra over the array of stations; (g) repeat steps (d) and (e) on the matched filter sum trace to obtain another estimate of the signal spectrum; (h) plot and save any or all of the above outputs.

The approach discussed above, is equally applicable to local arrays (e.g. LASA) and to continental-sized arrays (e.g. LRSM). Results on test cases (Alexander and Lambert, 1971) indicate that this approach allows reasonable spectral estimates to be obtained for Rayleigh waves at LASA (using 9 elements) down to individual station signal-to-noise levels approaching unity (where S/N is the maximum signal trace amplitude divided by the RMS level of the noise in the band .02-.065 Hz) and that

the best spectral estimates are obtained from the matched filter sum trace. We have also computed spectra at LASA for events of different magnitude from the Kuriles, Hokkaido, and the Greenland Sea (Table 1) using this approach. Figure 5 shows the spectral shapes observed at LASA for a Kurile Island pair representing M_b = 5.6 (reference event 21 November 1966) and M_b = 4.3 (19 Apr. 1967) in Table I(b); the distance is 7346 km. The spectra shown have been summed over LASA and noise corrected (normalized noise spectrum is shown). The directly computed spectrum (DIR) and the matched filter computed spectrum (MF) for the small event are shown. The values given at the top show the relative power in the two events (2400 vs 4.3 or 4.9). This is approximately what is expected from the body wave magnitudes i.e. $(10^{5.6})^2$ vs $(10^{4.3})^2$. Note that the small event peaks at a higher frequency than the large event; this represents a difference in source excitation because the transmission paths are common for both. The earthquakes from Hokkaido show a systematic shift in their Rayleigh wave spectral peaks with magnitude, such that the smaller the event (at least to m_b=4.0) the higher the peak frequencies as seen in Figure 6. Such a systematic relationship was not observed for the Kurile events as seen in Figure 6.

Figure 6 shows the frequency at which the Rayleigh wave spectrum peaked vs M_b at LASA for several Hakkaido and Kurile Island events summarized in Table I. Also shown are the ranges (arrows) in peak frequency observed at LRSM stations along a single azimuth SW across the US for LONGSHOT and the 22 November 1965 Rat Island earthquake which was located very close to LONGSHOT (about 50 km) and which had the same body wave magnitude. Since for each source region the transmission path is essentially

TABLE IA - EPICENTER DATA FOR EVENTS FROM HOKKAIDO

Date	Latitude	Longitude	Origin Time (GMT)	Depth (KM)	Magnitude
26 Nov. 1966	42.7°N	144.5°E	17:05:08.0	54	3.9
2 Nov. 1966	43.1°N	145.5°E	17:25:48.0	63	4.1
25 Jul. 1967	42.3°N	148.1°E	15:24:17.3	75	4.2
27 May 1967	41.9°N	142.8°E	20:11:11.0	68	4.3
21 Apr. 1967	41.0°N	143.0°E	9:24:00.0	35	4.4
12 Nov. 1966	41.7°N	144.2°E	23:04:58.8	33	4.7
11 Dec. 1966	42.9°N	144.6°E	19:47:34.2	57	4.8
18 May 1967	41.9°N	144.7°E	11:33:31.6	41	4.9
31 Jan. 1967	42.8°N	145.4°E	17:43:56.2	44	5.1
29 May 1967	43.3°N	145.7°E	21:01:44.3	88	5.3
1 Dec. 1966	41.6°N	139.6°E	18:56:23.1	173	5.4
6 Jan. 1967	41.8°N	143.3°E	0:04:02.7	35	5.5
12 Nov. 1966*	41.8°N	144.1°E	12:49:43.6	33	5.8

*Reference Event

TABLE IB - EPICENTER DATA FOR EVENTS FROM KURILE ISLANDS

Date	Latitute	Longitude	Origin Time (GMT)	Depth (km)	Magnitude
2 Dec. 1966	43.9°N	149.0°E	23:46:55.2	98	4.1
26 Jun. 1967	45.0°N	147.3°	4:53:43.5	88	4.2
19 Apr. 1967	45.4°N	150.8°E	10:46:49.0	33	4.3
29 Mar. 1967	44.4°N	148.4°E	10:01:10.2	26	4.4
19 Jan. 1967	48.7°N	155.1°E	19:46:28.3	29	4.5
18 Jun. 1967	47.6°N	154.3°E	2:42:45.1	32	4.6
11 Nov. 1966	50.3°N	155.5°E	16:03:38.0	145	4.9
22 Dec. 1966	48.6°N	154.3°E	19:24:06.5	77	5.2
1 Apr. 1967	45.8°N	151.7°E	14:00:33.8	23	5.4
1 Apr. 1967	46.3°N	152.0°E	5:56:00.0	40	5.5
21 May 1966*	46.7°N	152.5°E	12:19:27.3	40	5.6
1 Apr. 1967	45.8°N	151.8°E	5:54:19.1	40	5.7
11 Apr. 1967	45.7°N	161.8°E	12:28:35.5	40	5.9

*Reference Event

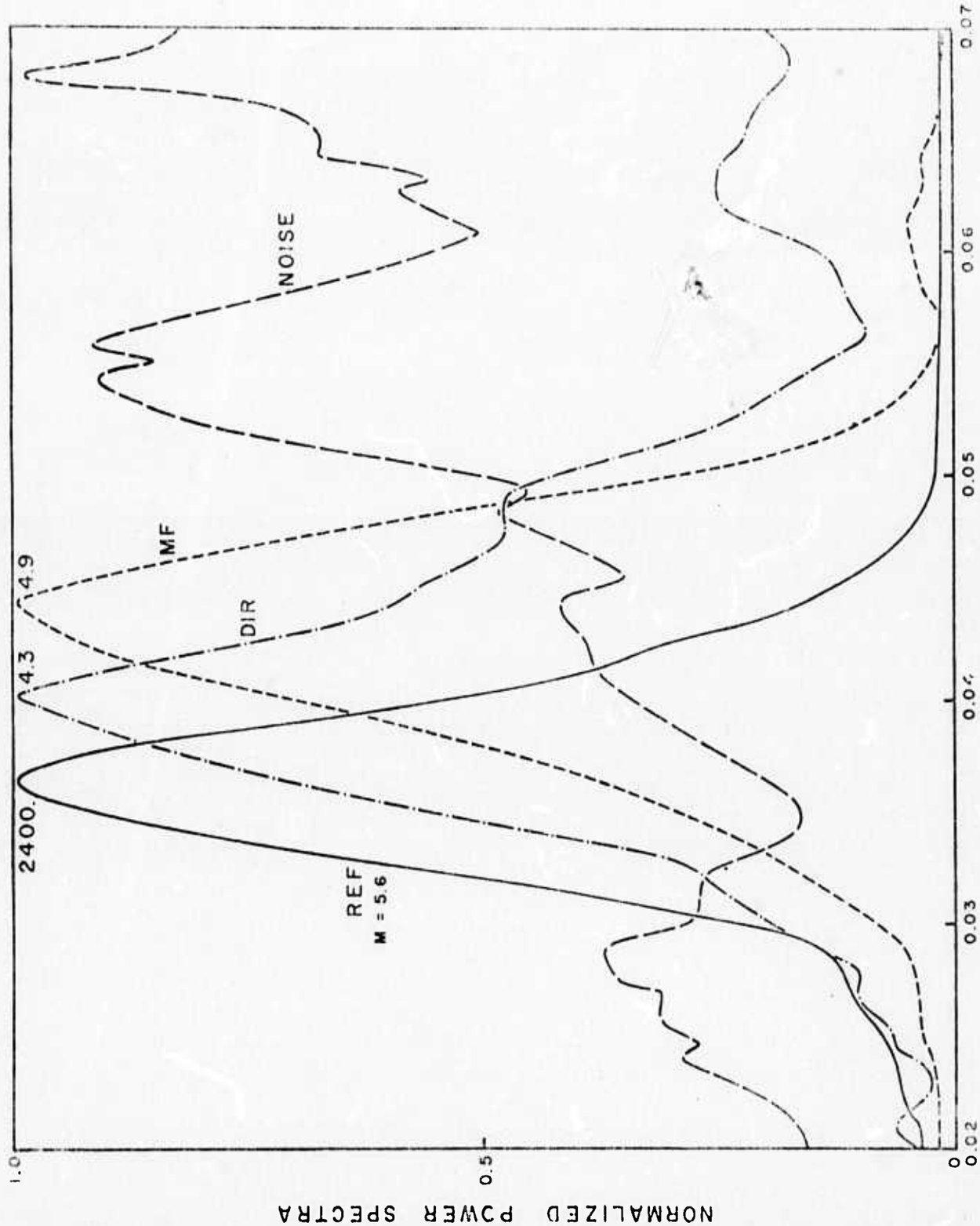

Figure 5. KURILE EVENTS

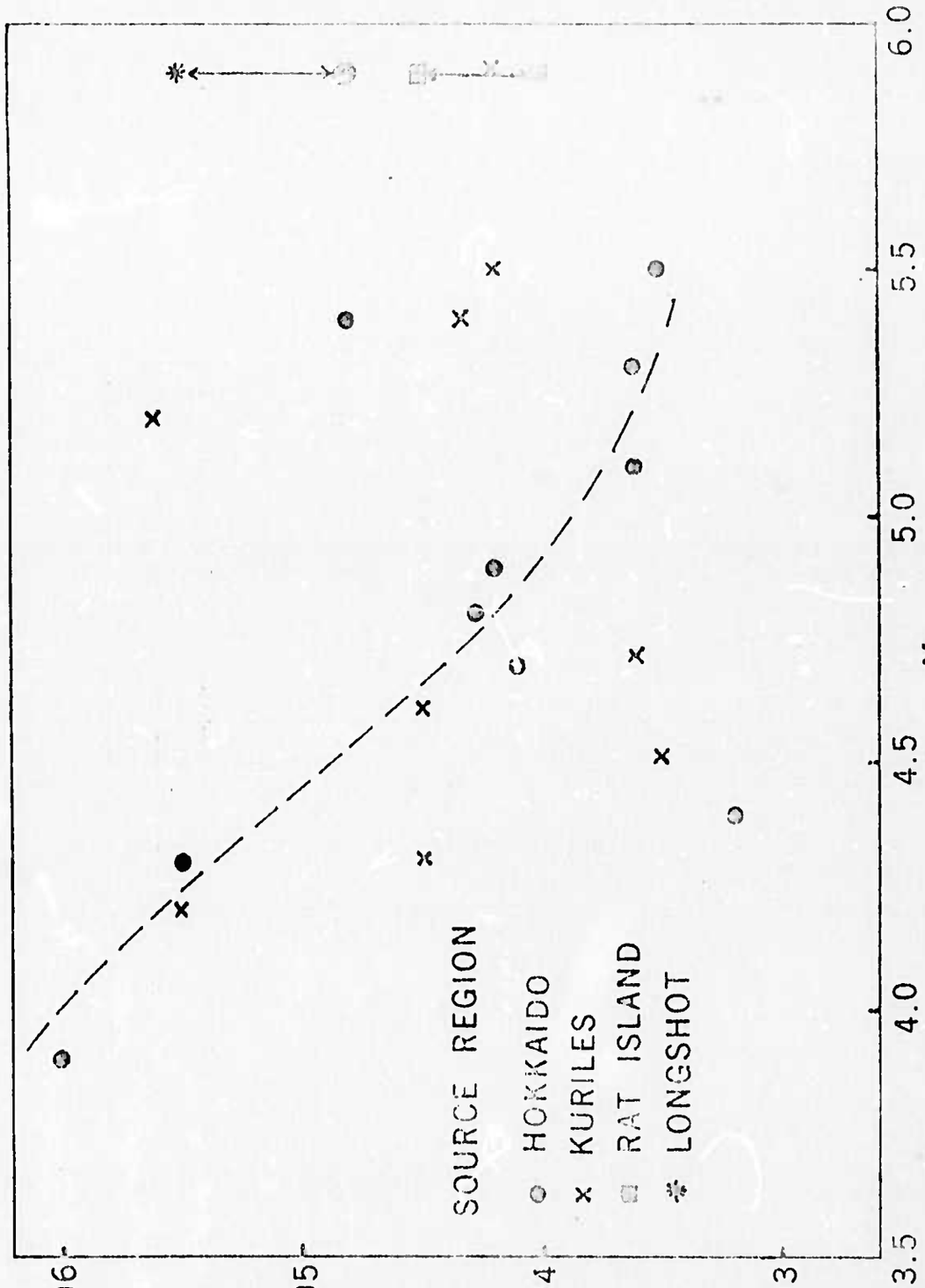
PEAK FREQUENCY (HZ)
.06
.05
.04
.03
3.5
4.0
4.5
5.0
5.5
6.0
M_b
SOURCE REGION
HOKKAIDO
KURILES
RAT ISLAND
LONGSHOT

Figure 6.

invariant the dependence of spectral peak on M_b is a measure of the differences in source excitation. The Hokkaido events appear to be reasonably systematic (dashed line) while the Kurile events show no systematic dependence on magnitude. The range observed for LCNGSHOT and the 22 November 1965 Rat Island earthquake is a manifestation of the effects of attenuation and/or other transmission factors in shaping the spectrum at each station along the profile.

Figure 7 shows the matched filter sum of the Rayleigh waves over LASA for these events. The sum is proportional to a surface wave amplitude measurement, hence, proportional to M_s with little scatter. These (time-domain) estimates include energy over the entire long-period frequency band, and the results show that the total Rayleigh energy varies smoothly vs the body-wave magnitude, even the Kurile events whose spectral peaks (shapes) were so scattered (Figure 6). Note that the events which show low surface wave values are deep; (depth values in parentheses). The arrows shifting two Hokkaido events to larger magnitudes result from a recomputation of M_b by Jarosch (1968) taking the observed body-wave radiation pattern into account. The Greenland Sea events show relatively large M_s/M_b values possibly reflecting significant body wave attenuation at the Mid-Atlantic ridge source. The fact that the slope of the observations seems to increase at the larger M_b values (dashed line) may be due to a systematic under-estimation of M_b at larger magnitudes by virtue of the way M_b is obtained (i.e. from short-period measurements at about 1 Hz); this excludes long-period P-wave excitation. Aki's w^2 model is shown for reference.

Also, the Greenland Sea events from one particular epicentral region

had spectral shapes which did not change significantly with magnitude. Again these data show that spectral shape is not a good diagnostic and that each source region of interest should be documented individually in order to establish any trend in the spectral excitation vs magnitude expected for earthquakes in that region. Wide azimuthal sampling (preferably 180° or more) is also needed to establish the consistency in spectral radiation patterns.

While these spectral techniques have been tested primarily on Rayleigh waves, the same methods apply equally well to Love waves. The only complication is in first separating the Love waves so that the spectral estimates are not contaminated by Rayleigh energy. The separation methods discussed earlier in this report can be used for this purpose.

3. Combined use of Love and Rayleigh waves for improved surface wave magnitude estimates.

By using the theory developed by Harkrider and Ben-Menahem (1964) for Rayleigh and Love wave excitation by various sources in a layered halfspace we have been able to calculate the effects of the fault parameters of strike, dip, slip, and depth on Rayleigh and Love magnitude estimates for realistic earth models (e.g. Gutenberg continental model). We have investigated various ways of combining Love and Rayleigh energy to obtain magnitude estimates which are invariant under changes in these parameters. Our results indicate that simply summing the Love and Rayleigh power spectra for 8 or more stations distributed approximately uniformly over any 180° azimuthal sector will nearly eliminate the effects of strike, dip, and slip on this combined magnitude estimate. However averaging Rayleigh waves alone is better for shallow source depths. In addition, measuring

the combined magnitude in the 30-50 second period range should largely eliminate the dependence on depth, at least for sources shallower than 50 km while comparisons at shorter periods can be used to estimate source depths.

The main difficulty in applying this approach is in correcting for propagation effects that can seriously alter the spectrum observed at a given station. However, for given source regions and a fixed network of stations distributed in azimuth, reliable relative magnitude can be obtained by applying this approach because the distortions introduced by propagation are common to magnitude estimates for each event. Thus, given sufficient azimuthal coverage, this technique will make the M_s vs m_b diagnostic more powerful because we can obtain more accurate magnitude estimates for earthquakes without any knowledge at all about their mechanism. If this approach is used in conjunction with the methods discussed earlier for detecting and separating weak Love and Rayleigh waves, it should be possible to obtain more reliable surface wave magnitude estimates for small earthquakes since only a few stations are needed.

In the process of making this combined magnitude estimate, detailed information on Love and Rayleigh waves individually will be obtained at each station, which in turn can be used to infer source mechanism parameters for the event. Details of this study are included in Appendix I.

4. Mode Separation

In addition to fundamental mode observations the relative excitation of surface wave modes is also potentially diagnostic of source type and depth. However, in order to use them it is necessary to isolate and identify particular modes. The basic approach of Alexander (1963) using

narrow-band filters and recent developments by other workers was used in this aspect of the study. The relative excitation of each mode, its group arrival time, and its local particle motion (ellipticity) can be obtained at each center frequency by superimposing the vertical and radial (rotated horizontal) output. Figure 8 shows an example of multiple filtering of a distant teleseism from Mongolia recorded at LASA. At each period contributions from several Rayleigh modes and one body are present and separable. Notice also the dispersion as the time of arrival of energy packets for each mode changes with period. More details concerning these techniques are contained in the thesis by Newton (1973).

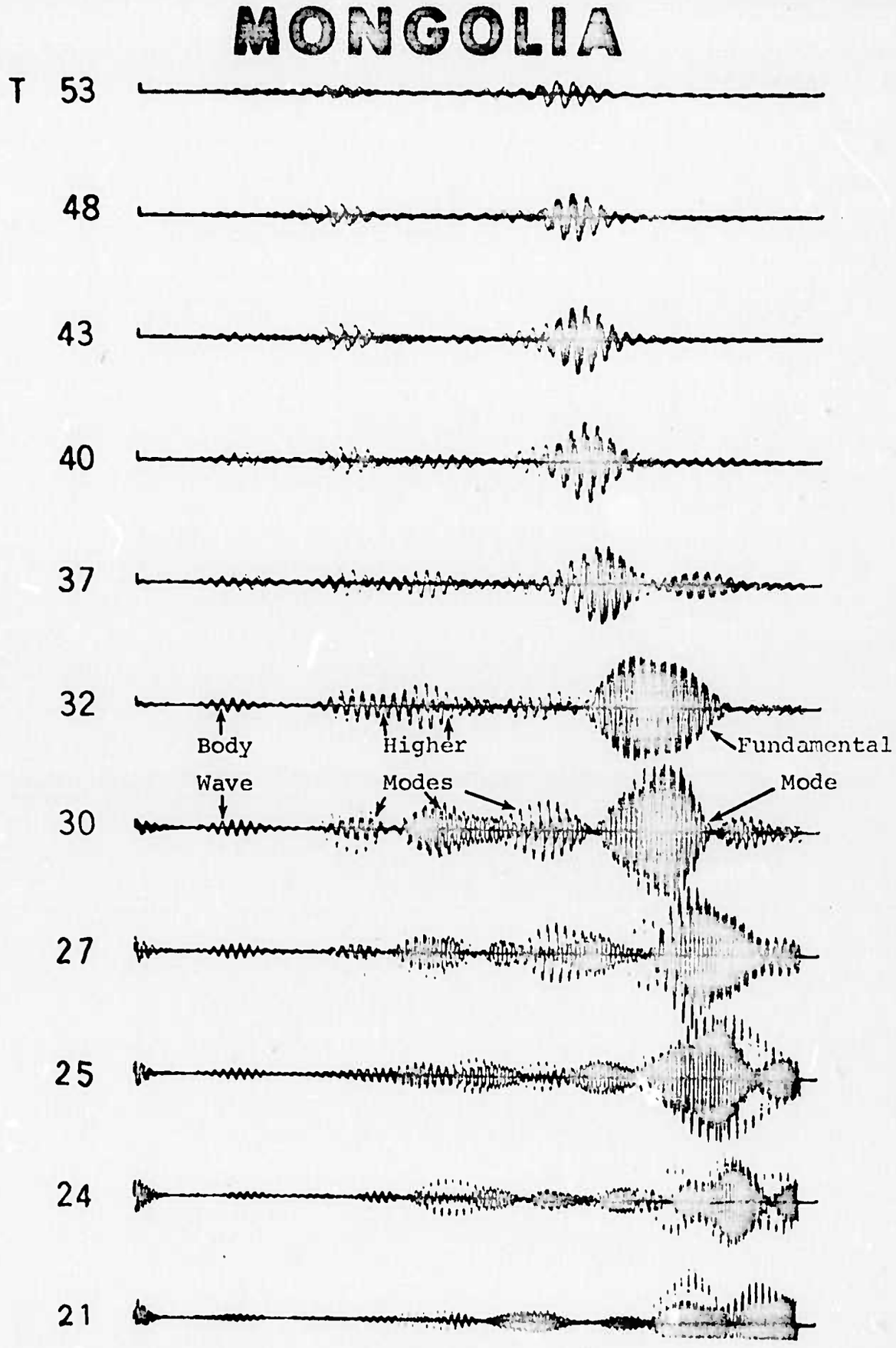
MONGOLIA
T 53
48
43
40
37
32
30
27
25
24
21
Body Wave
Higher Modes
Fundamental Mode
TIME

Figure 8.

Source Parameters

Ideally we would like not only to identify specific events as explosions on earthquakes but also to derive information on the source mechanism of earthquakes typical of a given source region and the stress system that produced them. Several results of this research that bear directly or indirectly on this problem are summarized in this section.

1. Use of entire seismic signatures for source information.

Typically only the short period P-waves and fundamental Rayleigh and Love waves have been used routinely to identify explosions (e.g. M_s v m_b, location from P-arrivals and depth from pP-P estimates). From theoretical considerations and observations of large explosions and earthquakes one expects that there should be a fundamental difference between the spectral distribution of energy emitted as shear waves vs compressional waves. In turn this is reflected in the temporal and spectral distribution of energy among various body wave arrivals and surface wave modes observed at regional and teleseismic distances. In an effort to make use in a practical way of this additional information several techniques were investigated.

a. Pattern Recognition and Energy Distribution Among Phases as a Possible Discriminant

Typically the information taken from seismograms for distinguishing earthquakes from explosions represents only a fraction of the total seismic signature. One reason for this is the difficulty in rapidly examining seismograms from many stations. We have developed a tractable approach to this problem that opens up interesting avenues for future applications.

Basically the idea is to compute the Fourier spectrum for each of a succession of overlapping, short time windows that taken together represents the spectrum as a function of time. (This is the basis for seismoprint or voiceprint displays of time varying spectra such as presented by Cohen (1969) for just the P wave portions of seismograms.) In this fashion we can see both the spectral and temporal distribution of energy in the entire seismogram.

Because of the fundamentally different source mechanisms for earthquakes and explosions the spectral distribution of energy among phase (e.g. P, S, Rayleigh, Love) should be different for the two types of events. We will show some examples that demonstrate this difference for the Shoal-Fallon events observed at LRSM stations shown in Figure 9.

Figure 10 is a comparison of the seismograms for the Shoal explosion and Fallon earthquake as observed at HLID. It is clear from visual comparison that the temporal distribution of energy is quite different for the two events.

Figure 11 shows the seismoprints for the vertical components of these seismograms with contours of equal power shown. The star denotes the maximum over the entire seismogram. Note the difference in the spectral as well as temporal distribution of energy that is not evident from visual examination of the seismograms; that is, the energy distribution pattern differs. A large fraction of the earthquake energy is concentrated in the surface wave (L_g) portion of record whereas most of the energy in the Shoal record is in the P-wave (P_g) portion. Since those events were very nearly the same body wave magnitude and most of the propagation path is common these differences represent actual differences in the sources.

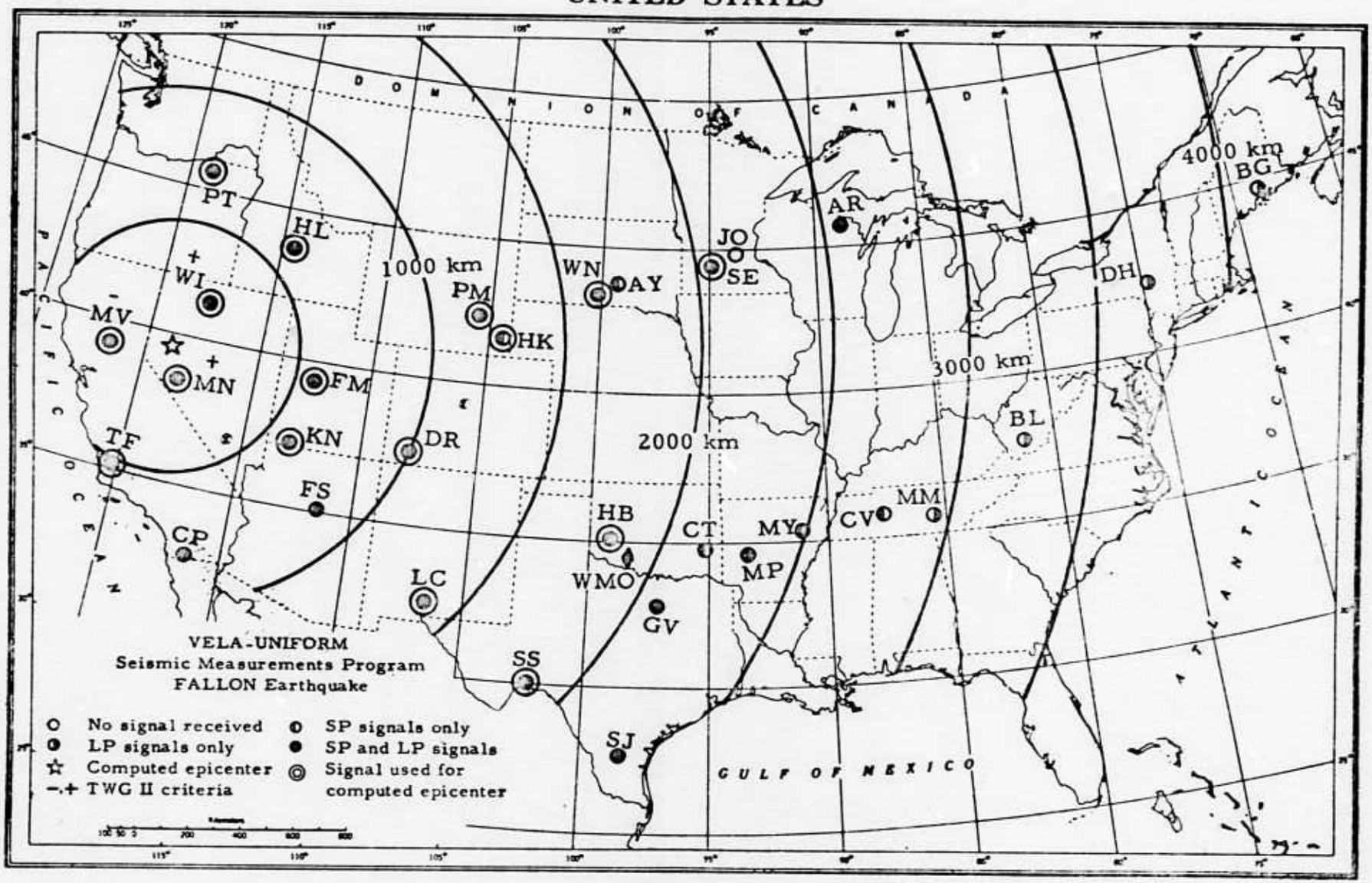

Figure 9. Source-station geometry for the Shoal-Fallon source area.

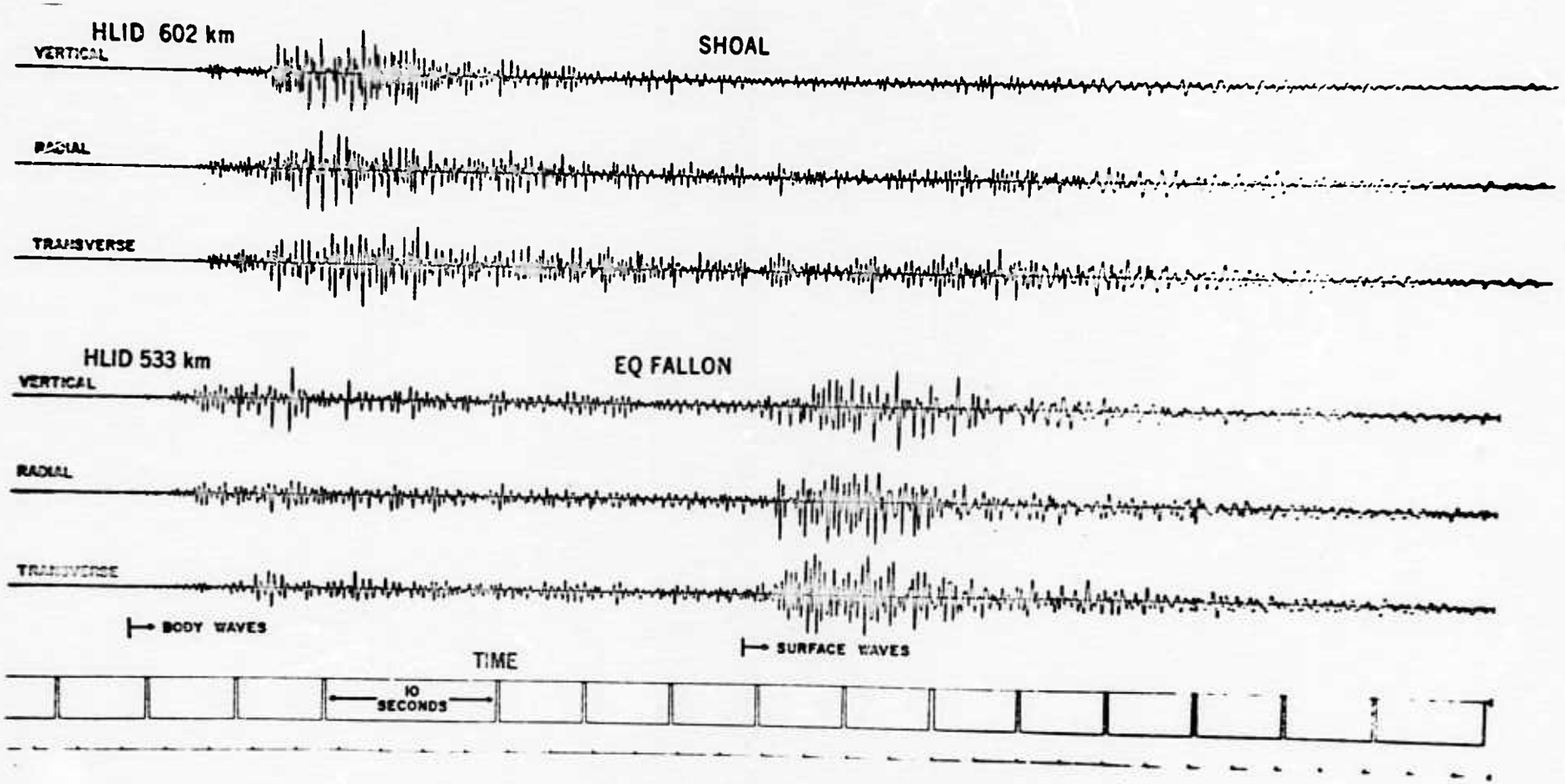

Figure 10. Seismograms for HLID

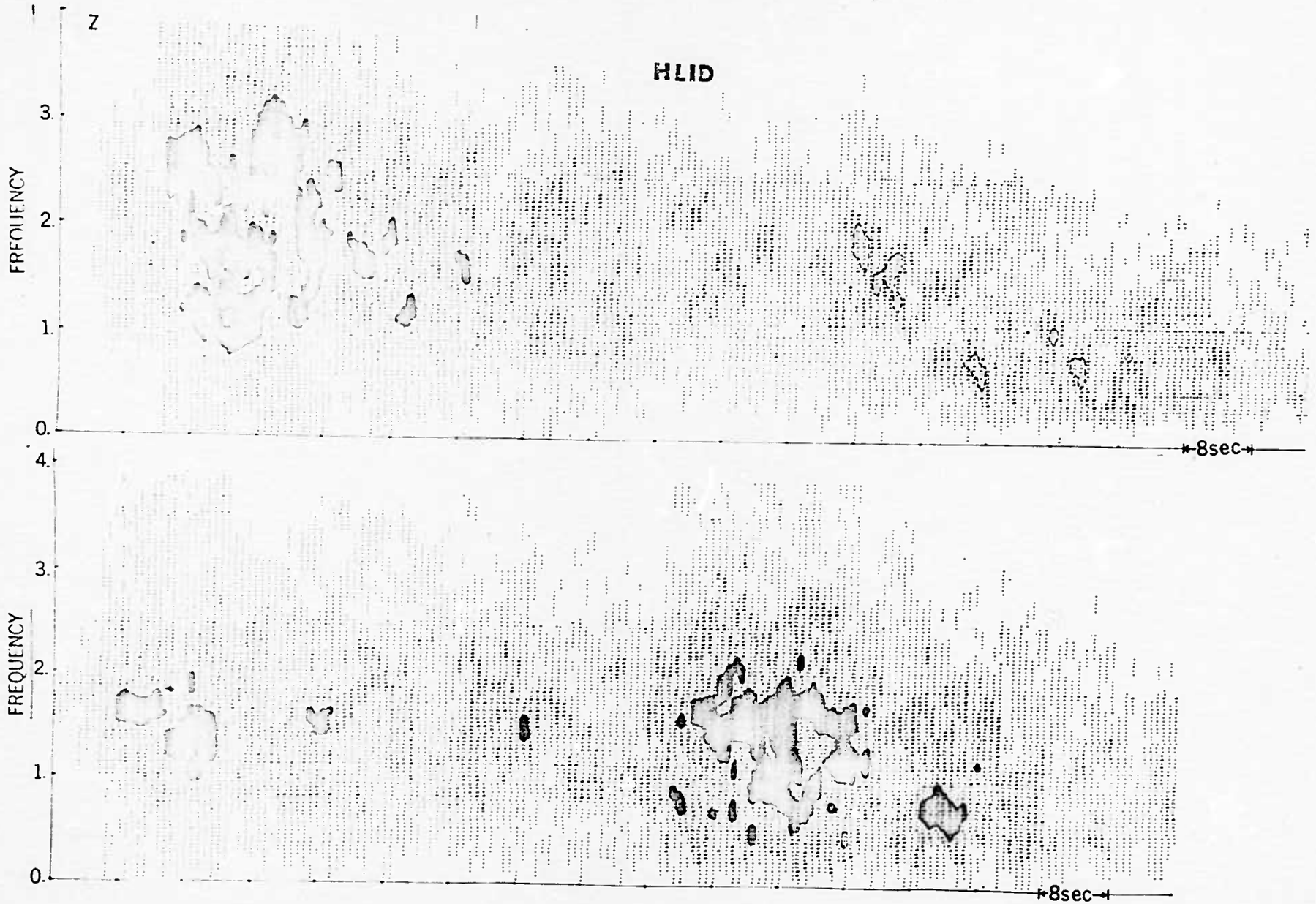

Figure 11. Seismoprints for Vertical Component seismograms at HLID. Top pattern is Shoal, bottom is Fallon.

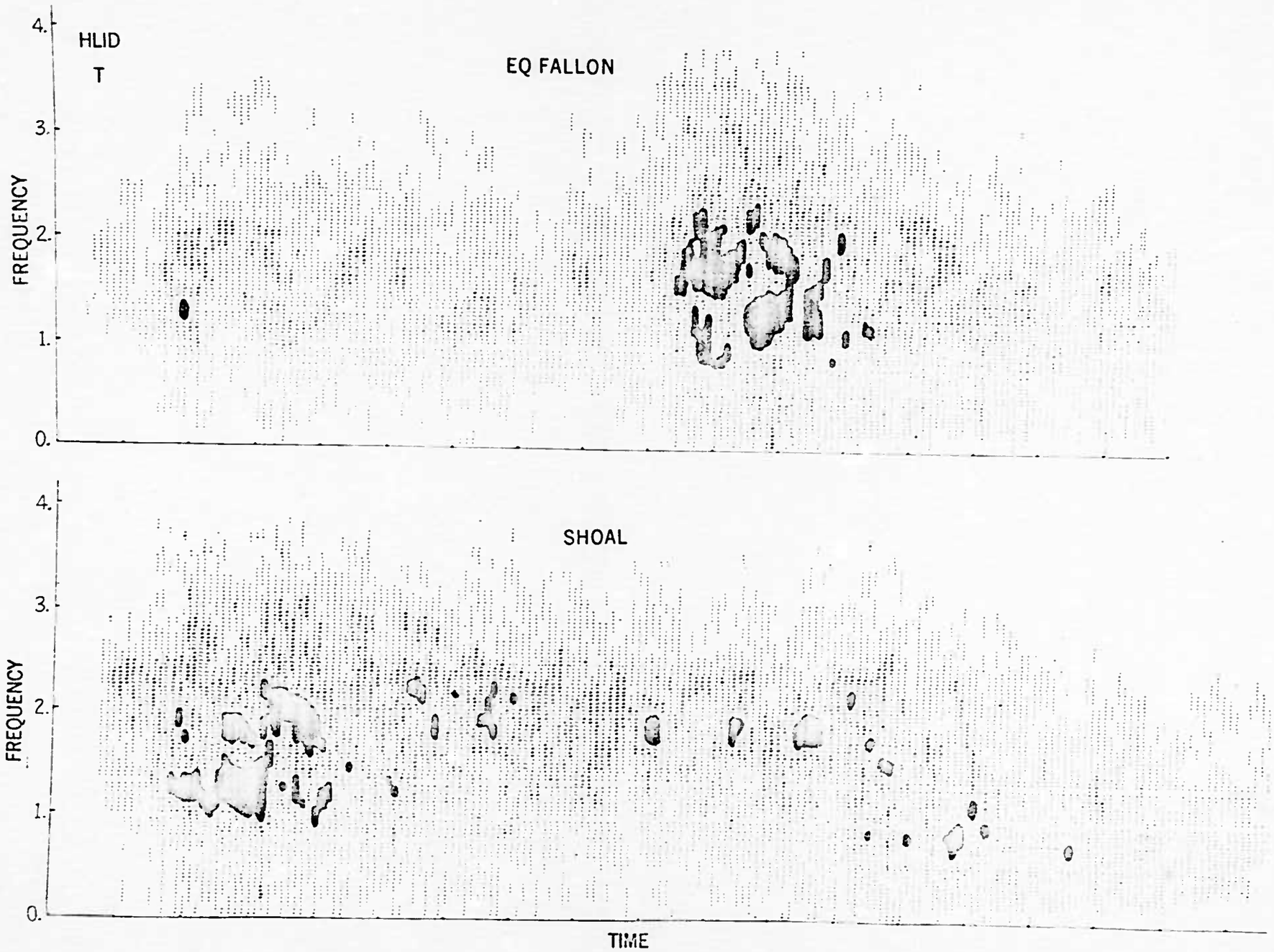

Figure 12. Seismoprints for Transverse Components (Love Waves) at HLID.

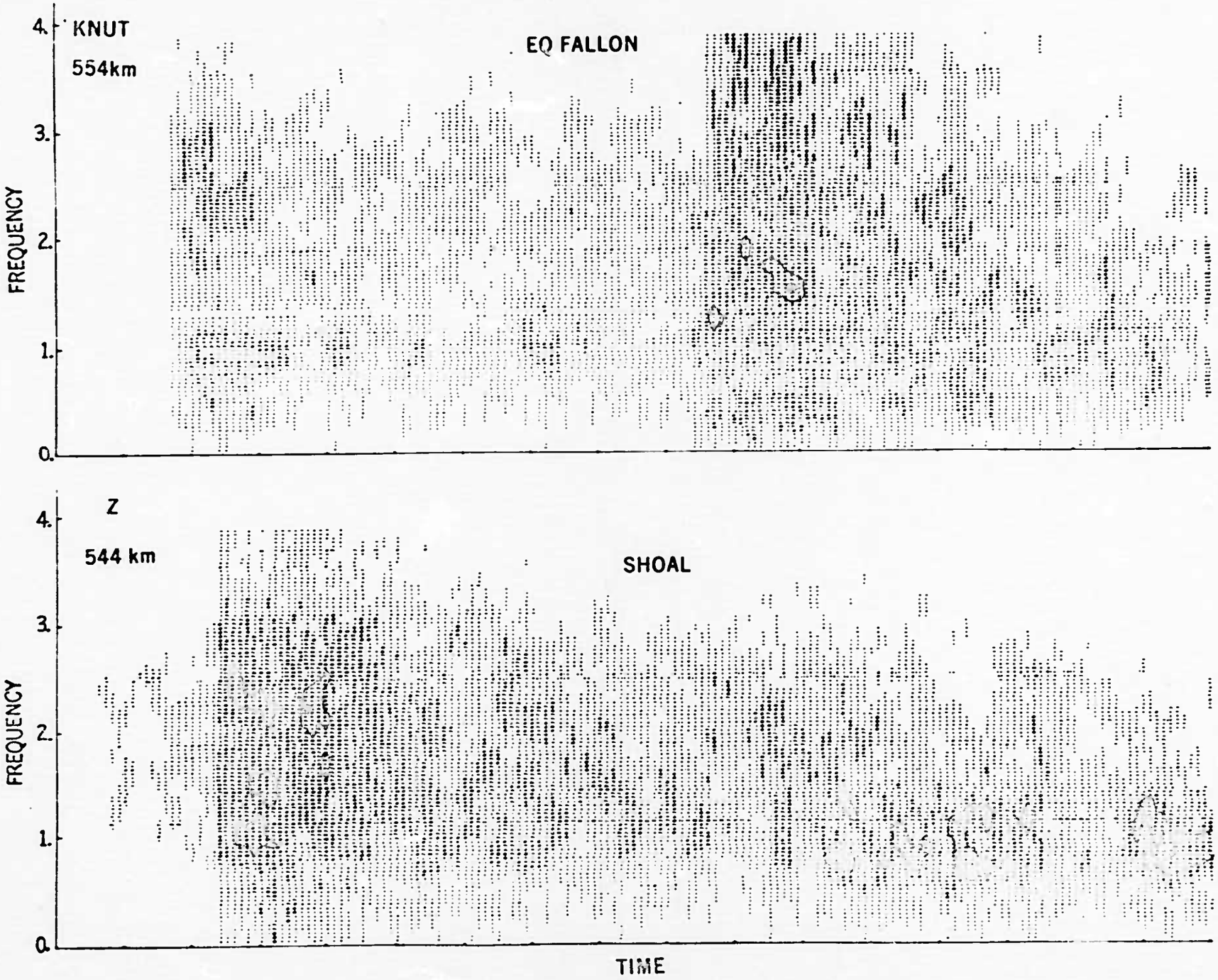

Figure 13. Seismoprints for Vertical Component seismograms at KNUT.

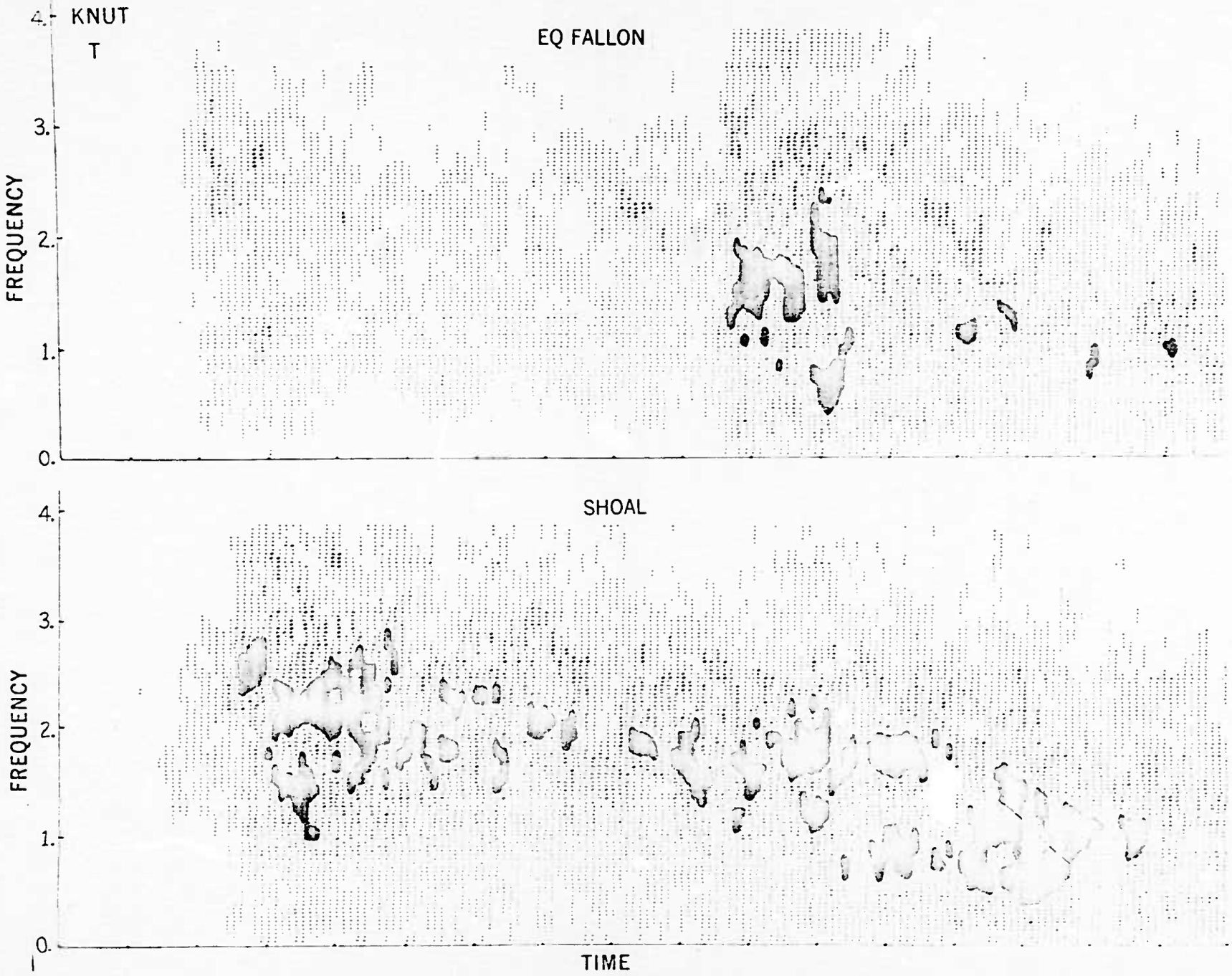

Figure 14. Seismoprints for Transverse Components (Love Waves) at KNUT.

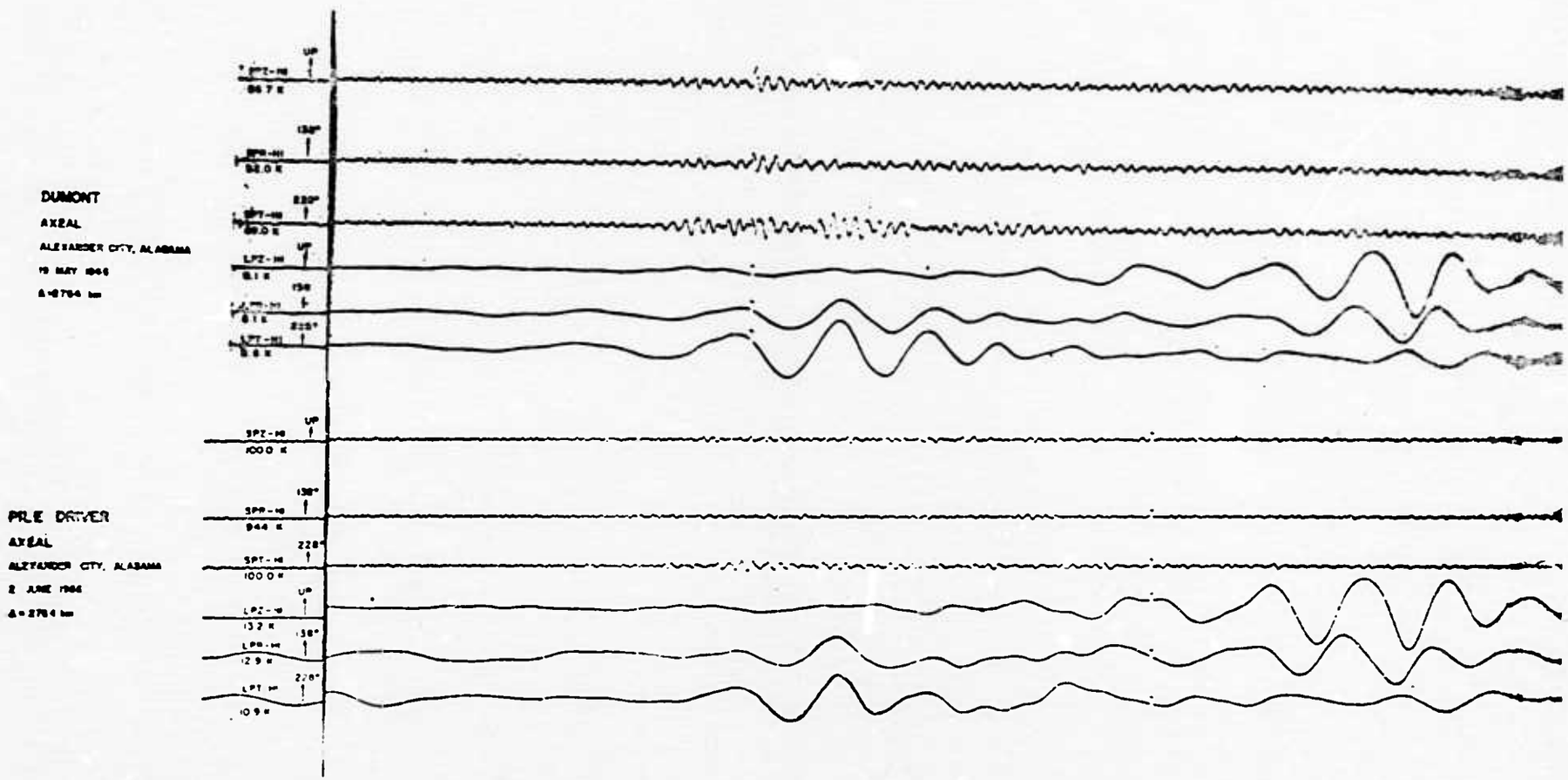

Figure 15. Seismograms for two NTS explosions observed at AX2AL at a distance of 2764 km.

Figure 12 shows the results for the transverse component at HLID. The Fallon (transverse) energy is more concentrated in the surface wave portion than was the vertical. Shoal (transverse) still has maximum energy in the body wave portion but some energy is arriving steadily throughout the record with a gradual shift to lower frequencies. The patterns for Shoal and Fallon are unmistakably different.

Figure 13 shows the seismoprints for Shoal and Fallon at KNUT. Here the differences are still more pronounced than for the cases discussed above with Fallon's energy again concentrated in the surface wave (L_g) portion. Figure 14 shows the results for the transverse component. It is evident that the earthquake's energy is heavily concentrated in the surface (Love) waves.

It is interesting to compare the seismoprints for similar components at the two different receivers (Figs. 11 and 13, Figs. 12 and 14). The pattern for the explosion and earthquake are very similar at both stations. This suggests that pattern recognition techniques can be used to advantage in classifying events provided they are sufficiently consistent. In this connection the signatures are quite consistent from explosion to explosion (at least for the long periods) as mentioned previously (Figure 4) and as illustrated in Figure 15 showing events DUMONT and PILEDRIVER as observed at AX2AL (2764 km). Notice also that the short period surface waves are clearly visible in both events, suggesting that the short-period energy distribution could be used for classifying events out to teleseismic distances in a manner analogous to the regional observations discussed above.

The principle advantages of this approach are: (1) that it is inexpensive in computing time and can be applied routinely to large

quantities of data, and (2) that spectra and spectral ratios among particular phases can be extracted directly from the seismoprints simply by extracting a window containing each phase of interest, and (3) the seismogram is cast into a form where both spectral and temporal energy patterns are immediately apparent.

Once the data are transformed into the seismoprint "domain" and stored a two-dimensional array in the computer, then it is extremely simple to compute energy distribution among phases, total energy ratios among phases, and spectral ratios among phases. To illustrate this approach the seismoprints discussed above (plus those from other LRSM stations) were used to compute the spectral ratios of the body waves to the surface (L_g) waves; a group velocity window beginning at approximately 5 km/sec was used as the beginning of the surface wave window (see Figure 10 where this is shown). Figures 16 to 19 show these spectral ratios for both Rayleigh and Love waves at HLID, KNUT, CPCL, and DRCO (see map in Figure 9). R is the ratio (db) of body-wave energy to surface wave energy for frequencies up to 3.5 Hz; note that R=0 means an equal amount of energy, positive values predominantly body wave energy, and negative values predominantly surface wave energy. (It is instructive to refer to the seismoprints in Figures 11 to 14 when examining Figures 16 and 17). It is clearly evident from these figures that there is 10 to 20 db difference in the ratio of body wave to surface wave energy between the Shoal and Fallon events. This is reflecting the usual differences in M_s vs m_b for earthquakes and explosions even though the surface waves here are higher modes (L_g, etc.). The separations become somewhat less pronounced at the lower frequencies but still remain apart for these two events. This example suggests that if high frequency (1-4 Hz) signals can be observed at

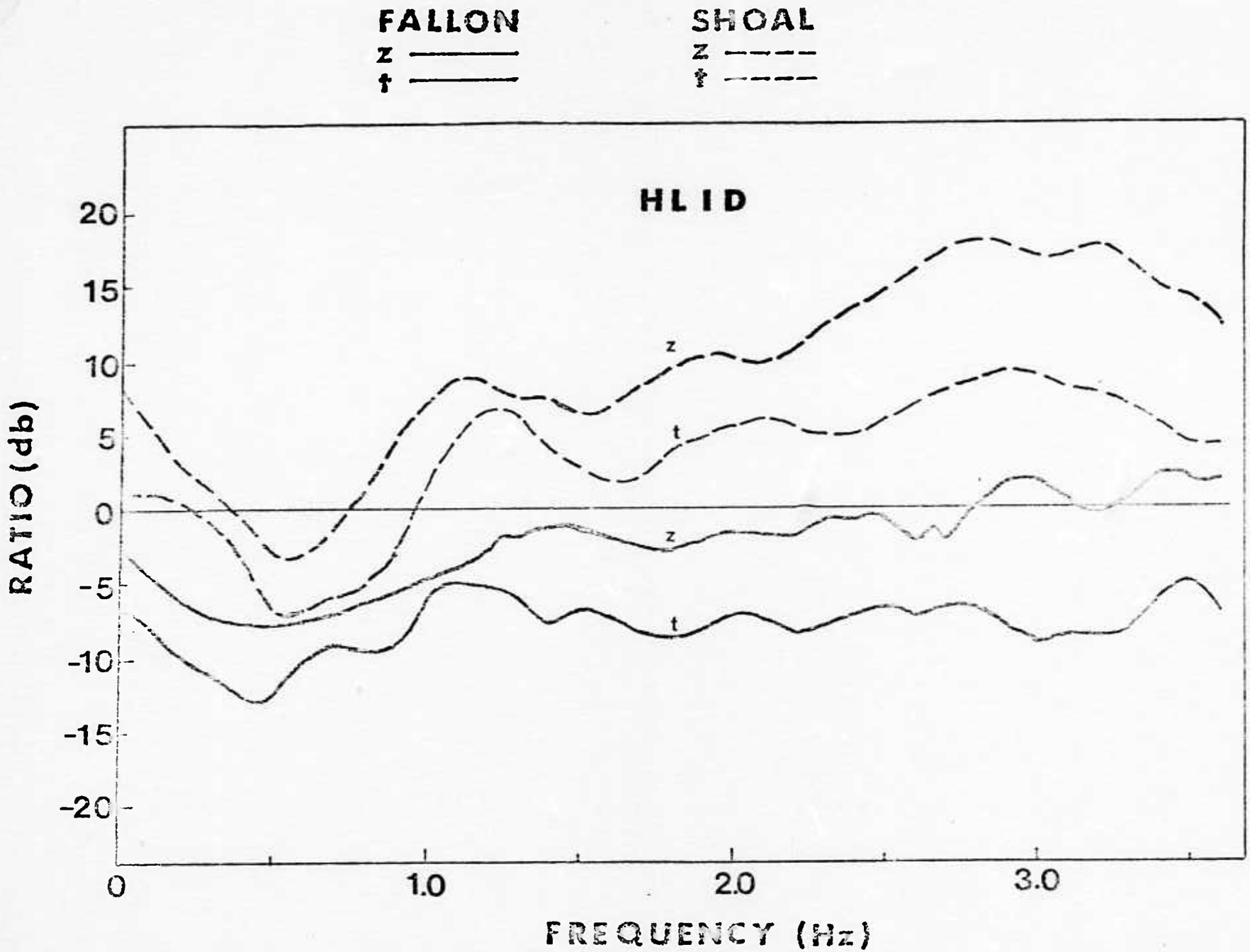

Figure 16. Body wave to surface wave (Lg) spectral ratios from seismoprints.

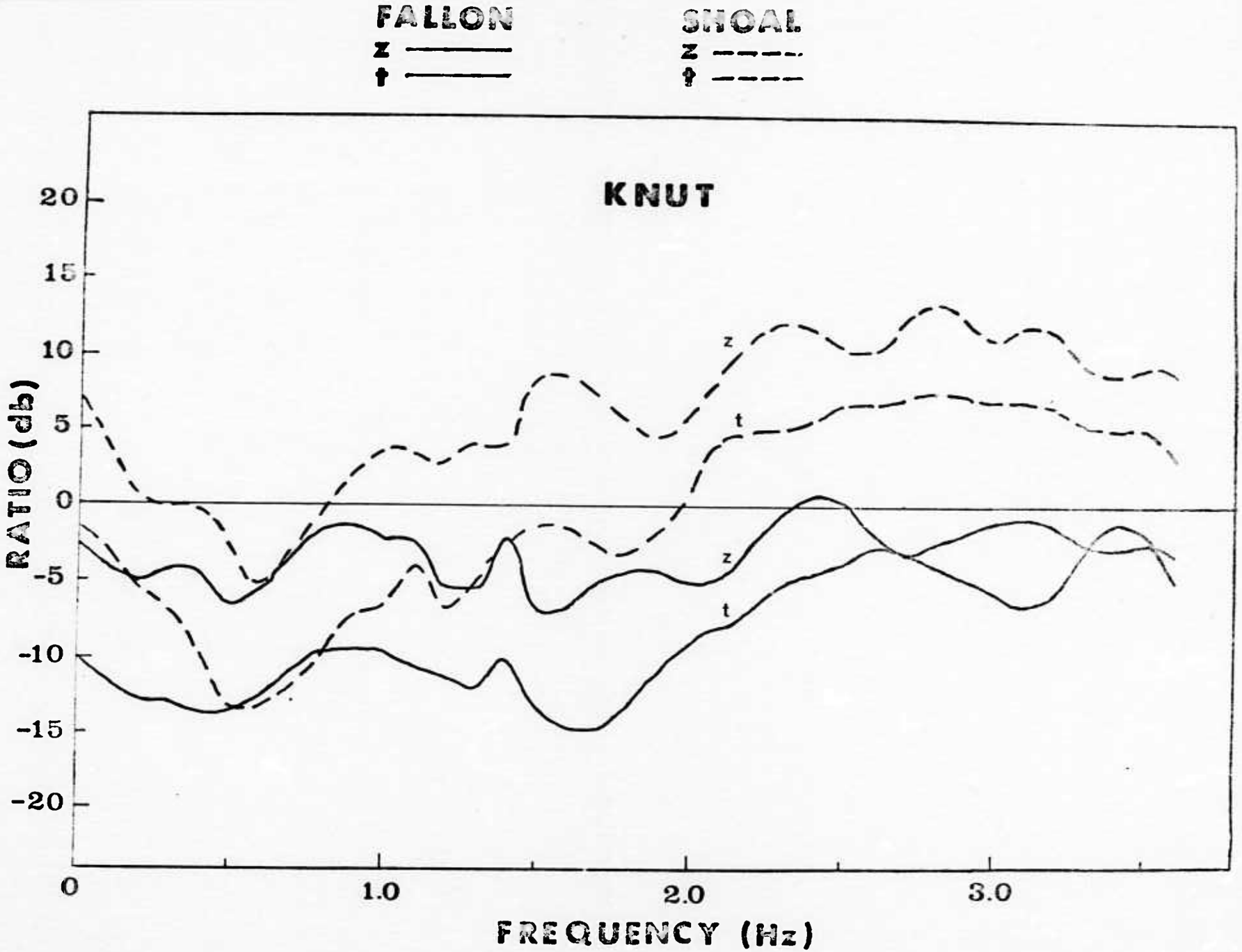

Figure 17. Body wave to surface wave (Lg) spectral ratios from seismoprints.

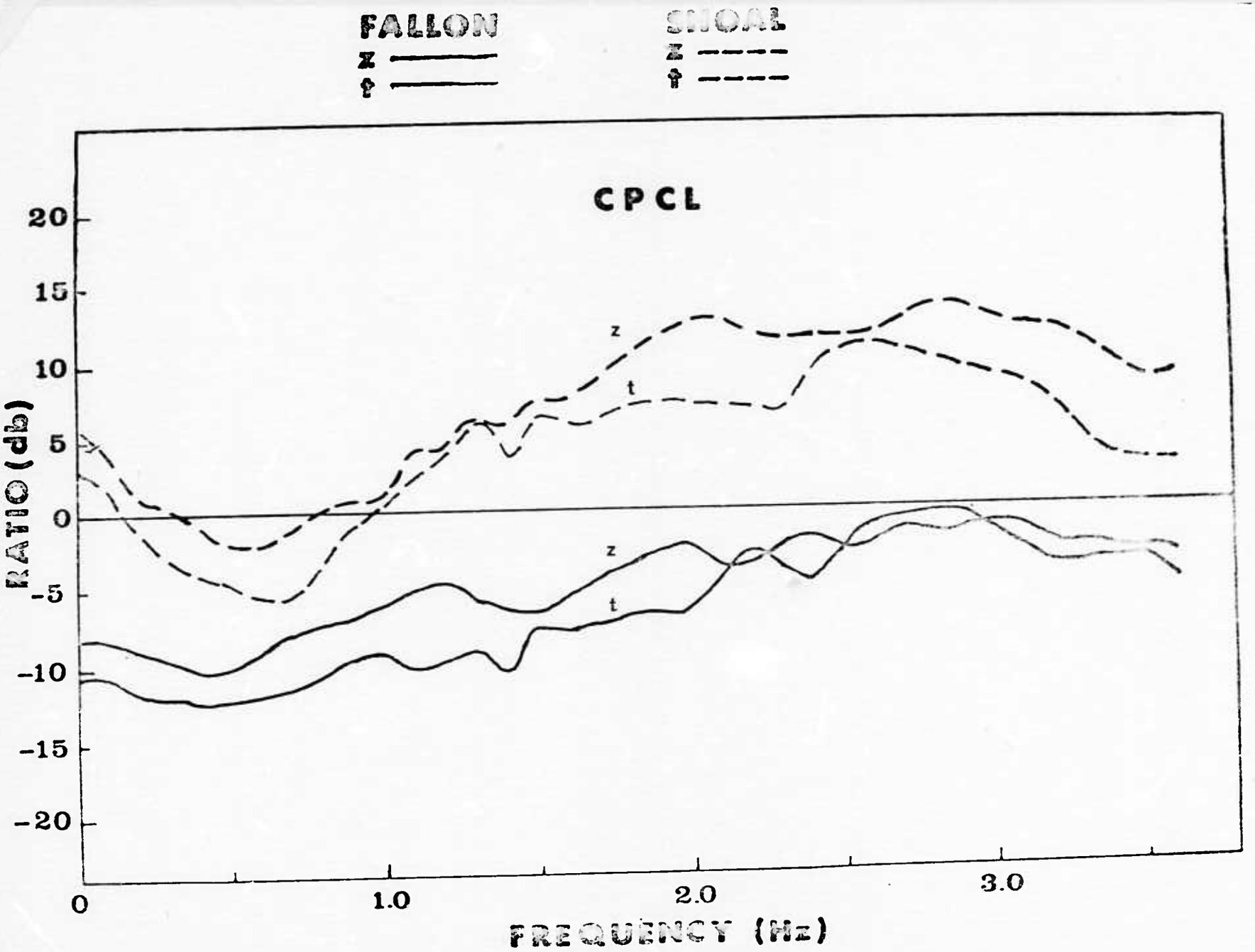

Figure 18. Body wave to surface wave (Lg) spectral ratios from seismoprints.

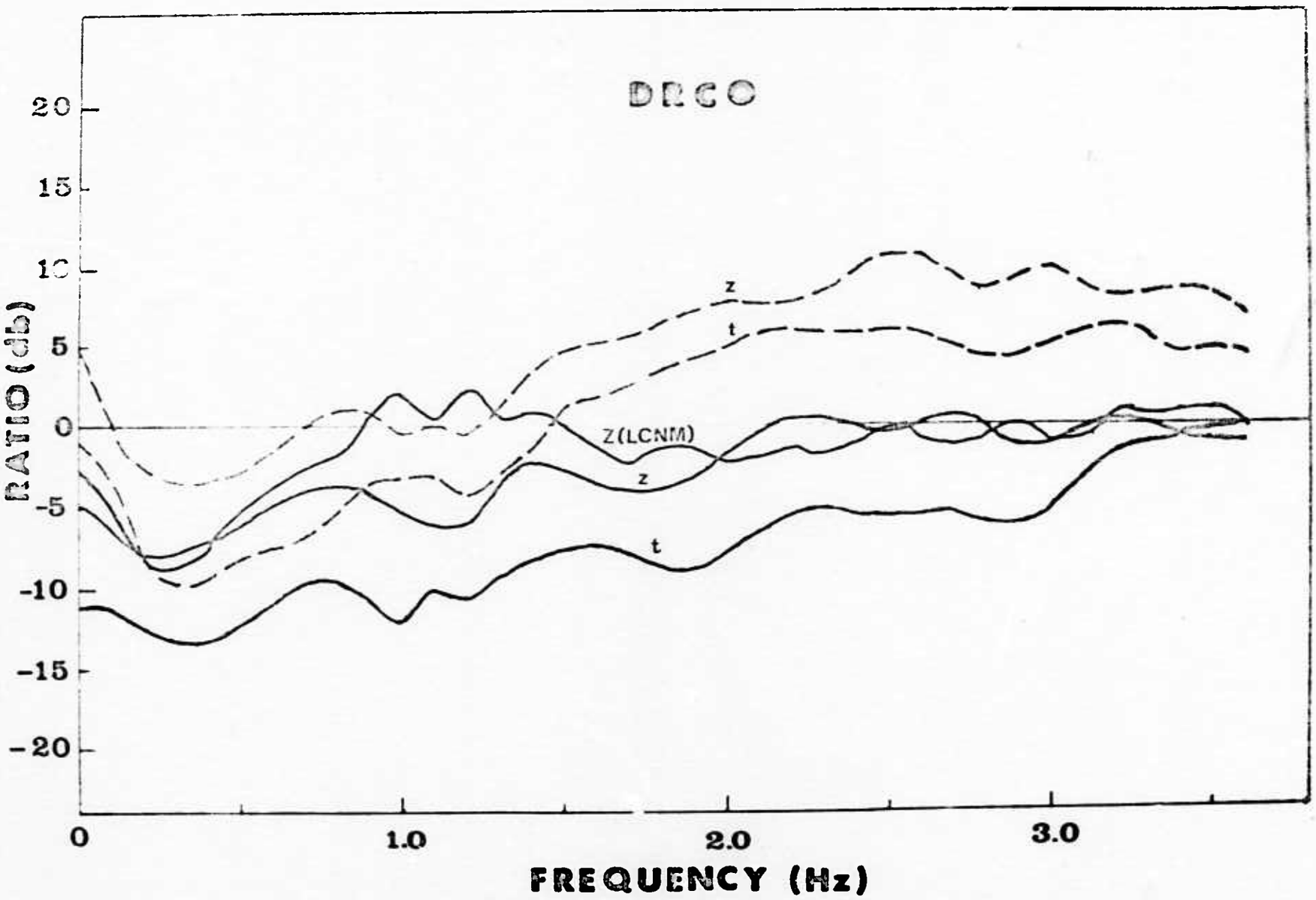

Figure 19. Body wave to surface wave (Lg) spectral ratios from seismoprints.

sufficiently high S/N levels, seismoprint analysis and spectral ratios can be used to distinguish between earthquakes and explosions. It should be noted, however, that attenuation will begin to sap the energy from the high frequencies at larger distances; therefore favorable (high Q) propagation paths to receivers are highly desirable.

Conclusions

1. Using the approaches discussed, the entire seismogram can be used to classify the event, provided the characteristic energy distribution patterns are consistently different for earthquakes and explosions.

2. There appear to be pronounced differences in the energy distribution of short-period waves generated by earthquakes and explosions.

3. The method provides a practical means of extracting discriminant parameters such as Lg/P, S/P, and body wave spectral splitting.

b. Multiple Estimates of Source Parameters From Each Seismogram.

Each separable body or surface-wave phase potentially contains source information (e.g. pP, PcP, PP, S, sS, ScS) but typically only the direct waves are used to obtain source information from spectra such as corner frequency and seismic moment. We have developed a practical procedure for routinely computing spectra of the various phases; it simply consists of keying on standard travel-time curves to define the time windows containing each phase and transforming the arrivals in each such window to obtain the spectral excitation of that phase.

A few examples will illustrate this approach. For the Shoal-Fallon pair spectra of windows that bracketed the P, Pg, and Lg arrivals were computed for several LRSM stations. Figure 20 compares the P-wave spectra at HLID: Shoal exhibits a distinct corner frequency at about 2.5 Hz while Fallon's P-wave spectrum is very irregular with no well-defined corner. Figure 21 compares the Pg spectra for HLID. In this case the observed corner frequency for Shoal is at about 3 Hz whereas that for Fallon is at about 1.7 Hz; this reflects the difference in source dimensions for these events and potentially constitutes a means of identification provided the events have about the same propagation path. Figure 22 shows the results for the Lg portion of the HLID seismograms; no easily identifiable corner frequency is evident and this was found to be typical of other LRSM stations. Evidently the ensemble of higher modes masks or at least subdues any manifestation of source dimensions through corner frequencies.

Figure 23 compares the P-wave spectra for KNUT and again there is a distinct corner for Shoal but not Fallon. Figure 24 shows the results for Pg at KNUT; the corner for Shoal is again very clear at about 3 Hz but scalloping prevents an unambiguous selection for Fallon. Figure 25

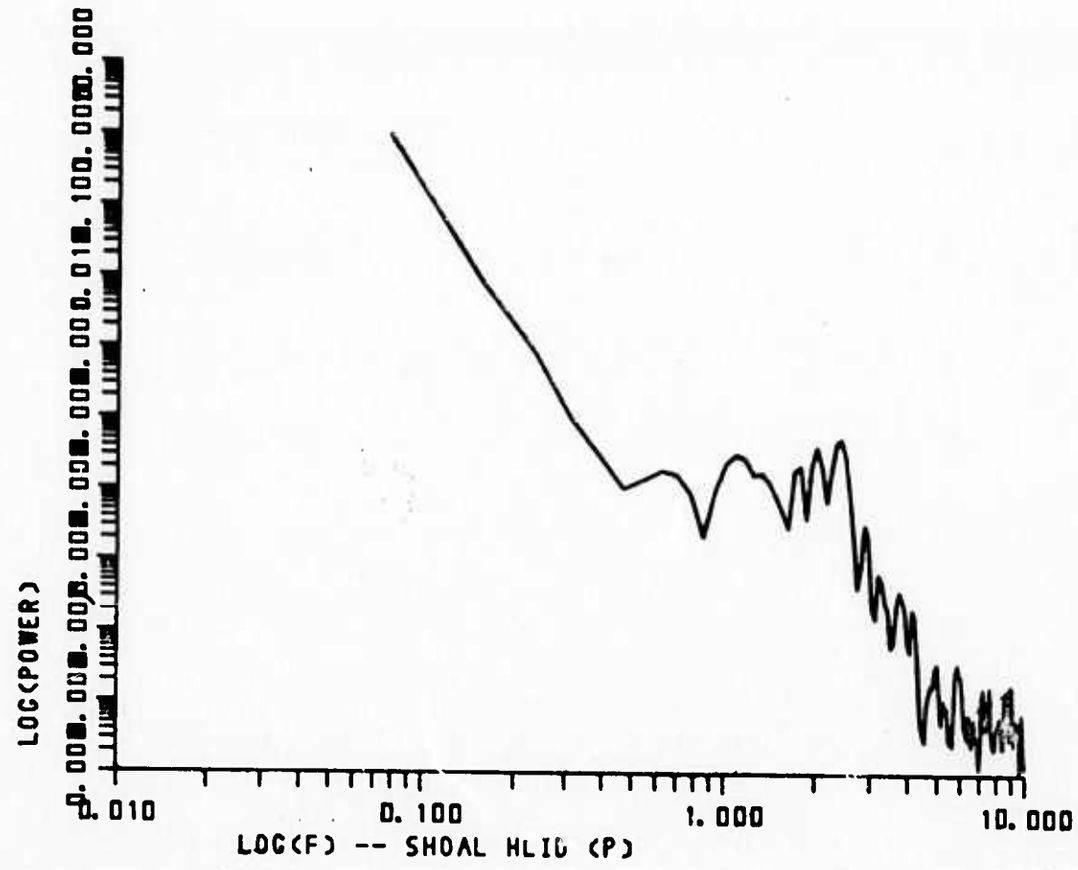
LOG(POWER)
0.010
0.100
1.000
10.000
LOG(F) -- SHOAL HLID (P)

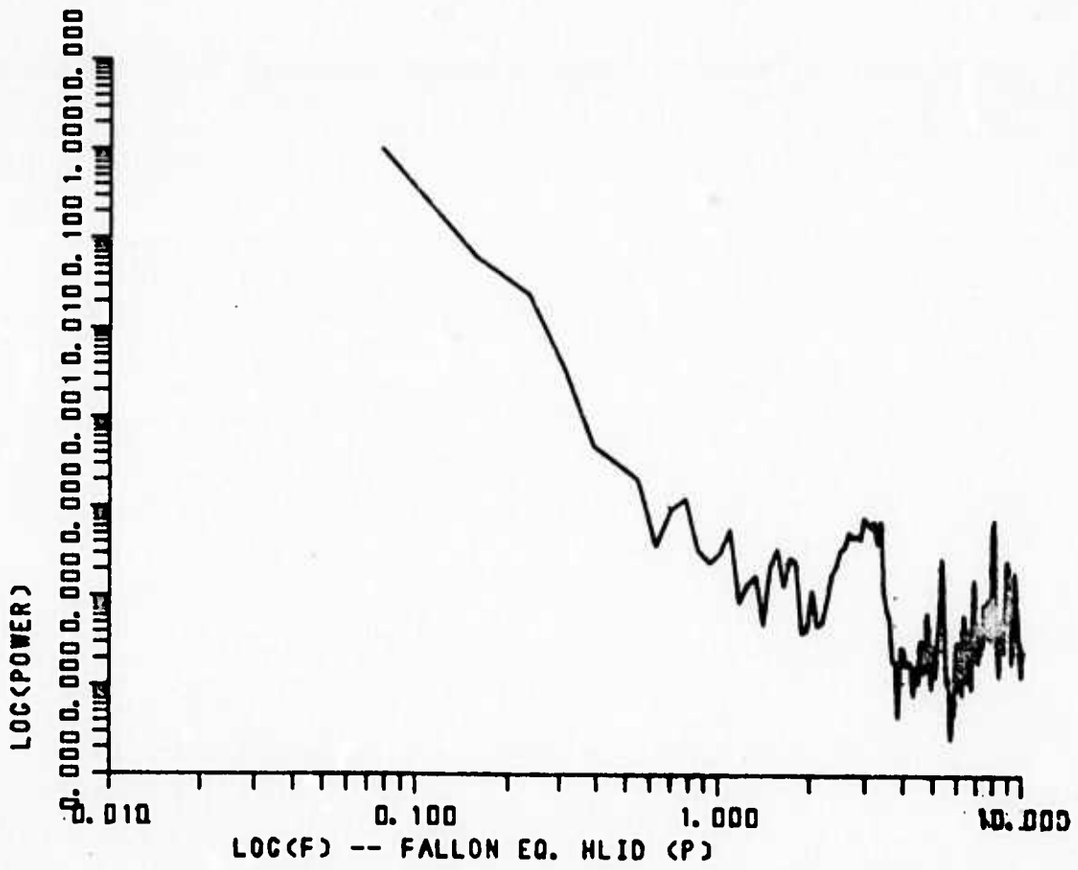
LOG(POWER)
0.010
0.100
1.000
10.000
LOG(F) -- FALLON EQ. HLID (P)

Figure 20.

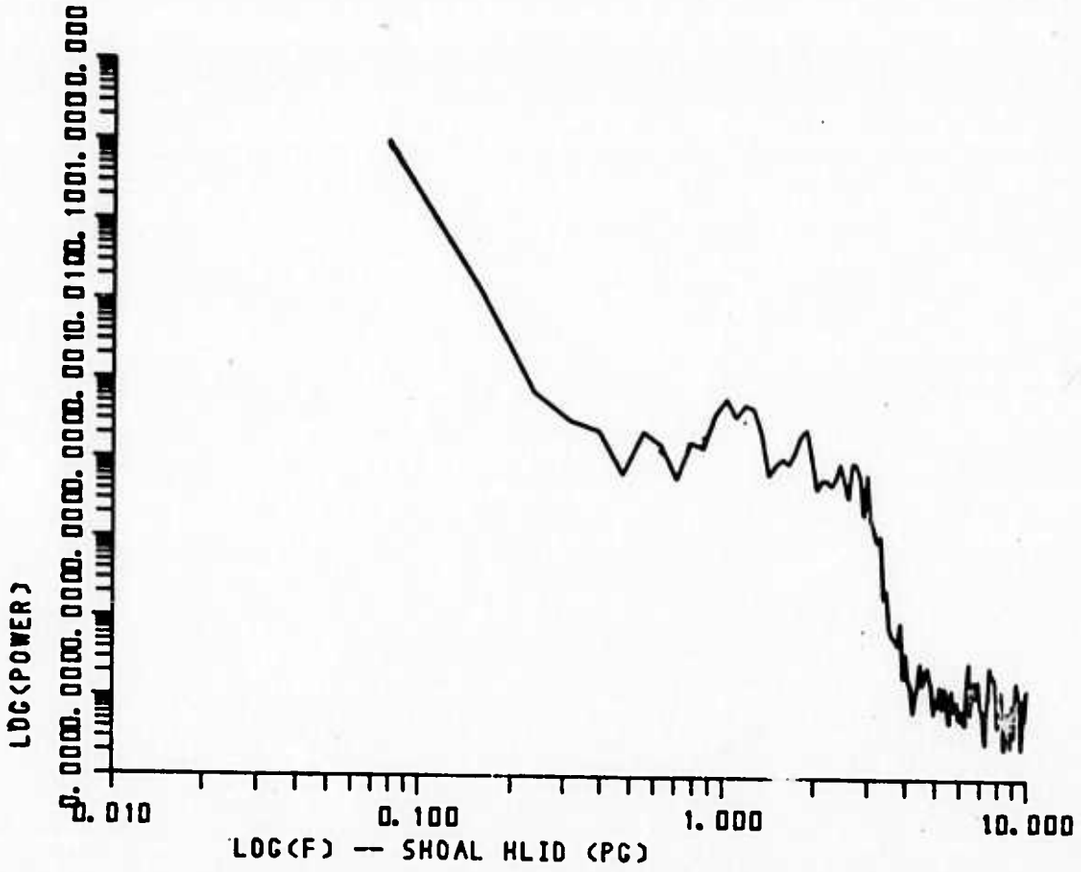
LOG(POWER)
0.010
0.100
1.000
10.000
LOG(F) -- SHOAL HLID (PC)

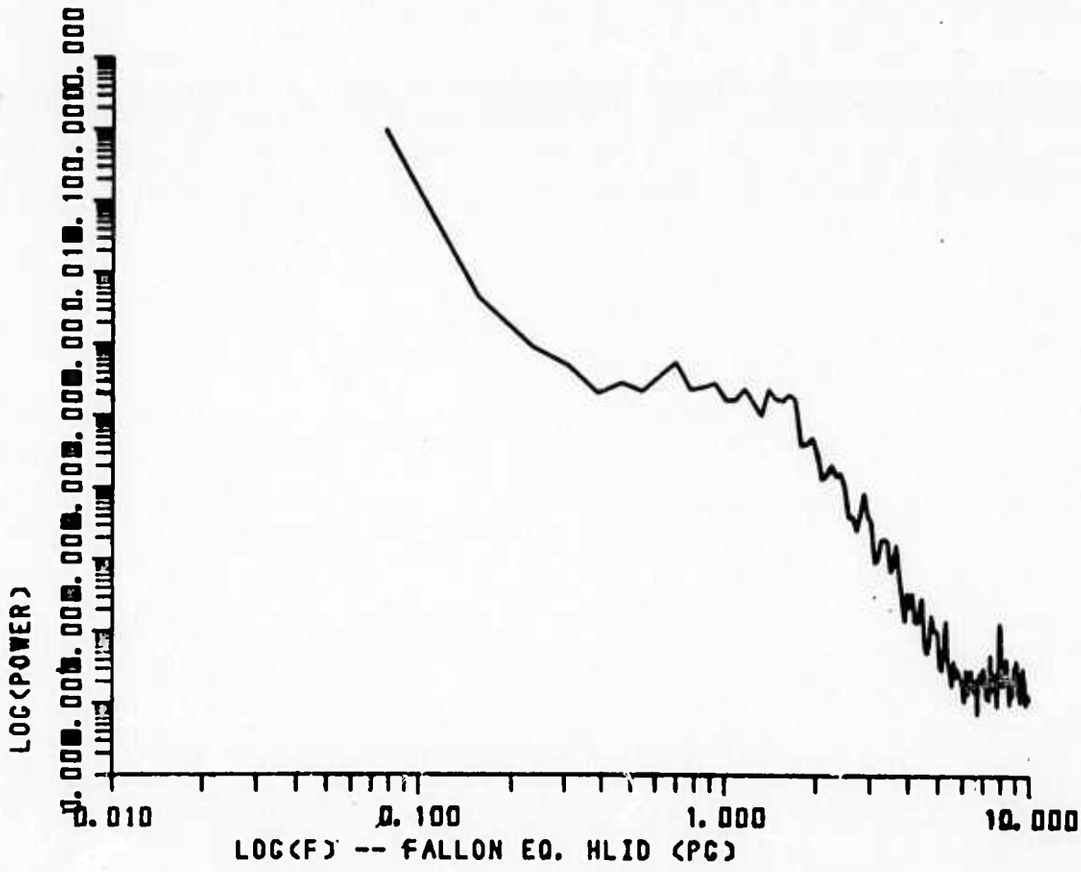
LOG(POWER)
0.010
0.100
1.000
10.000
LOG(F) -- FALLON EQ. HLID (PC)

Figure 21.

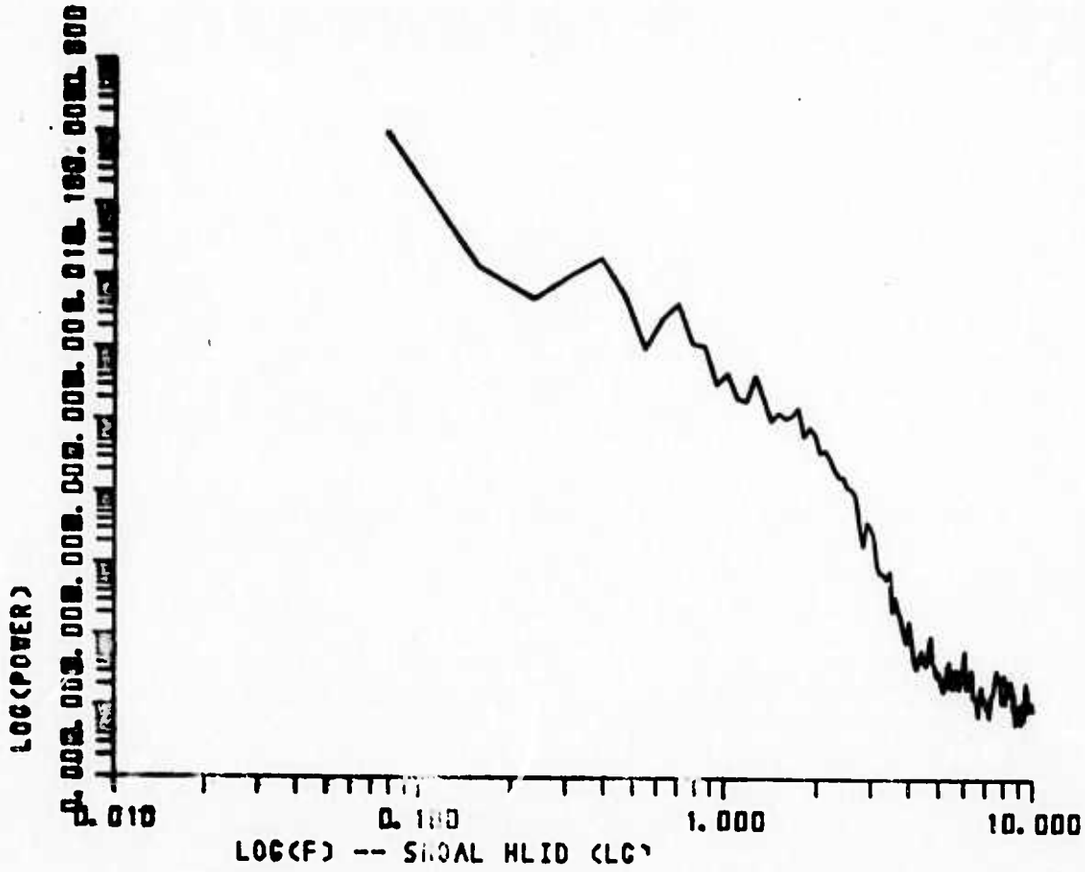
LOG(POWER)
0.010
0.100
1.000
10.000
LOG(F) -- SIGNAL HLID (LC)

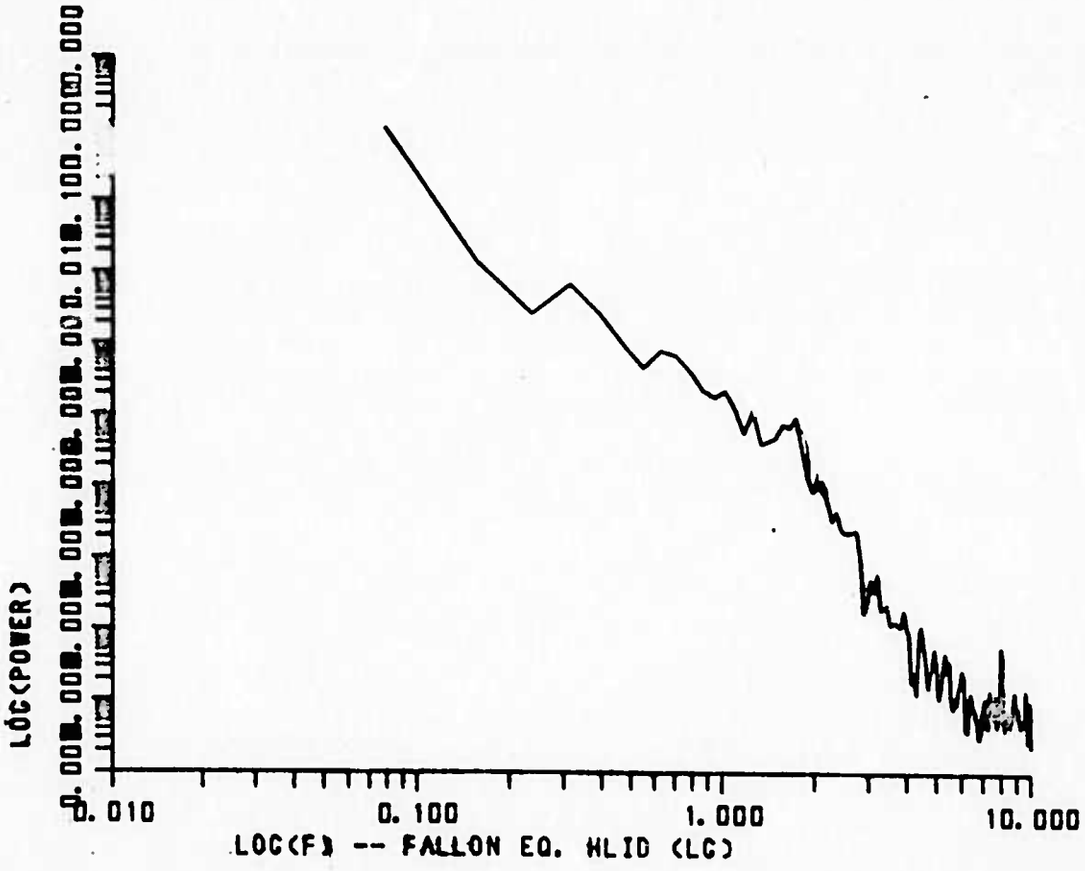
LOG(POWER)
0.010
0.100
1.000
10.000
LOG(F) -- FALLON EQ. HLID (LC)

Figure 22.

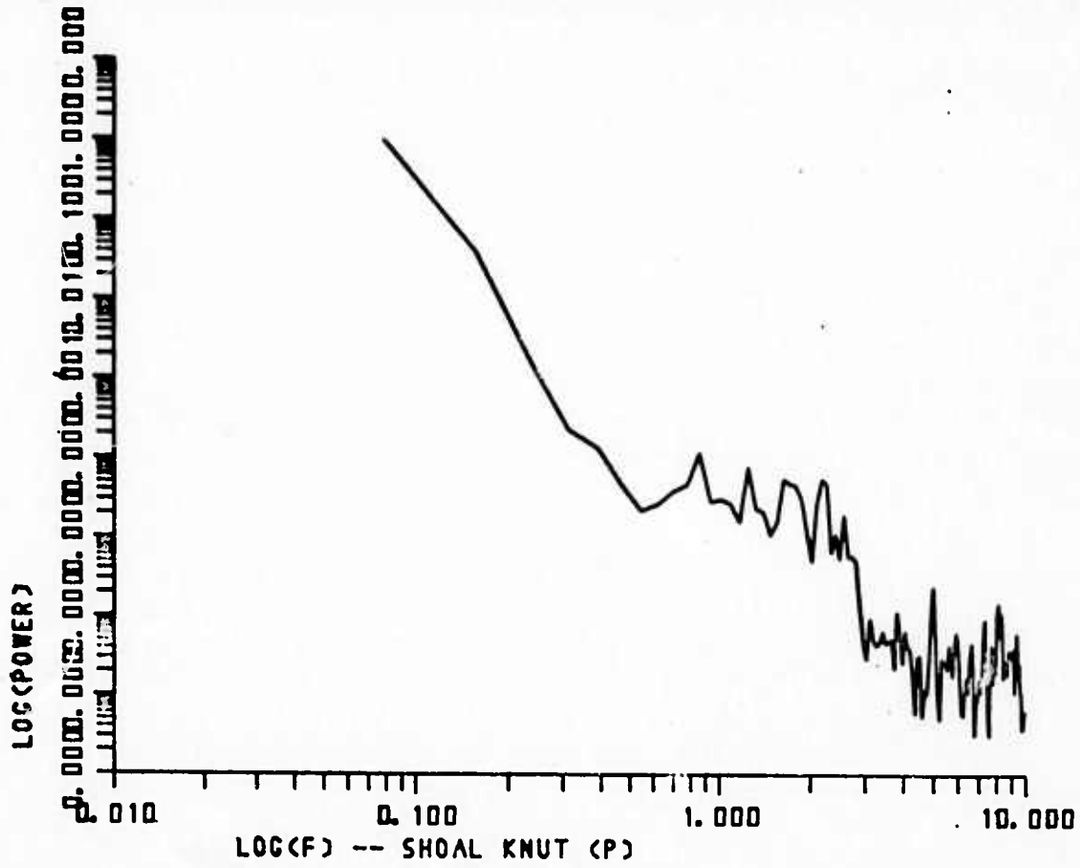
LOG(POWER)
0.010
0.100
1.000
10.000
LOG(F) -- SHOAL KNUT (P)

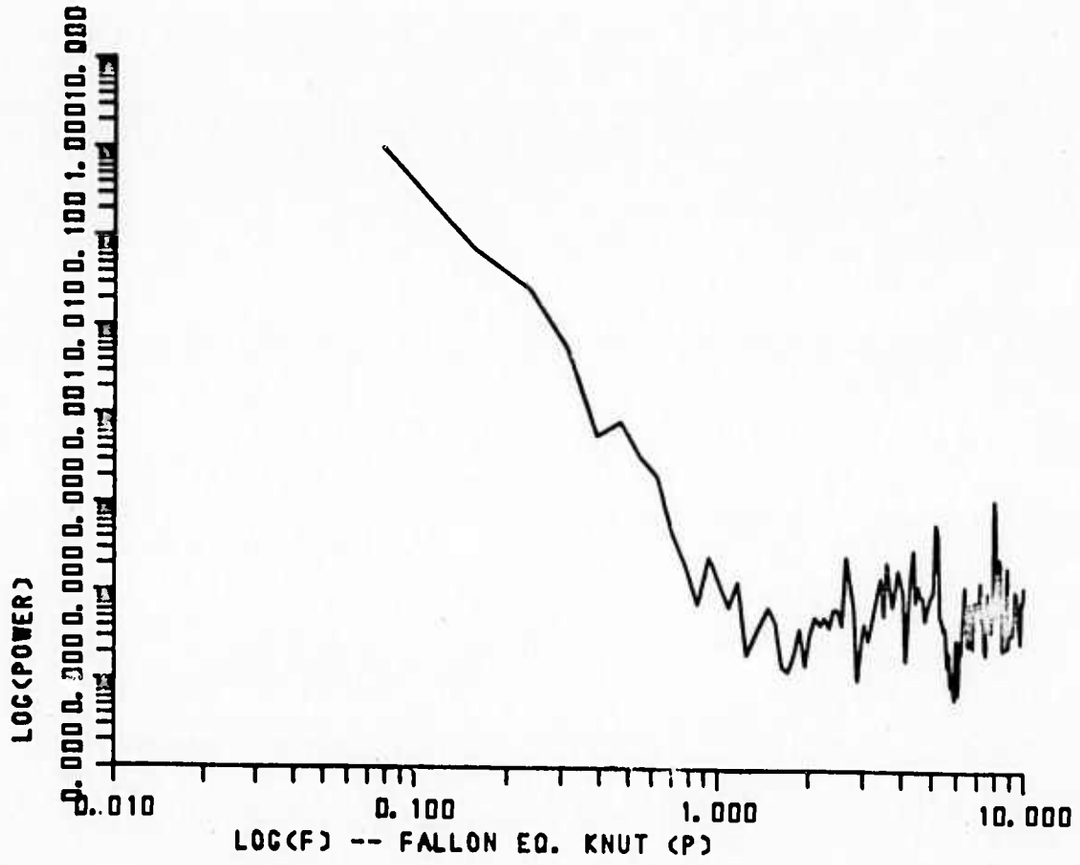
LOG(POWER)
0.010
0.100
1.000
10.000
LOG(F) -- FALLON EQ. KNUT (P)

Figure 23.

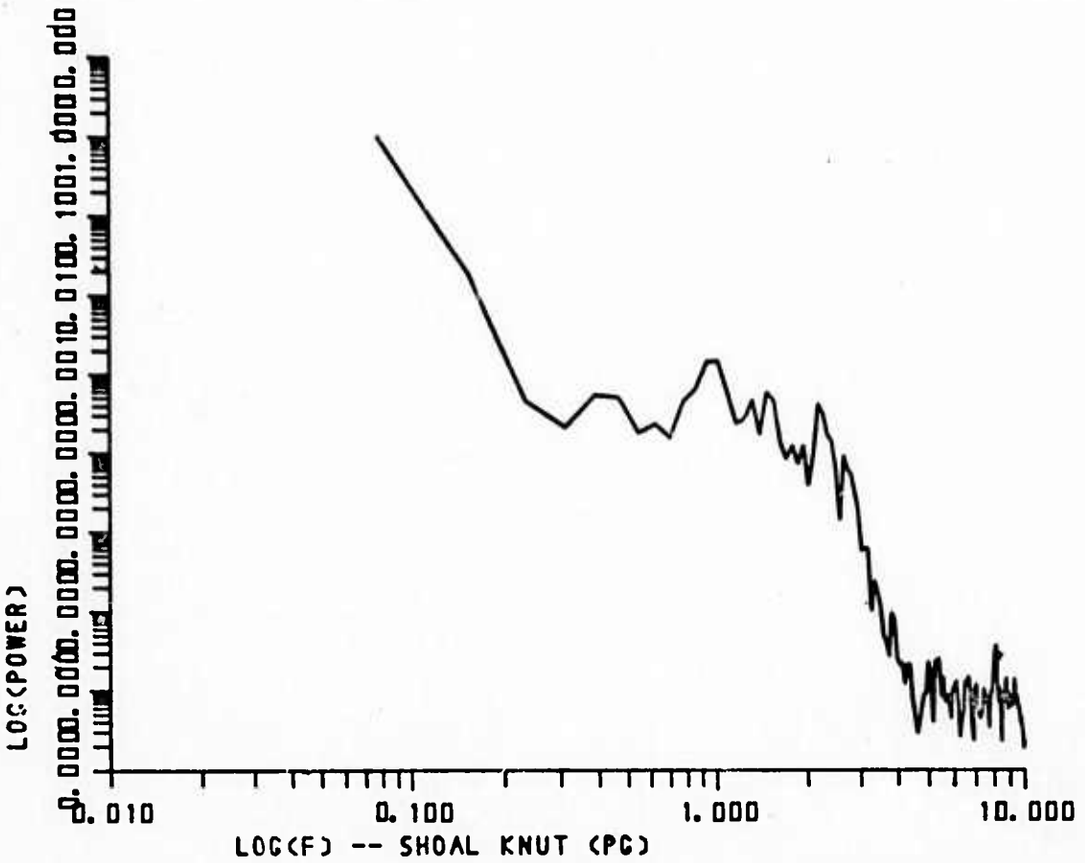
LOG(POWER)
0.010
0.100
1.000
10.000
LOG(F) -- SHOAL KNUT (PG)

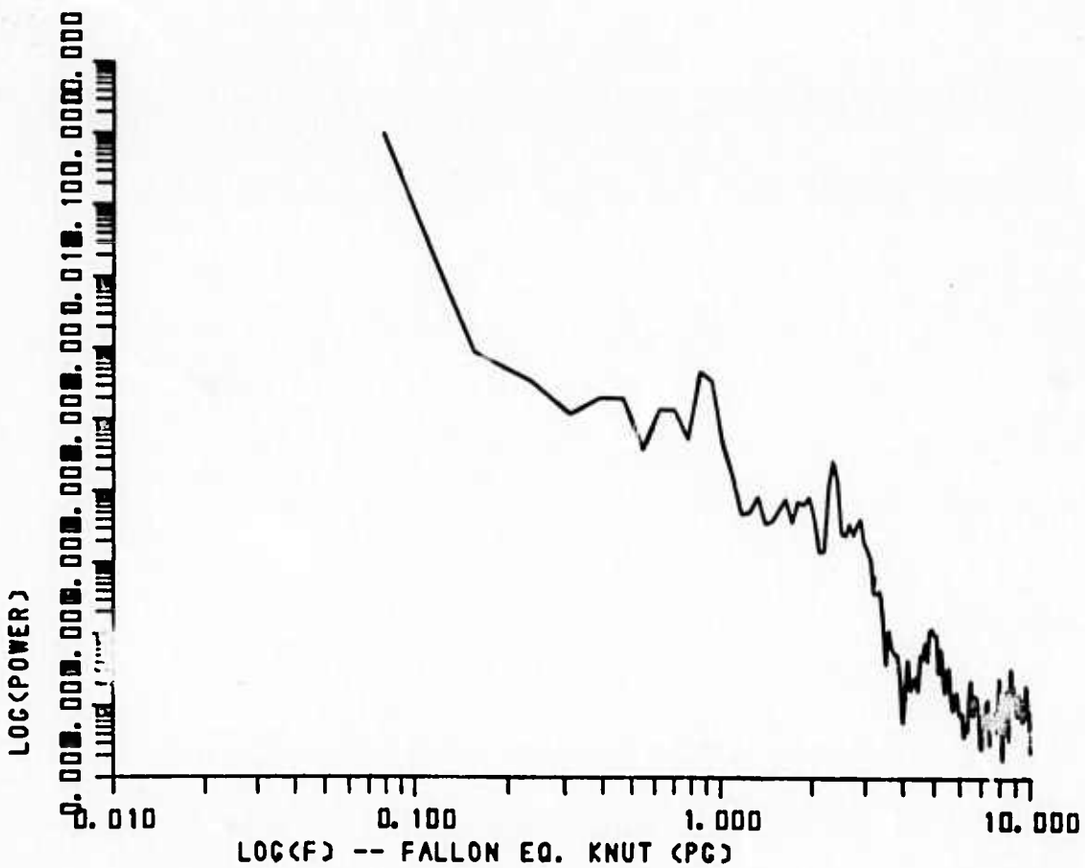
LOG(POWER)
0.010
0.100
1.000
10.000
LOG(F) -- FALLON EQ. KNUT (PG)

Figure 24.

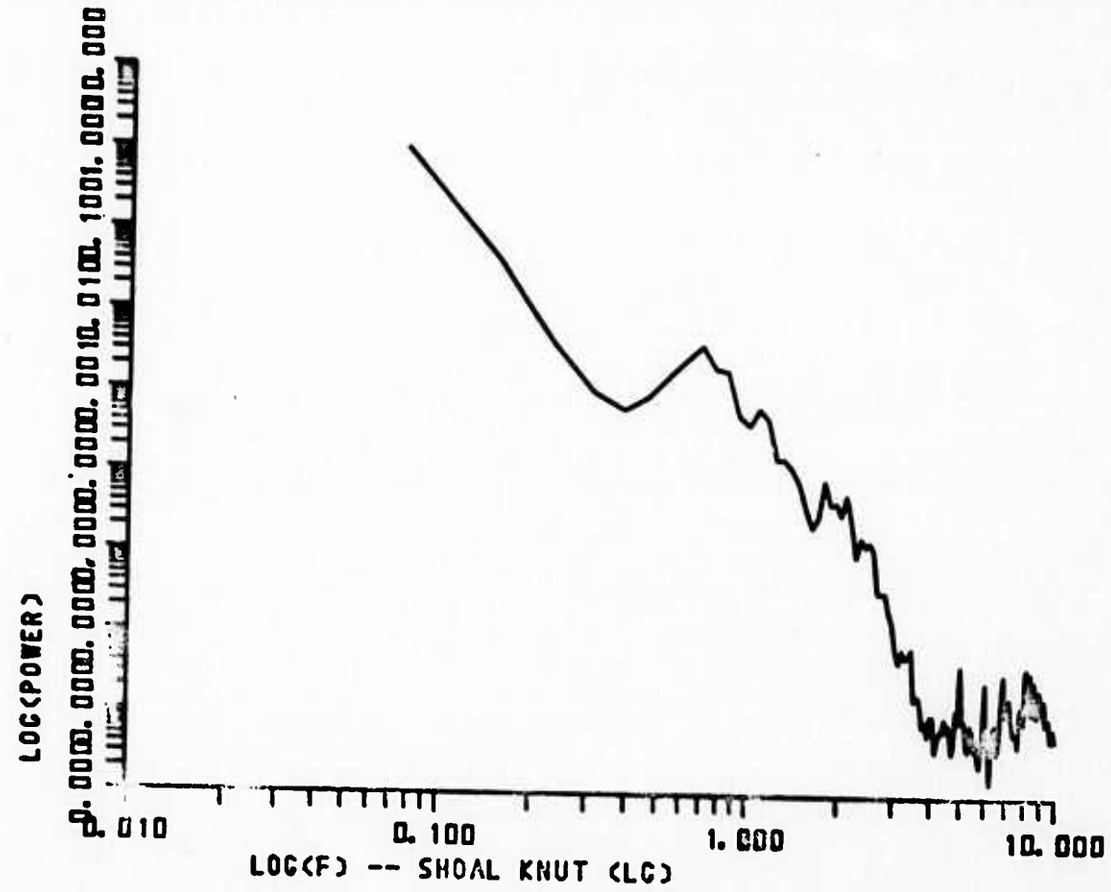
LOG(POWER)
0.010
0.100
1.000
10.000
LOG(F) -- SHOAL KNUT (LG)

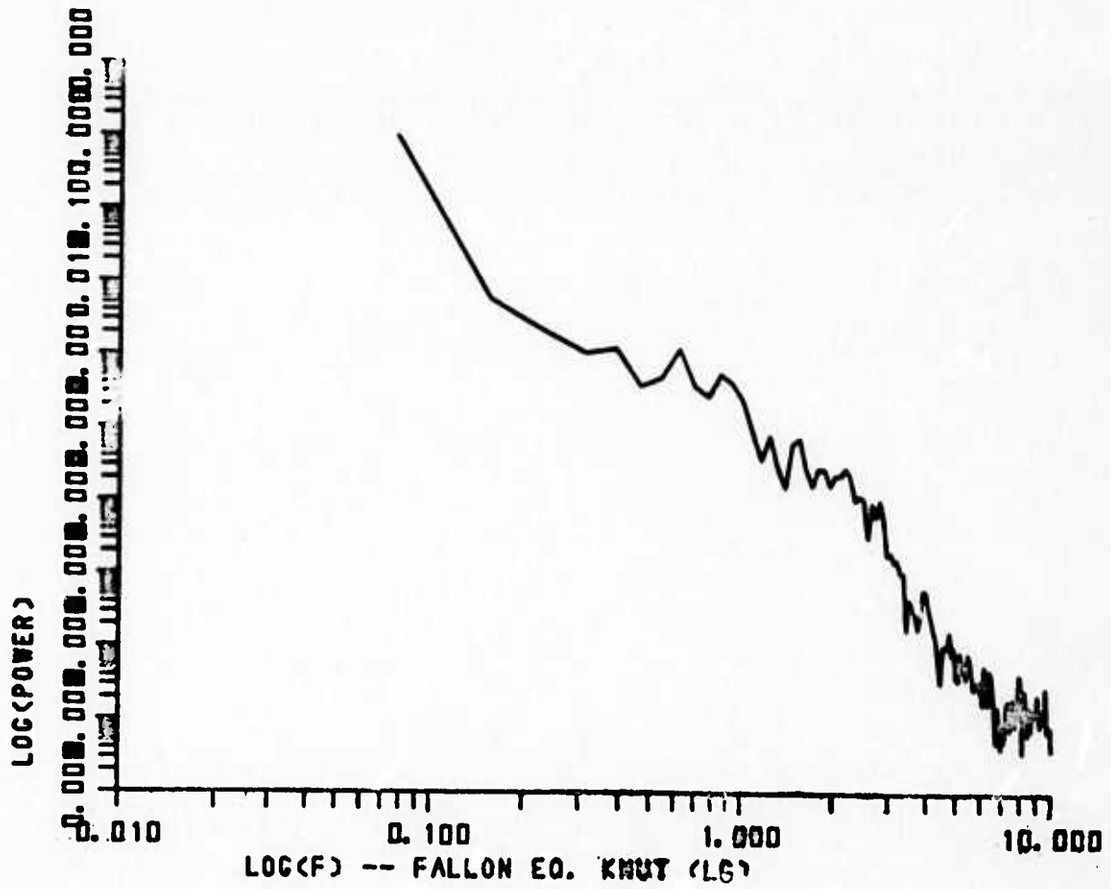
LOG(POWER)
0.010
0.100
1.000
10.000
LOG(F) -- FALLON EQ. KNUT (LG)

Figure 25.

shows the results for Lg at KNUT and no corner frequency is evident.

Figure 26 compares the P-wave spectra for LCNM at a distance of over 1000 km. In this case apparent corner frequencies are present at around 1 Hz but no appreciable difference in the corner frequencies can be discerned; this is primarily the effect of path attenuation stripping away the high frequency corner-frequency information at around 3 Hz and producing a similarly shaped spectrum for both events. Figure 27 compares the Pg spectra at LCNM; in this case the apparent Shoal corner frequency is at about 1.7 Hz while that of Fallon is at about 1 Hz. Thus, the corner frequency distinction is still discernable but not to the same degree as at the closer stations. Figure 28 compares the Lg spectra at LCNM. As before, no corner frequency information can be inferred.

Thus it appears that at regional distances the Pg portion of the seismograms contains the most diagnostic information on source dimensions and that the Lg portion contains essentially none. It should also be noted that estimates of corner frequencies of different arrivals can also be obtained directly from the seismoprint displays such as those in Figures 11-14.

An example of multiple phase spectral estimates for long-period teleseismic recordings is given by results for the SCP seismograms shown in Figure 29 for an earthquake in Paraguay on 13 January 1968 at a depth of 192 km; the epicentral distance is 7407 km. Figures 30 and 31 give the P and pP spectra obtained by the "automated" method of selecting time windows. The apparent corner frequencies agree approximately (at about .10 Hz) with the pP perhaps shifted slightly toward a lower value. Figures 32

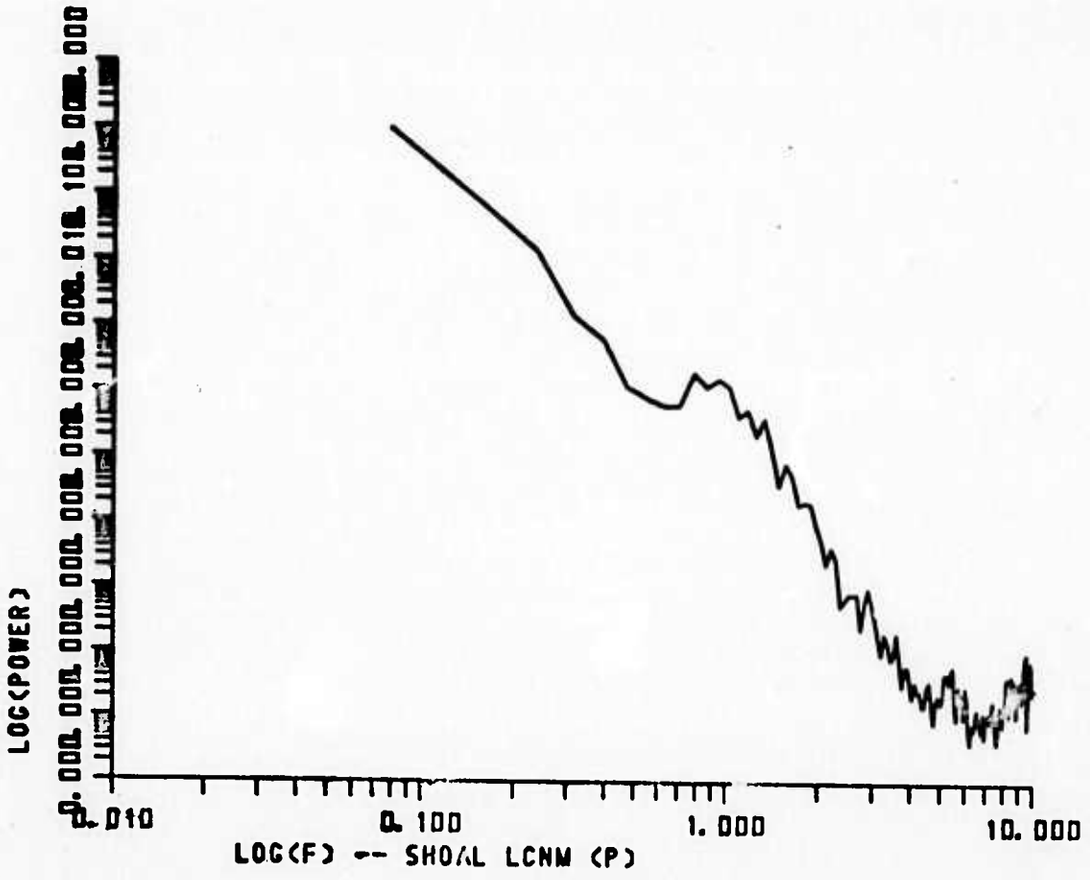
LOG(POWER)
0.010
0.100
1.000
10.000
LOG(F) -- SHOAL LCHM (P)

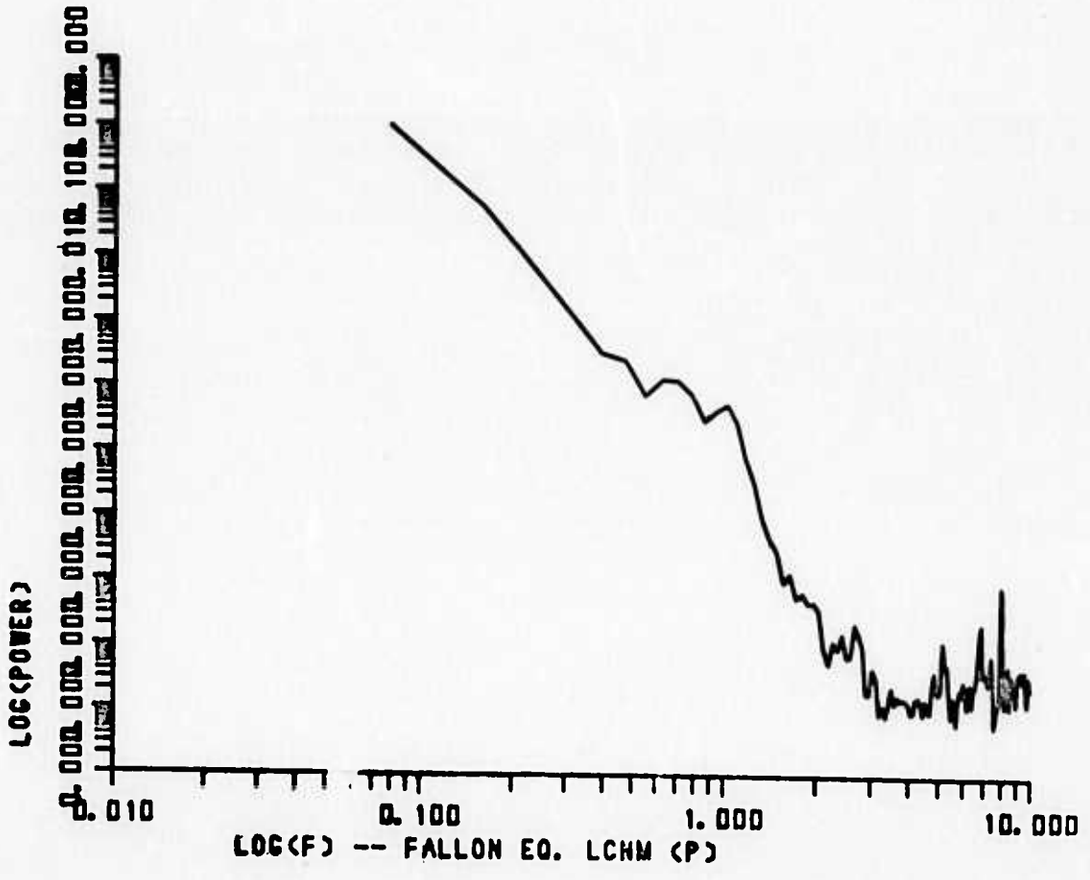
LOG(POWER)
0.010
0.100
1.000
10.000
LOG(F) -- FALLON EQ. LCHM (P)

Figure 26.

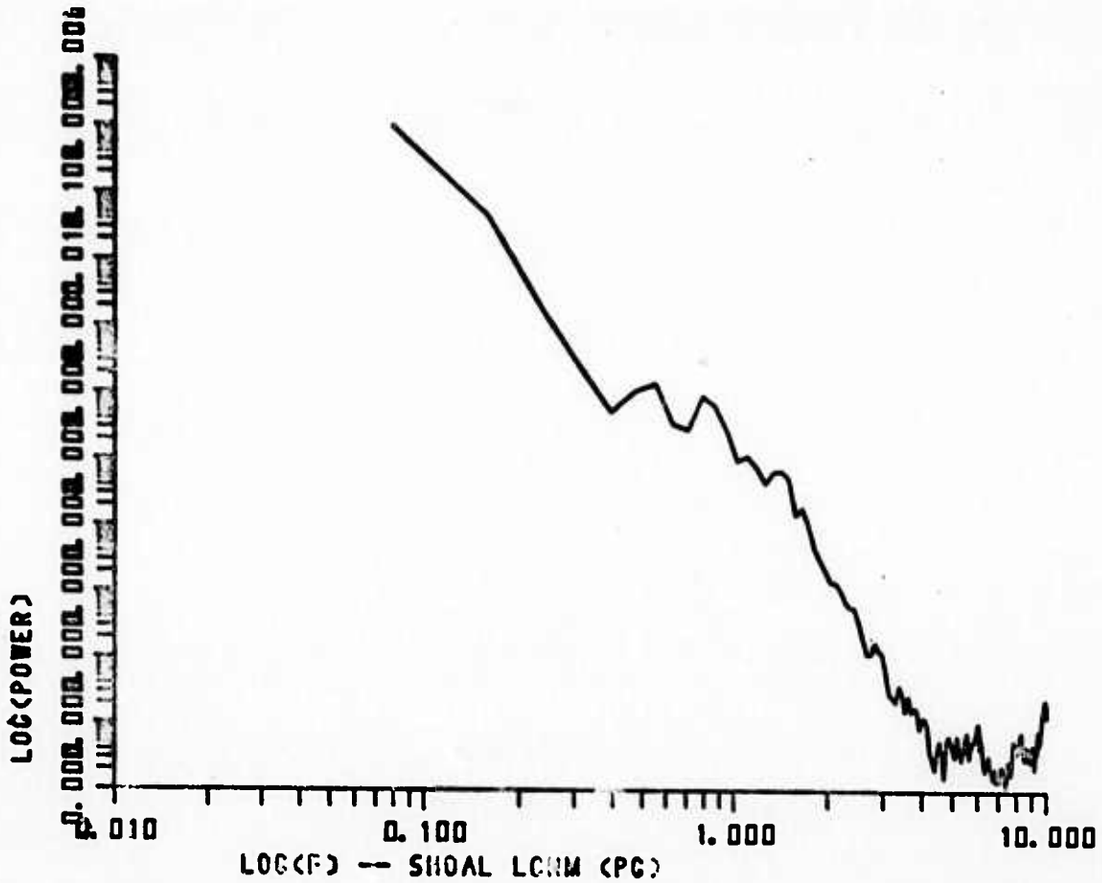
LOG(POWER)
0.010
0.100
1.000
10.000
LOG(F) -- SHOAL LCNM (PG)

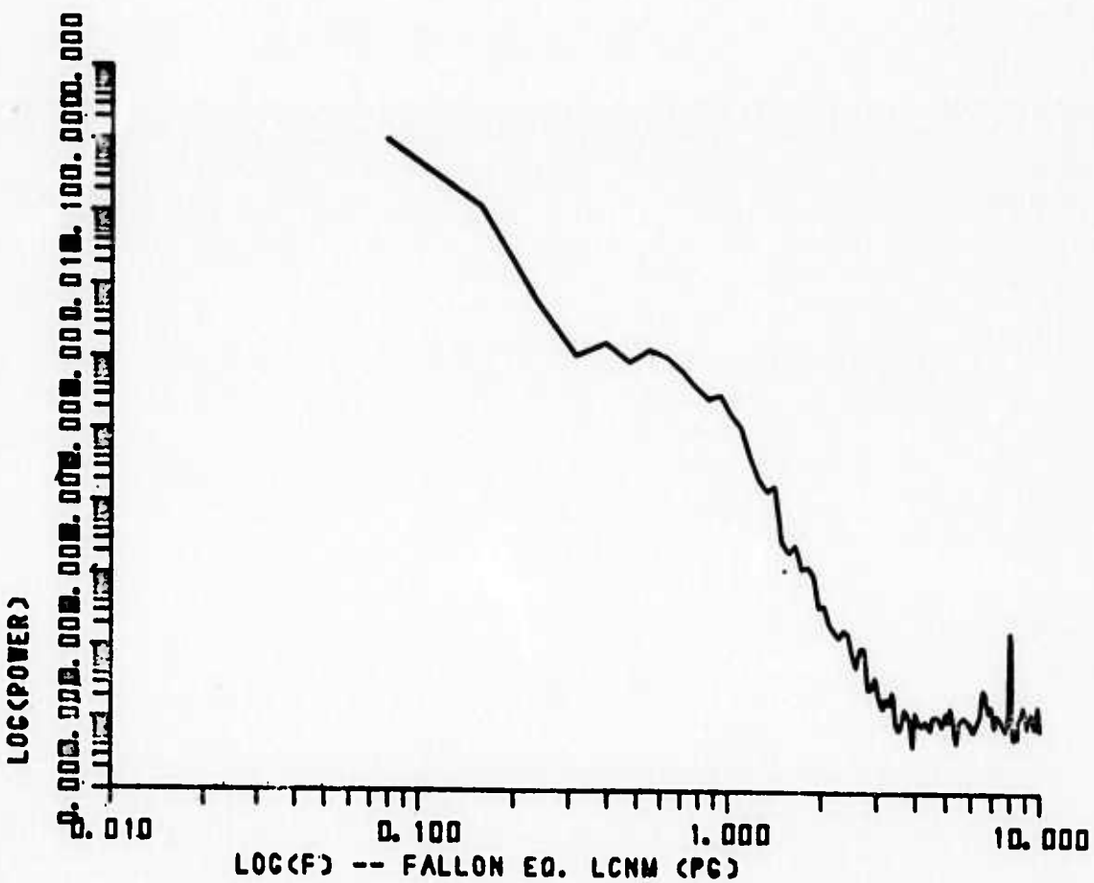
LOG(POWER)
0.010
0.100
1.000
10.000
LOG(F) -- FALLON EQ. LCNM (PG)

Figure 27.

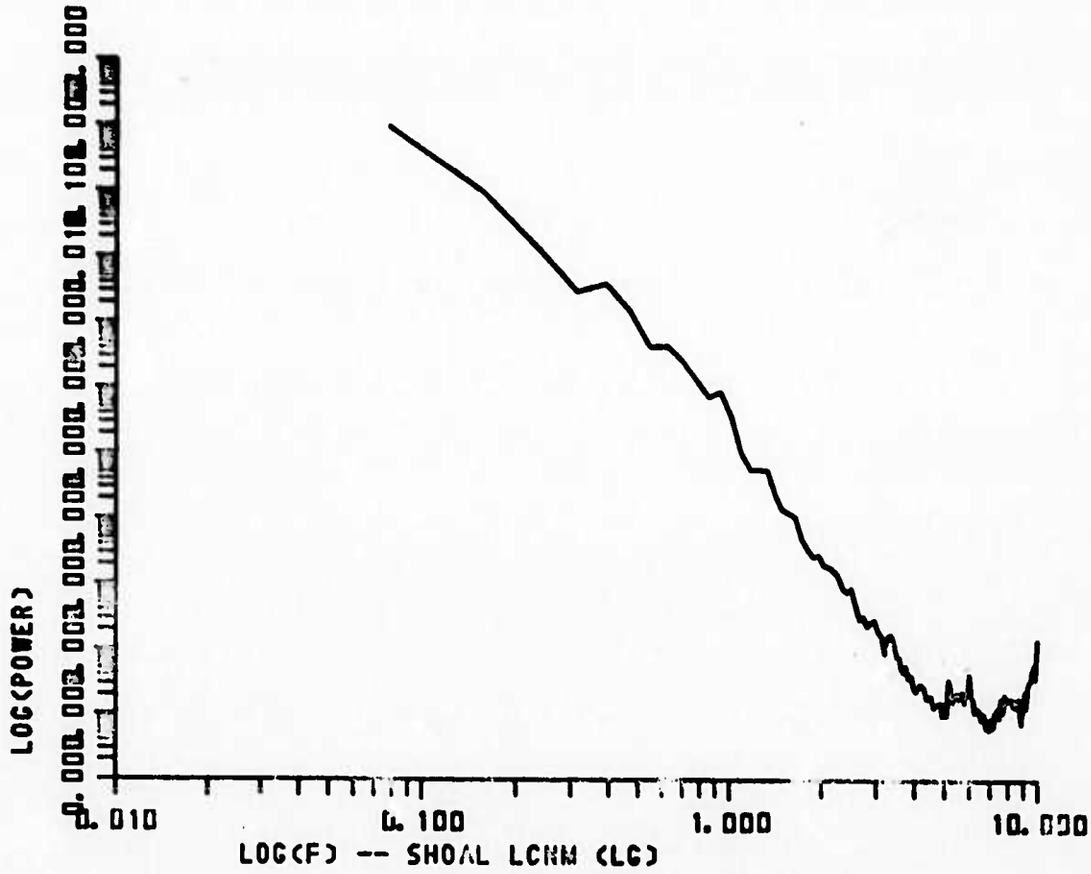
LOG(POWER)
0.010
0.100
1.000
10.000
LOG(F) -- SHOAL LCNM (LC)

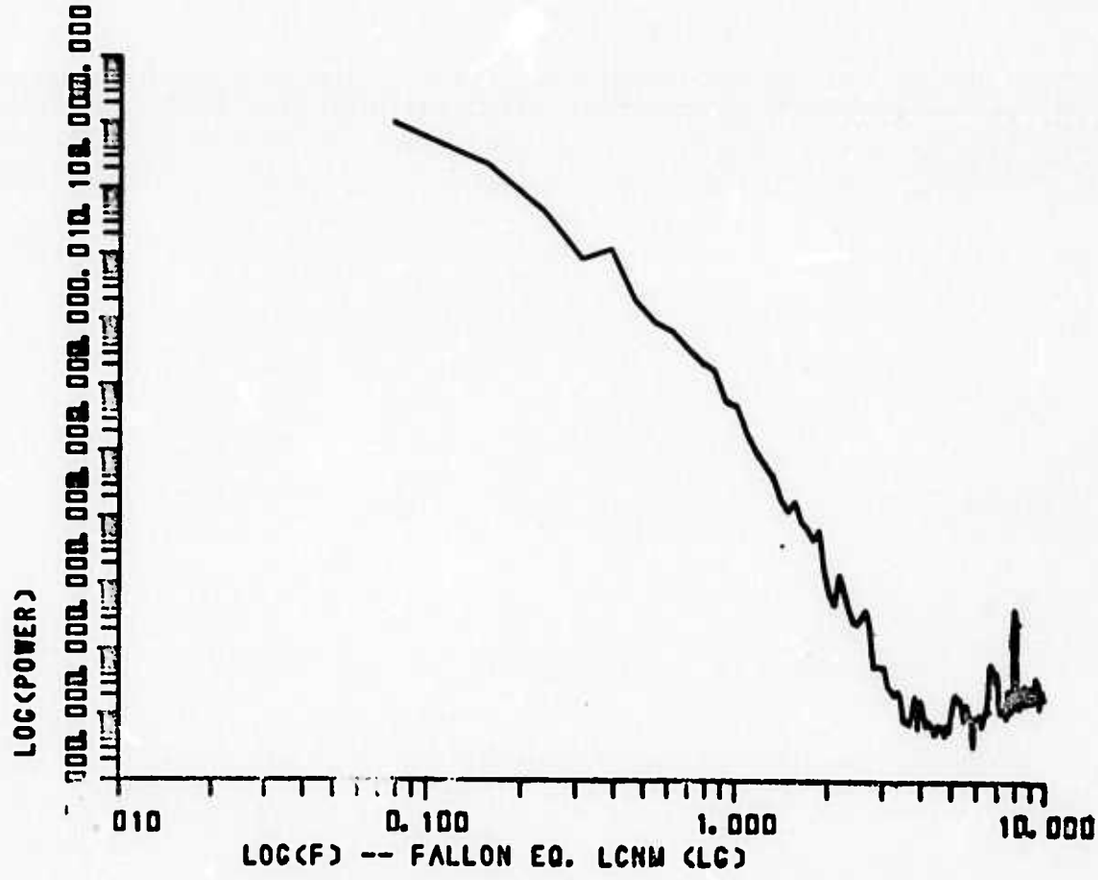
LOG(POWER)
010
0.100
1.000
10.000
LOG(F) -- FALLON EQ. LCNM (LC)

Figure 28.

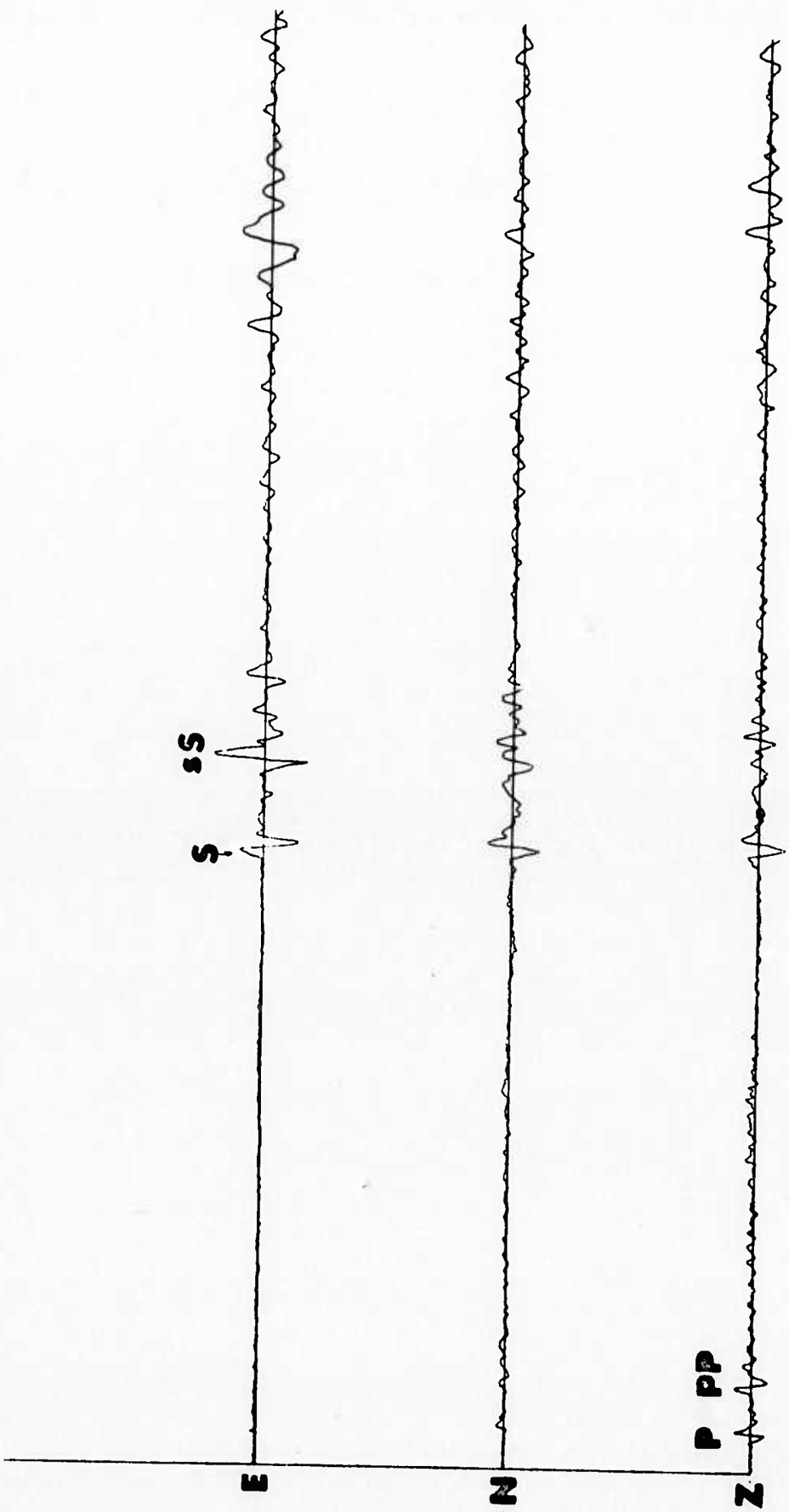

Figure 29.

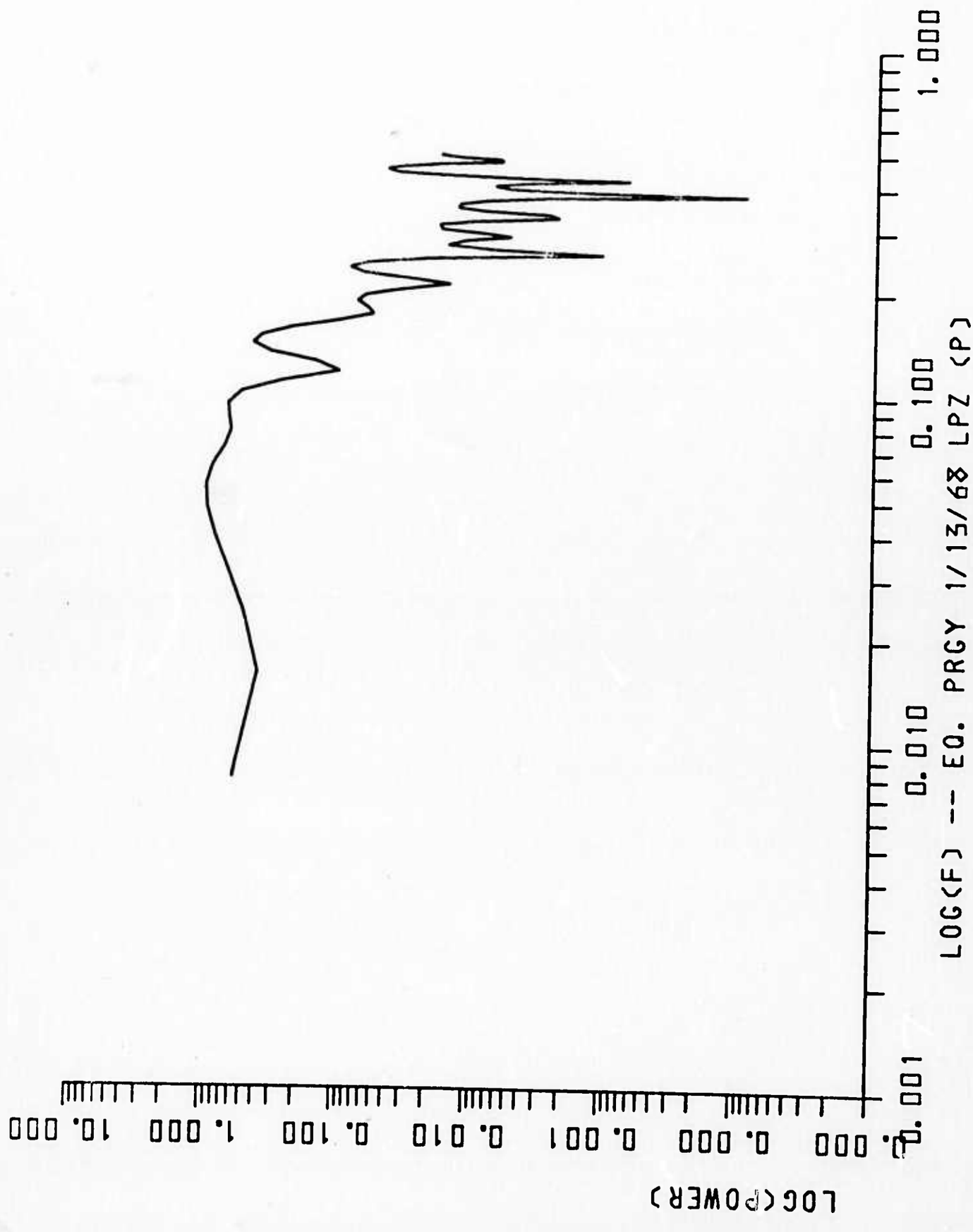
LOG(POWER)
0.000
0.001
0.010
0.100
1.000
10.000
LOG(F) -- EQ. PRGY 1/13/68 LPZ (P)
0.001
0.010
0.100
1.000

Figure 30.

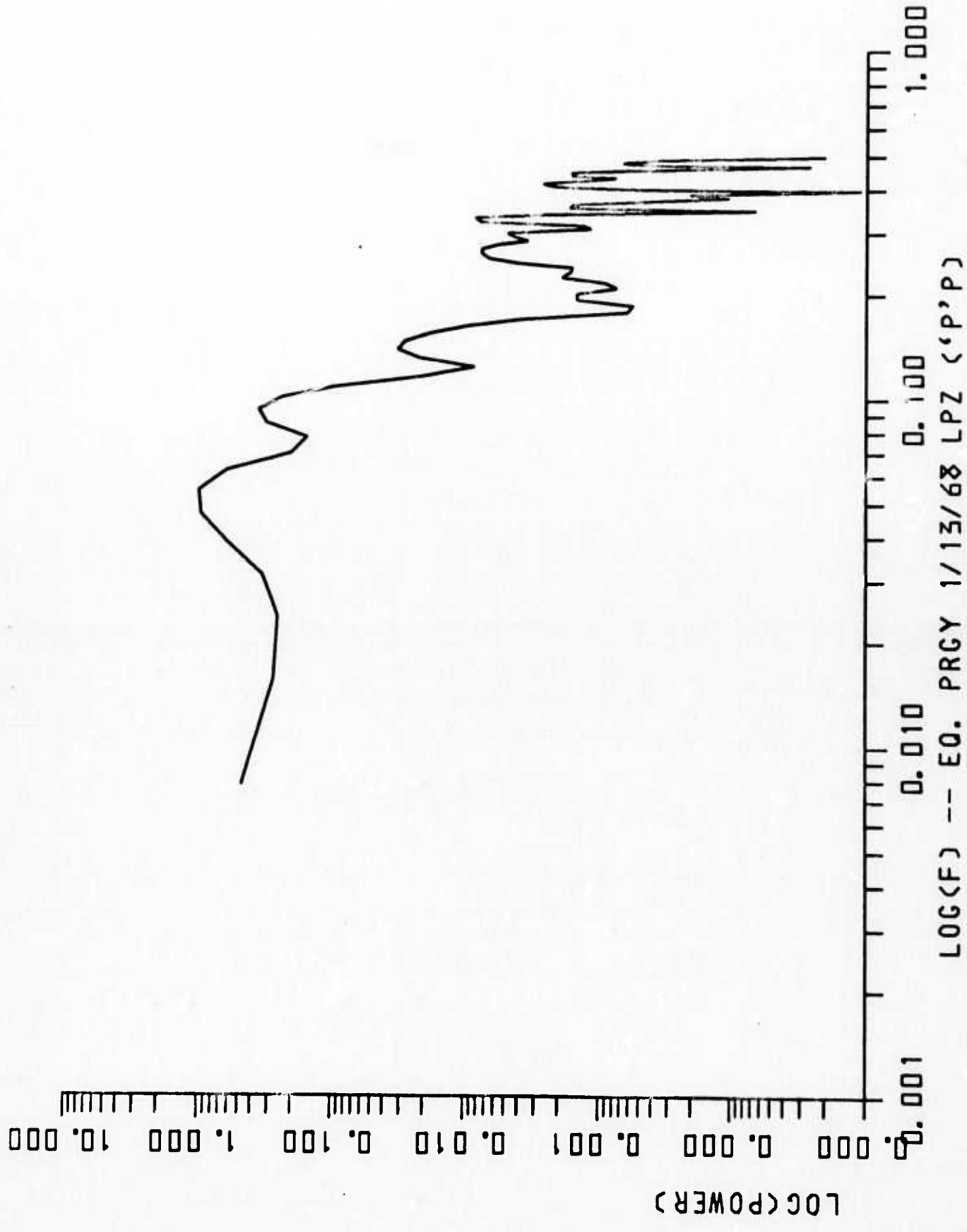
LOG(POWER)
0.000
0.000
0.001
0.010
0.100
1.000
10.000
0.001
0.010
0.100
1.000
LOG(F) -- EQ. PRGY 1/13/68 LPZ ('P'P)

Figure 31.

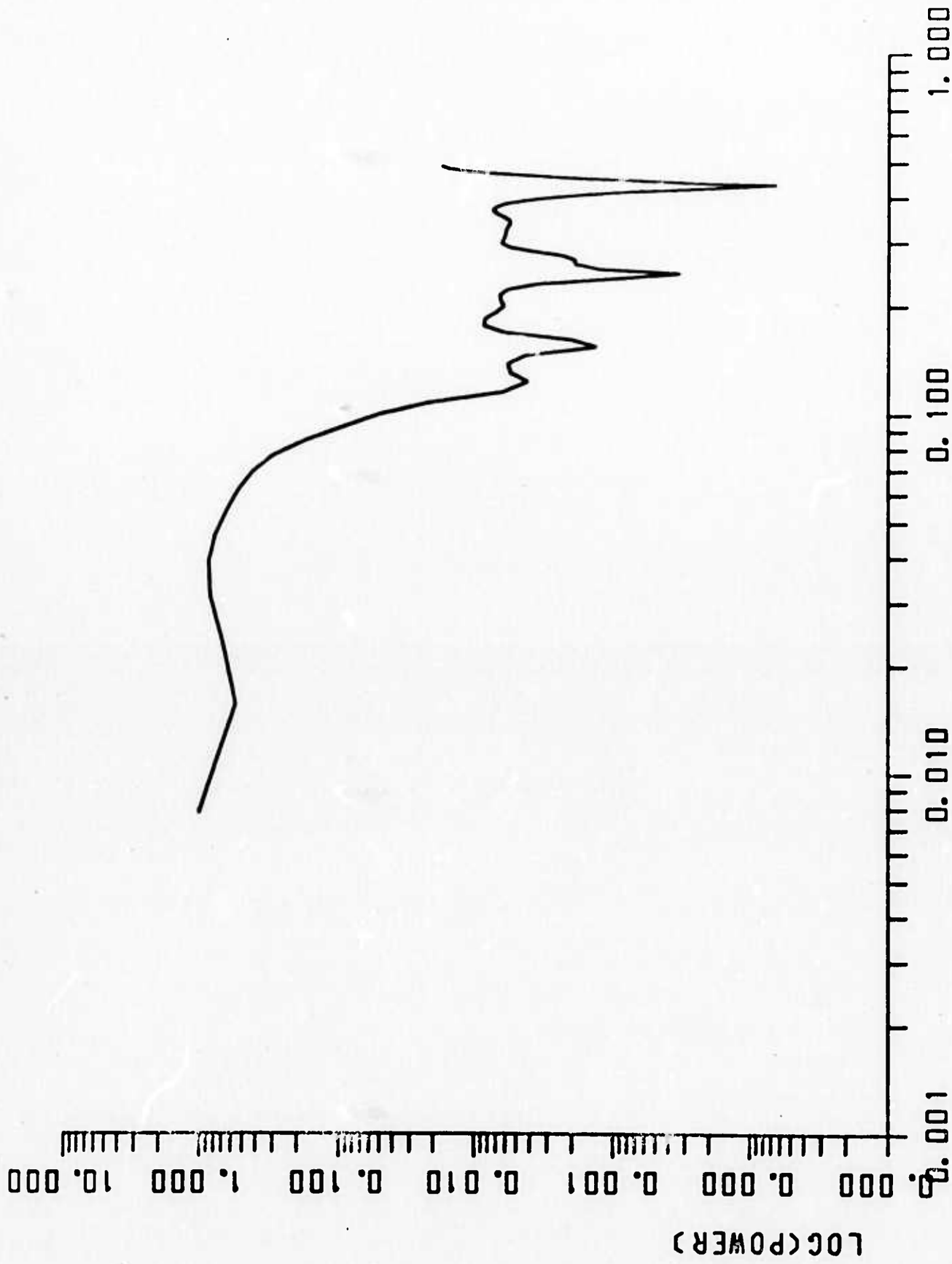
LOG(POWER)
0.000
0.000
0.001
0.010
0.100
1.000
10.000
0.001
0.010
0.100
1.000
LOG(F) -- EQ. PRGY 1/13/68 LPE (S)

Figure 32.

and 33 compare the S and sS spectra. Again there is close agreement with the corner located in the vicinity of .06 Hz. Note that the ratio of corner frequencies is approximately in the ratio of S/P velocities as suggested by recent source theory. The fact that the sS arrival has essentially the same spectrum as S indicates that there is not a low Q zone above this source.

Thus, by applying this approach and perhaps combining spectra of like body waves (e.g. P and pP) more reliable estimates of source parameters, especially source dimensions, can be obtained.

2. Mechanism of Love wave generation by NTS explosions.

One important result obtained in the course of this investigation concerns Love wave generation by NTS explosions. This has been a subject of long and inconclusive debate centering around the question of whether near-source P-SH and SV-SH conversion due to complicated geologic structure or tectonic release in the immediate vicinity of the explosive source produced the substantial but variable Love waves observed. In this study the combination of two observations provide conclusive evidence that Love waves are generated primarily by tectonic release induced by the explosion and not by conversion.

The first is the fact that cavity collapses following some explosions produce almost no long-period Love waves while the long-period Rayleigh waves so generated are almost perfect replicas (with a π phase difference) of the explosion signal; this shows that conversion cannot be important because the explosion and collapse source points and propagation paths to given receivers are identical. Figure 34 shows an outstanding (typical) example of this phenomenon for the Bilby explosion and collapse recorded

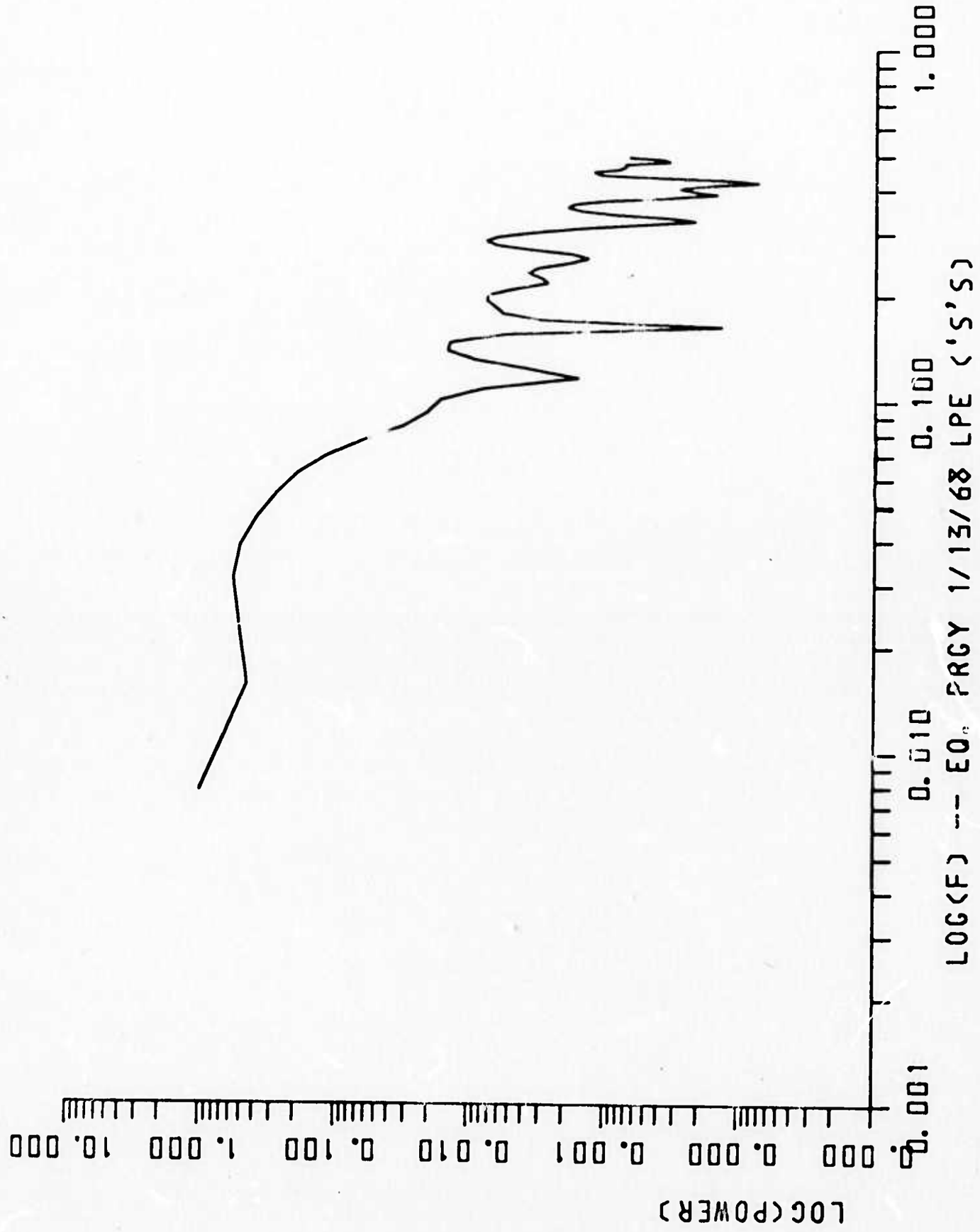
LOG(POWER)
0.000
0.000
0.001
0.010
0.100
1.000
10.000
0.001
0.010
0.100
1.000
LOG(F) -- EO. PRGY 1/13/68 LPE ('S'S)

Figure 33.

at Winnemucca, Nevada; the Love waves are clipped for the explosion and absent for the collapse.

The second line of evidence is provided by the differential dispersion of Love waves generated by nearby sources. Figure 35 shows the Love waves generated by the explosions Pile Driver, Tan, and Half-Beak as observed at HNME with epicentral distances of 4059, 4064, and 4073 km, respectively. The vertical line represents a common time base with respect to the known origin times. It is clear that there is differential dispersion of the Love waves even though there is only 14 km maximum difference in source-receiver distance; careful measurements show that the dispersion is that appropriate for the Basin and Range (NTS) source region and this indicates that in each instance the signals were generated in the immediate vicinity of each source. Further evidence of this is the fact that in opposite directions similar results and conclusions are obtained.

Thus these two lines of evidence lead to the conclusion that explosive sources generate long-period SH energy in the immediate vicinity of the point of detonation.

An apparent dilemma is posed by the fact that Rayleigh waves show little influence of S-wave generation by the explosion as evidenced by the similarity of wave-forms from explosion to explosion with different Love wave levels and between explosion and collapse and that there are no long-period teleseismic observations of SH energy even for explosions that generate large Love waves.

The first of these was investigated theoretically and based on the results we believe that the fact that Rayleigh waves in the period range observed are not strongly affected by the tectonic release induced

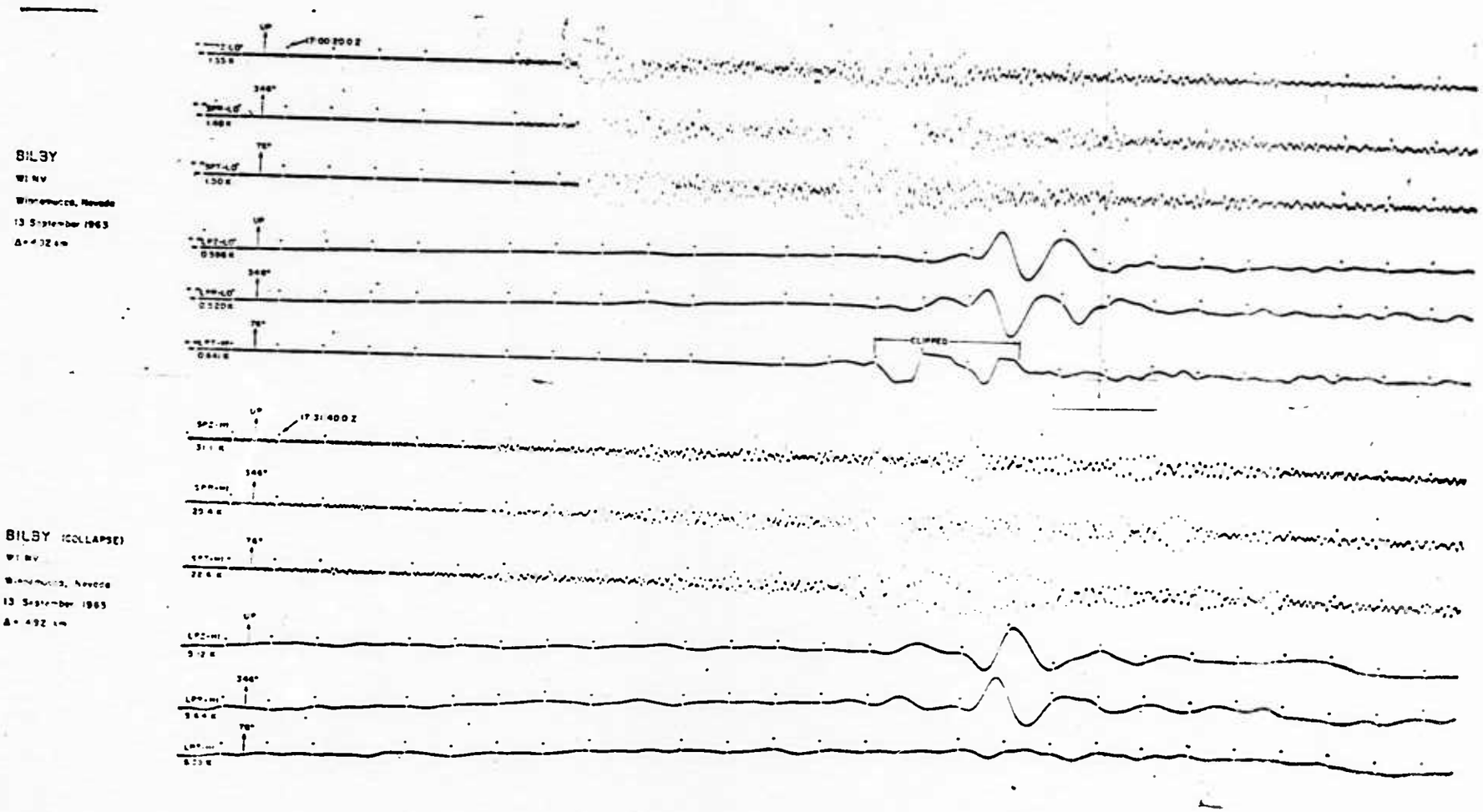
BILSY
Wilkinson, Nevada
13 September 1963
CLIPPED
BILSY (COLLAPSE)
Wilkinson, Nevada
13 September 1963

Figure 34.

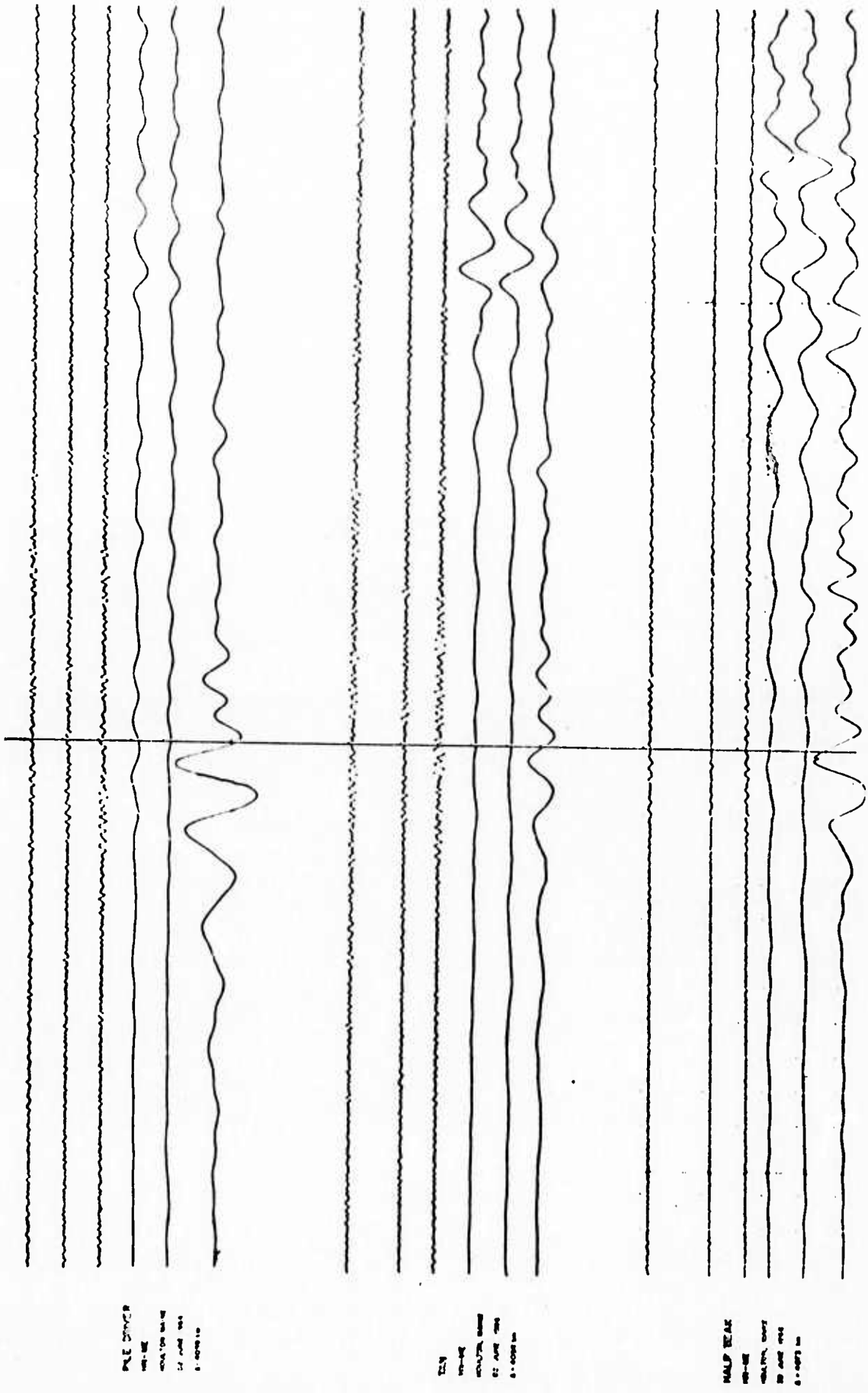

Figure 35.

by NTS explosions is due to the prevailing stress system in Nevada. That is, for vertical strike-slip faulting that is typical of the NTS area Love wave excitation should be approximately 20 times greater than Rayleigh excitation in the period range 10-50 seconds: Thus if the observed Love and Rayleigh signal amplitudes are roughly comparable, as is common, then the Rayleigh waves would be perturbed only by about 5 percent due to the tectonic release.

The reason explosions generate SH sufficient to produce large Love waves but apparently do not emit long period SH body waves may be that the cracking induced by the explosion is predominantly lateral (horizontal) with crack orientations controlled by the regional and local tectonic stress, while fewer cracks propagate downward. Thus most of the SH energy from fracturing that is emitted preferentially in a horizontal direction is trapped in the crust and interferes constructively to produce Love waves.

3. Least-squares estimates of source parameters from Love and Rayleigh modes.

Some work was completed that showed the feasibility of utilizing frequency dependent radiation patterns of Love and Rayleigh modes to find source parameters, strike, dip, slip, depth, and seismic moment.

A non-linear least squares technique has been developed for determining seismic source parameters (fault strike, dip, and slip) for earthquakes using surface wave spectra at different azimuths. A multipolar source representation in a layered half space, derived from the mathematical source description of Harkrider, is used for computing trial radiation patterns. Regression analysis of the difference between observed and calculated spectra is implemented by using a Taylor series approximation for variations of radiation patterns with strike, dip, and slip. The

limitations of the method in terms of the required azimuthal coverage and convergence have been investigated by analysis of realistic test cases for a double couple source at different depths in a Gutenberg model. In practice it is desirable to normalize observed spectra by those from a well-documented reference event in order to eliminate propagation path and receiver effects. This work is continuing as part of the Ph.D. thesis research by L. S. Turnbull.

Crustal Structure

1. Remote measurements of crustal structure in seismic source regions.

We have developed a method whereby dispersion measurements in a given source region can be made by using a single distant receiver. In brief, the method consists of using an array of sources in the same fashion an array of receivers is used conventionally for tripartite or multipartite phase and group velocity measurements. Since all of the transmission paths are in common except in the immediate source area the relative travel-times provide a direct measure of propagation in the source region, just as relative times across an array of receivers reflect propagation there. Figure 35 in the previous section illustrates the feasibility of this approach.

The analysis is identical to the usual multipartite phase and group velocity measurements and the standard least-squares programs previously developed can be used. It is especially important to note that the early and simple time domain visual method of matching peaks and troughs across a tripartite array can be used here; this means that elaborate computing facilities are not required for obtaining useful dispersion data, using this approach.

To obtain reliable dispersion estimates using this method one must have accurate relative locations of the events used and accurate relative origin times. Because standard epicenter locations are usually not nearly accurate enough we devised a method (discussed later in this report) for determining relative locations using only the standard USC&GS P-wave arrival times at a fixed network of stations. Relative location accuracies using this method are around 2 km (Spence, 1973). Relative origin times we believe can be determined to better than 1/2 second for most events.

We experimentally tested this source array dispersion technique both by using an ultrasonic model for generating Rayleigh waves under controlled conditions and by analyzing Rayleigh and Love waves from the larger NTS explosions whose origin times and locations are known precisely. The model experiment gave the expected dispersion, and both Rayleigh and Love wave dispersion estimates for NTS are reasonable and similar in shape and value to the average for the Basin and Range.

The importance of this method is potentially very great not only for helping to distinguish between explosions and earthquakes but generally for studying crustal structure and source mechanism in tectonically active areas which are inaccessible for direct measurements. By using many events from a given region and several different receiver azimuths, differences in initial phase spectra will tend to average out in the overall least-squares solution thereby giving reliable average dispersion estimates. Once the dispersion is known then individual initial phase spectra can be compared pair-wise for any of the events because differences due to propagation can be removed. Also, better relative locations using surface waves can be made for subsequent events.

Taylor (1972) explored this use of relative event analysis both using ultrasonic model studies and analyzing events on the Mid-Atlantic Ridge. These results are summarized in Appendices II and III containing preprints of papers describing the method and results.

2. Site structure from ellipticity dispersion.

As a by-product of the methods for separating Love and Rayleigh waves discussed earlier we obtain at each frequency estimates of Rayleigh wave ellipticity, that is the ratio of radial to vertical particle motion. The

ellipticity is dispersed (i.e. frequency dependent), different for each mode, and dependent only on the earth structure beneath the recording site. As a result, ellipticity dispersion in principal can be inverted in a fashion analogous to phase and group velocity dispersion to estimate site structure.

We have made fundamental mode ellipticity observations as LASA stations in the period range 15-60 seconds for several events. Comparison of these results with theoretical curves for layered models based on refraction and surface wave dispersion analysis show good agreement. Moreover, the observations provide additional evidence for east-west lateral variations in the deeper part of the crust under LASA.

Provided ellipticities for a number of events are combined to obtain statistically reliable ellipticity spectra, point-wise estimates of crust and upper mantle structure can be obtained anywhere a three-component long-period station exists. A Ph.D. thesis by C. A. Newton (1973), completed under sponsorship of this Grant, presents in detail the various aspects of the observation and interpretation of Rayleigh wave ellipticity summarized here.

Relative Location of Events

Accurate relative locations are required in order to use the approach discussed above to determine crustal structure in a seismic region from an array of sources and to compare individual source time functions. We have developed methods for using short-period P-waves and surface waves for relative locations.

1. Relative locations from short-period P-wave travel time observations.

This method consists of plotting P-wave travel time differences for each event at a common network of stations as a function of azimuth, using

if possible a reference event whose location is well known. These travel time differences fall on a curve of the form $A \cos(\alpha + \alpha_o + \pi/2)$ where A is the distance separating the events (times $dT/d\Delta$) and α_o is the azimuth connecting the two events. Observed travel time differences are fit to this function by least squares to obtain "best" estimates of A and α_o. Since receivers are usually located at different distances a correction for variations in take-off angle is made before fitting the curve; this in effect equalizes all receivers to a common distance. Tests of this method on NTS nuclear events whose locations are precisely known and on Lake Superior chemical explosions were made. In both cases relative location accuracies were good to within approximately 2 km, including one case at NTS where the event separation was as large as 174 km. See also Spence (1973) for a more exhaustive treatment of relative location methods and results for other areas. We conclude therefore that we can estimate relative locations of events to approximately 2 km, provided lateral variations in near-source structure are not significantly more extreme than for these areas. Better relative locations were obtained by using only teleseismic observations, because the take-off angles for these distances are small and rather insensitive to structural variations in the source region. By forcing the closer station data to fall on the "best fit" cosine curves for teleseismic observations we were able to obtain estimates of $\frac{dT}{d\Delta}$ for the nearer distances. In turn these can be inverted to obtain shallow velocity structure along different azimuths from the source region. This also provides a possible means of inferring lateral variations in crustal structure in active seismic areas.

This approach, then, provides us with relative locations which are sufficiently accurate to use the surface wave method described earlier for

obtaining surface wave dispersion measurements using an array of sources and only a few distant recording stations. It has the important advantages that only the standard USC&GS P-wave arrival times are required and effects of travel time anomalies and station corrections are avoided.

2. Relative locations using surface wave observations.

Once the dispersion is known for a given source region relative locations can also be obtained using Rayleigh or Love waves in a manner analogous to that described above. Again we take advantage of the fact that the transmission path to each receiver is the same except for a portion in the immediate source region. The group or phase arrival time differences for each frequency are plotted versus azimuth, fitted with a cosine curve and interpreted in an analogous fashion to the body-wave case except that no distance corrections are needed. Although time differences accurate to about .5 sec must be made for this approach to be competitive with the body wave method, the fact that an estimate is obtained for each frequency of the dispersed signal may allow us to relax this accuracy somewhat for individual frequencies.

Computational Programs

In the course of this study a number of programs were written for the IBM 360/67 computer and others were adapted from existing programs obtained at Penn State and elsewhere for use on this machine. These programs implement the methods discussed above and permit them to be used on digital data appropriate to each technique. Although our purpose was primarily to develop methods rather than exhaustively apply them, these programs for the most part can be used in the routine processing of long-period data.

One important development was an economical and efficient method for digitizing analog (paper) records. Basically one only samples as often as necessary to resolve the highest frequency arriving at that time (peaks, troughs, and inflections) and interpolates to a desired uniform sampling rate using a cosine interpolation.

The basic processing programs now fully operational include:

(a) Combined matched filter and spectral analysis.

This program has many options for analyzing both individual seismograms and arrays. Input is primarily from magnetic tapes and results are displayed using computer graphics routines and printer plotting.

(b) Multiple narrow-band filtering.

This program applies a suite of narrow-band digital filters of arbitrary shape and center frequency and plots each filtered seismogram and its envelope. It is used for separating Rayleigh and Love modes, computing spectra of each mode, and obtaining dispersion curves experimentally.

(c) Single station ellipticity dispersion and propagation direction.

Three orthogonal components are combined to give Rayleigh wave ellipticity and propagation directions as a function of frequency, for various modes. This program is used for mode separation and site structure.

(d) Synthetic seismograms.

From input spectra, attenuation, and phase velocity values theoretical seismograms are computed for any desired distance. Provision is made for composite paths with segments differing in attenuation and phase velocity.

(e) Least-squares dispersion estimates.

Relative arrival times for a multipartite array of stations (or sources) are combined to obtain least-squares estimates of phase and group velocity and propagation direction.

(f) Frequency-wave number analysis.

An array of N seismograms is doubly transformed into frequency-wave number space. Plots at each frequency give power spectra, propagation vectors, and propagation velocity for signals common to all the array elements. This is used successively on horizontal and vertical components to separate Love and Rayleigh and measure Rayleigh wave ellipticity dispersion.

(g) Theoretical surface wave dispersion.

Programs written by D. G. Harkrider were adapted for use on Penn State's computer. They calculate multimode Love and Rayleigh wave dispersion for an N-layered elastic half-space. They also provide certain additional parameters needed for calculating excitation spectra and radiation patterns for explosive and earthquake sources at any depth.

(h) Theoretical surface wave spectra and magnitude calculations.

This program takes the results of program (h) above and computes Love and Rayleigh excitation spectra, spectral ratios, radiation patterns, and average magnitude for explosive sources at any depth and earthquake sources of any orientation and depth in a multi-layered half-space. Data from this program along with program (d) above can be used to calculate theoretical seismograms at any desired distance.

(i) Seismoprints and energy ratios.

This program generates the seismoprint displays and computer desired energy or spectral ratios.

(j) Dynamic finite element codes.

These programs calculate body and surface wave excitation for seismic sources in complicated geologic structures.

(k) Non-linear least squares estimates of source parameters.

This program fits observed or theoretical radiation patterns to obtain source strike, dip, slip, and seismic moment.

(l) Data tape conversion.

This program (BCDCUT) converts CDC 7-track block BCD card image data tapes to an IBM 9-track "standard" format digital tape. This program is essential for using LRSM, Observatory, and array data from the Seismic Data Laboratory in Alexandria, Virginia, the primary source for our experimental data. A copy of this tape conversion program was given to the SDL for the convenience of other IBM 360 users of their CDC data tapes.

(m) Miscellaneous programs.

Many subroutines and additional small programs of general usefulness were written or adapted for use in this project (e.g. distance-azimuth, body wave travel time, and crustal transfer functions). Complete listings of these as well as the programs mentioned above are on file in the Department of Geosciences, Geophysics Section at The Pennsylvania State University.

References

Alexander, S. S. and D. B. Rabenstine, 1967A, Detection of Surface Waves from Small Events at Teleseismic Distances, Seismic Data Laboratory Report No. 175, Teledyne Industries, Inc., also Trans. A.G.U., vol. 48, no. 1, 1967.

Alexander, S. S. and D. B. Rabenstine, 1967B, Rayleigh Wave Signal-to-Noise Enhancement for a Small Teleseism Using LASA, LRSM and Observatory Stations, SDL Rpt. No. 194, Teledyne Industries, Inc.

Alexander, S. S., 1963, Surface Wave Propagation in the Western United States, Ph.D. Thesis, Calif. Inst. Tech., Pasadena, Calif.

Alexander, S. S. and J. H. Lambert, 1973, Long-Period Spectra Estimates from Earthquakes and Explosions, SDL Rpt. No. 307, Teledyne Geotech Alexandria, Va., 37 pp.

Alexander, S. S. and J. H. Lambert, 1971, Single-Station and Array Methods for Improved Surface Wave Spectral Estimates, SDL Rpt. No. 264, Teledyne Geotech, Alexandria, Va., 104 pp.

Cohen, T. J., 1969, Seismoprints, SDL Rpt. No. 238, Teledyne Geotech, Alexandria, Va., 73 pp.

Newton, C. A., 1973, An Investigation of Rayleigh Wave Ellipticity with Applications to Earth Structure, Ph.D. Thesis, The Penna. State Univ., University Park, Pa.

Spence, W. J., 1973, Crustal and Upper Mantle P-Wave Velocity Heterogeneity and the Problem of Earthquake Location, Ph.D. Thesis, The Penna. State Univ., University Park, Pa.

Taylor, R. W., 1972, Remote Determinations of Earth Structure from Relative Event Analysis with Applications to the Mid-Atlantic Ridge, Ph.D. Thesis, The Penna. State Univ., University Park, Pa.

von Seggern, D., 1969, Effects of Radiation Patterns on Spectra and Magnitude Estimates, SDL Rpt. No. 233, Teledyne Geotech, Alexandria, Va.

APPENDIX I

APPENDIX I

Long Period Seismic Methods for Identifying Small, Underground Nuclear Explosions

I. Abstract

The theory of earthquakes and explosive sources in multi-layered media developed by Ben Menahem and Harkrider has been used to determine what combinations of Love and Rayleigh waves can be used to obtain improved surface wave magnitude estimates. For deeper sources averaging the total Love and Rayleigh energy over approximately 8 stations distributed over any 180° sector will give a surface wave magnitude that is nearly independent of strike, dip, and slip of the source, while for shallow sources (~5 km) the Rayleigh waves alone averaged in the same manner azimuthally gives the best estimate. At periods shorter than 30 seconds these averages also can give estimates of source depth. These combined averages yield improved magnitude estimates only for fundamental mode Love and Rayleigh waves. In practice it is highly desirable to make relative magnitude estimates, keying on a well-documented explosion or earthquake in the source region of interest in order to eliminate propagation effects. In turn the same data used for the improved magnitude measurements can be used to infer source parameters.

II. Introduction

The motivation for this investigation was to develop procedures for obtaining improved surface-wave magnitudes in order to take better advantage of a distributed network of stations in identifying explosions and earthquakes using the M_s vs m_b and depth of focus criteria. In addition as a by-product we expect to obtain observations necessary to infer the

source mechanism parameters of strike, dip, slip, and depth for earthquakes.

III. Theoretical Development

The basic theoretical development used in this paper is that of Ben-Menahem and Harkrider (1964). One of the main characteristics of the source-time function they consider is that it is separable. Since the source is in the form of a delta function in time, the spectra we obtain are really the impulse response of the layered half space.

The source description used by Ben-Menahem and Harkrider (1964) considers a shear type fault with arbitrary dip and slip in a layered earth. An equivalent force system is used to replace the physical fault, with this force system generated from a single force. The time dependence of the force is that of a Dirac delta function. The geometry of the fault plane is the same as that adopted by Ben-Menahem and Harkrider, 1964, p. 2607.

The double-couple source used in this analysis is obtained by the superposition of two equal couples at right angles so that the total moment of the system is zero. To obtain the far-displacement field for this system we use:

$$\vec{U}^{dc} = -(\hat{n}\cdot\text{grad})\vec{U}^{s}(\vec{R}) - \left(\frac{\vec{R}}{|R|}\cdot\text{grad}\right)\vec{U}^{s}(|R|\hat{n})$$

Performing the above operations we obtain general formulas for the far field of Love and Rayleigh waves. This field may be written as

$$\vec{U} = |R|\,|n|\,k_n e^{-i3\pi/4}\, N(h)\chi(\theta)$$

where: k_n = either k_R or k_L

N_h = either $N_\theta(h)$ or $N_{rz}(h)$, where N_θ is the Love wave response of the medium to a horizontal force, and $N_{rz}(h)$ is the horizontal response due to a vertical force.

$\chi(\theta)$ = complex radiation pattern function that accounts for all of the effects of source parameters (strike, dip, and slip) excepth depth; it is the effects of this function that we shall seek to eliminate by combinations of modes and azimuths.

This complex function is defined as

$$\chi(\theta) = d_o + i(d_1\sin\theta + d_2\cos\theta) + d_3\sin 2\theta + d_4\cos 2\theta$$

The coefficients d_i are given in Ben-Menahem and Harkrider (1964, p. 2609) λ is measured counterclockwise from the positive strike direction, and δ is measured downward from the negative dip direction. The dimensionless entities A, B, C, and G are given by

$$A(h) = N_{rr}(h)/N_{rz}(h)$$

$$B(h) = \left(N_{rr}(h) + \frac{2}{k_R}\frac{\partial N_{rz}(h)}{\partial h}\right)/N_{rz}(h)$$

$$C(h) = \left(N_{rz}(h) + 1/k_R\frac{\partial N_{rr}(h)}{\partial h}\right)/N_{rz}(h)$$

$$G(h) = \frac{\partial N_\theta(h)}{\partial h}/k_L N_\theta(h)$$

IV. Theoretical Results

For the Gutenberg model we calculated the Love and Rayleigh fundamental mode response, exclusive of the $\chi(\theta)$ (radiation pattern) effects, for 3 source depths. These response curves are shown in Figure 1. One important feature of this figure is that the fundamental mode Love and

Rayleigh responses are approximately the same for each depth, indicating that depth affects both wave-types in approximately the same fashion in the period range 10-50 seconds; thus if the effects of the $\chi(\theta)$ term can be eliminated, it should be possible to infer depth from either Love or Rayleigh waves or both combined.

A similar plot is given in Figure 2 for the Rayleigh wave response for an explosive source at the same 3 depths plus a surface value. One sees basically the same shaped responses and depth dependences as for the double couple case.

Using the above theoretical development, we sought to examine the effect of the source parameters on averages of the real (measurable) quantities R^2, L^2, R^2+L^2, and L/R. For a Gutenberg earth model the quantities were examined as a function of azimuth from strike for 3 depths (5.5 km, 33.25 km, 56 km), 4 dips and slips (10°, 30°, 60°, 90°), and periods 10 sec. through 50 sec.

Because of the symmetry properties of the amplitude radiation patterns (Ben-Menahem and Harkrider, 1964, p. 2614), we only need to examine a 180° sector of the pattern. Furthermore, it was found that one need only use eight stations (or a minimum number of eight azimuths spanning the 180°). This was determined by averaging the quantities of interest over sucessively larger azimuthal intervals and determining if the average stayed within 10% of the largest and smallest values. This is analogous to the procedure and used by von Seggern (1969).

Figures 3a to 3d show representative results for 8-station averages of total surface wave energy (R^2+L^2) for dips of 10, 30, 60 and 90, degrees, respectively, and the depths indicated. In each case the shaded area

represents the ranges attributed to the variation in slip direction on the fault plane. Note that in each instance these average curves cluster closely around the corresponding curve in Figure 1 indicating that this average estimate is effective in eliminating radiation pattern effects. The one exception is for the case of a 90° dip at a 5.5 km depth where there may be more than an order of magnitude variation in the average energy at the longer periods. As we shall see presently this is due to the Love wave variations for this dip. Thus in general we can expect $R^2+ L^2$ to give a good magnitude estimate for most source orientations and depths.

Figures 4a to 4d show for a source depth of 5.5 km the ranges expected for the average quantities L^2, R^2, 4R, and R^2+L^2, respectively, for all combinations of the dips and slips given. The area of darker shading is obtained when the 90° dip is excluded. It is clear from examining these figures that the best average to use for magnitude estimates is the Rayleigh wave around 20 to 30 seconds period. Clearly it is the Love wave that varies pathologically with changes in fault orientation at 5 km depth.

Figures 5a to 5d show for a source depth of 33 km the ranges expected for the average quantities L^2, R^2, L/R, and R^2+L^2, respectively, for all combinations of dips and slips given. Again the area of darker shading is gotten by eliminating the 90° dip case. At this depth it is the Rayleigh wave that is strongly influenced by slip for a vertical fault (90° dip). However, R^2+L^2 gives the best average to use for events at this depth.

Figures 6a to 6d show for a source depth of 56 km the range expected for the average quantities L^2, R^2, L/R and R^2+L^2, respectively, for all combinations of dips and slips given. It is clear that again the R^2+L^2

average is least influenced by source geometry and should be used for magnitude estimates.

Conclusions

1. For all except very shallow sources (~5 km) the most reliable estimates of surface wave magnitude can be gotten from azimuth averages of total surface wave energy, R^2+L^2.

2. For shallow sources it is best to use an azimuthal average of Rayleigh waves alone, R^2, preferably in the period range 20-30 seconds.

3. Effects of radiation patterns on magnitude can be satisfactorily minimized by averaging about 8 stations distributed over any 180° sector of azimuth.

4. The data required for the above averages can also be used to fi by least-squares the best strike dip and slip for an event of interest, provided propagation effects can be accounted for either directly or by use of a reference event.

References

Ben-Menahem, A., and D. G. Harkrider, 1964, Radiation Patterns of Seismic Surface Waves from Dipolar Sources in a Flat, Stratified Earth, Jn. Geophys. Res., 69, 2605-2620.

von Seggern, D., 1969, Effects of Radiation Patterns on Spectra and Magnitude Estimates, SDL Report No. 233, Teledyne-Geotech, Alexandria, Va.

FIGURE CAPTIONS

Figure 1. Fundamental Rayleigh and Love response for a double couple source at 3 depths in a Gutenberg model.

Figure 2. Fundamental mode Rayleigh response for an explosive source at various depths, a_s is the cavity radius and $\bar{\rho}_o$ is stress on the cavity wall.

Figure 3. (a) Average total Rayleigh and Love wave energy for 3 depths and a dip of 10°;

(b) the same for a 30° dip;

(c) the same for a 60° dip;

(d) the same for a 90° dip.

Figure 4. Range in averages for 5.5 km depth for all indicated slips and dips for: (a) L^2; (b), R^2; (c), L/R; (d) $R^2+ L^2$. Darker area is obtained by eliminating 90° dip.

Figure 5. Range in averages for 33 km depth for all indicated slips and dips for: (a) L^2; (b), R^2; (c), L/R; (d) R^2+L^2. Darker area is obtained by eliminating 90° dip.

Figure 6. Range in averages for 56 km depth for all indicated slips and dips for: (a) L^2; (b), R^2; (c), L/R; (d) R^2+L^2. Darker area is obtained by eliminating 90° dip.

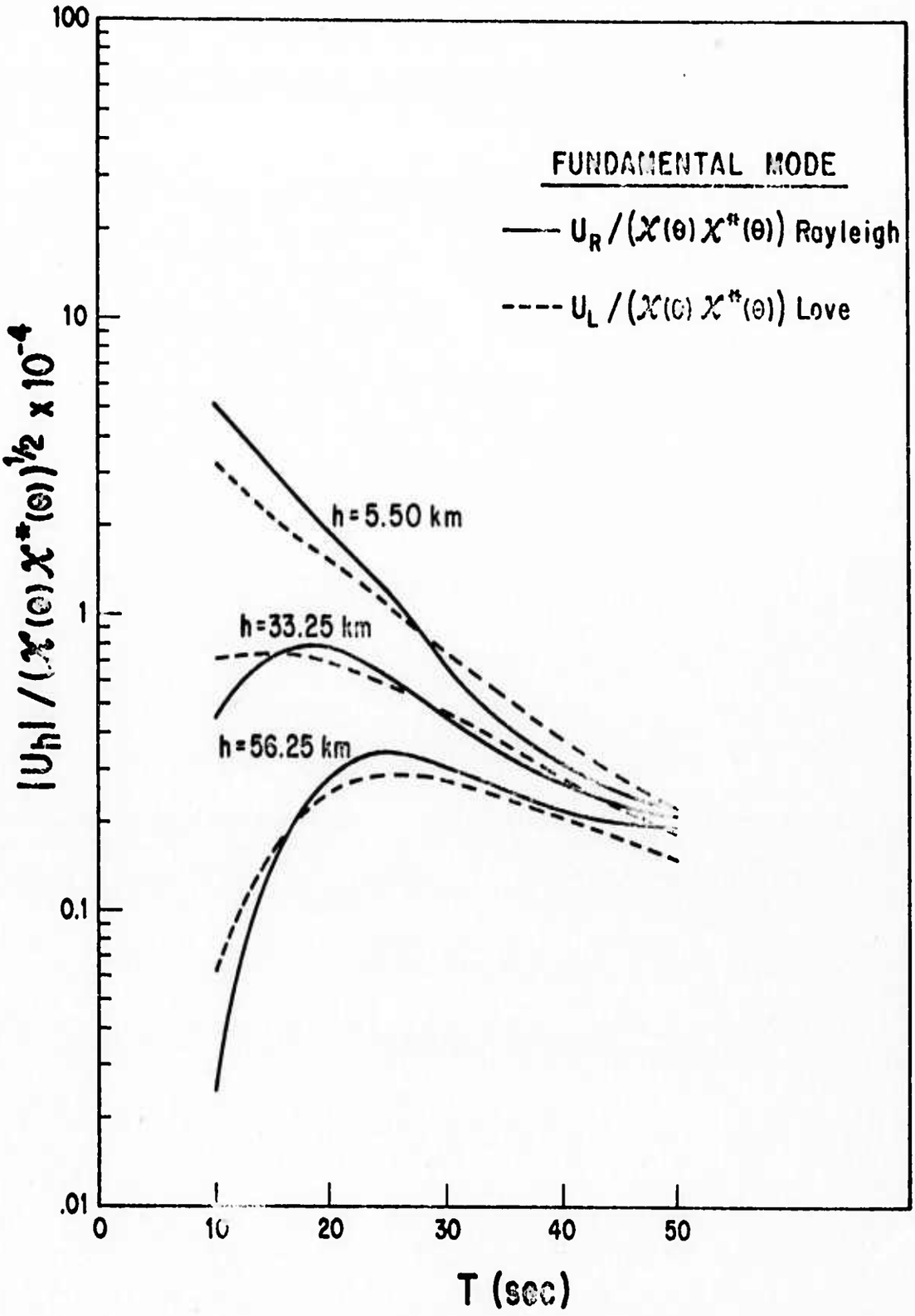
FUNDAMENTAL MODE
$U_R / (\chi(\theta)\chi^*(\theta))$ Rayleigh
$U_L / (\chi(\theta)\chi^*(\theta))$ Love
h = 5.50 km
h = 33.25 km
h = 56.25 km
$|U_h| / (\chi(\theta)\chi^*(\theta))^{1/2} \times 10^{-4}$
100
10
1
0.1
.01
0
10
20
30
40
50
T (sec)

Figure 1.

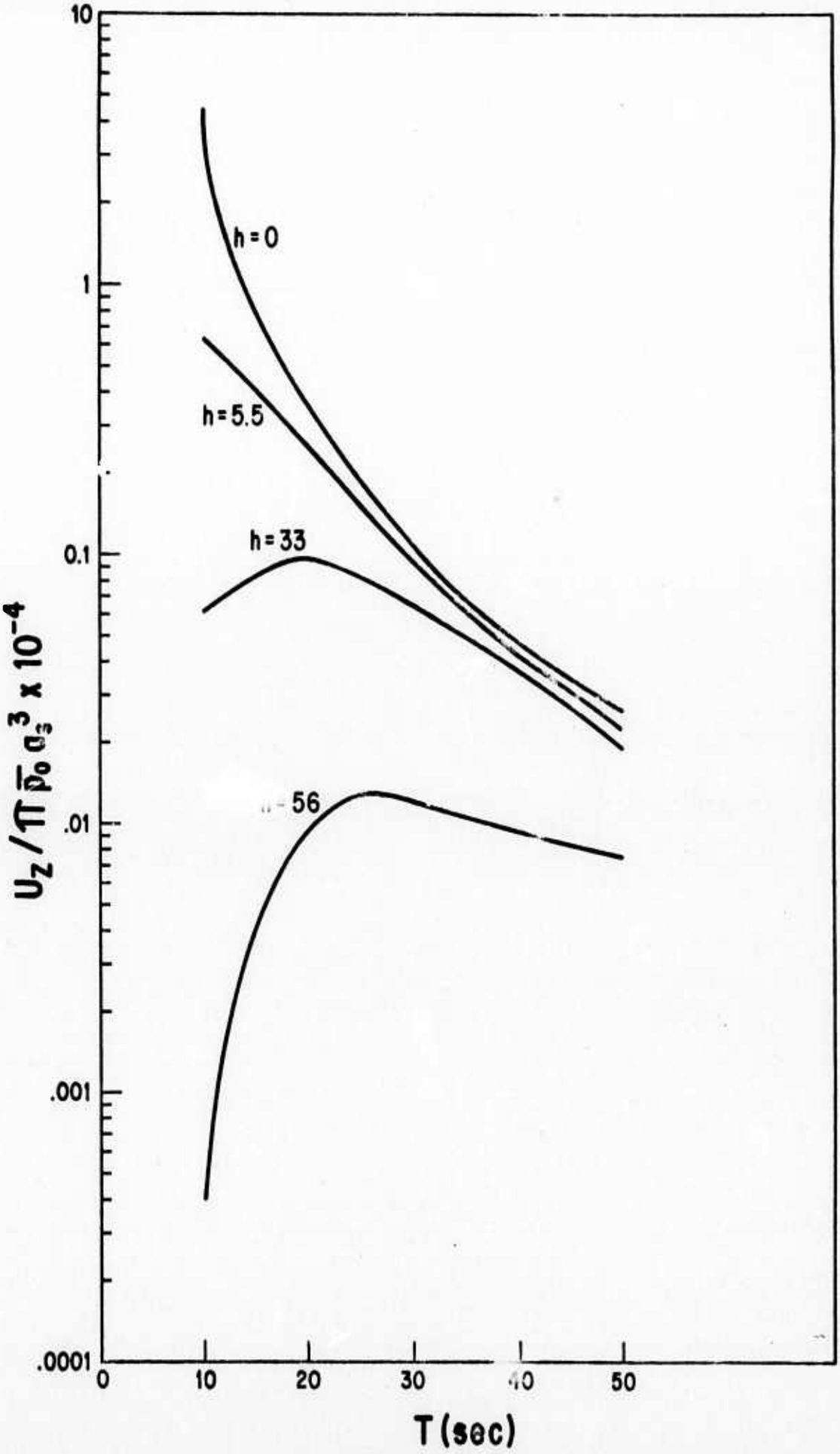
10
1
0.1
.01
.001
.0001
h = 0
h = 5.5
h = 33
h = 56
$U_z / \pi \bar{\rho}_0 a_3^3 \times 10^{-4}$
0
10
20
30
40
50
T (sec)

Figure 2.

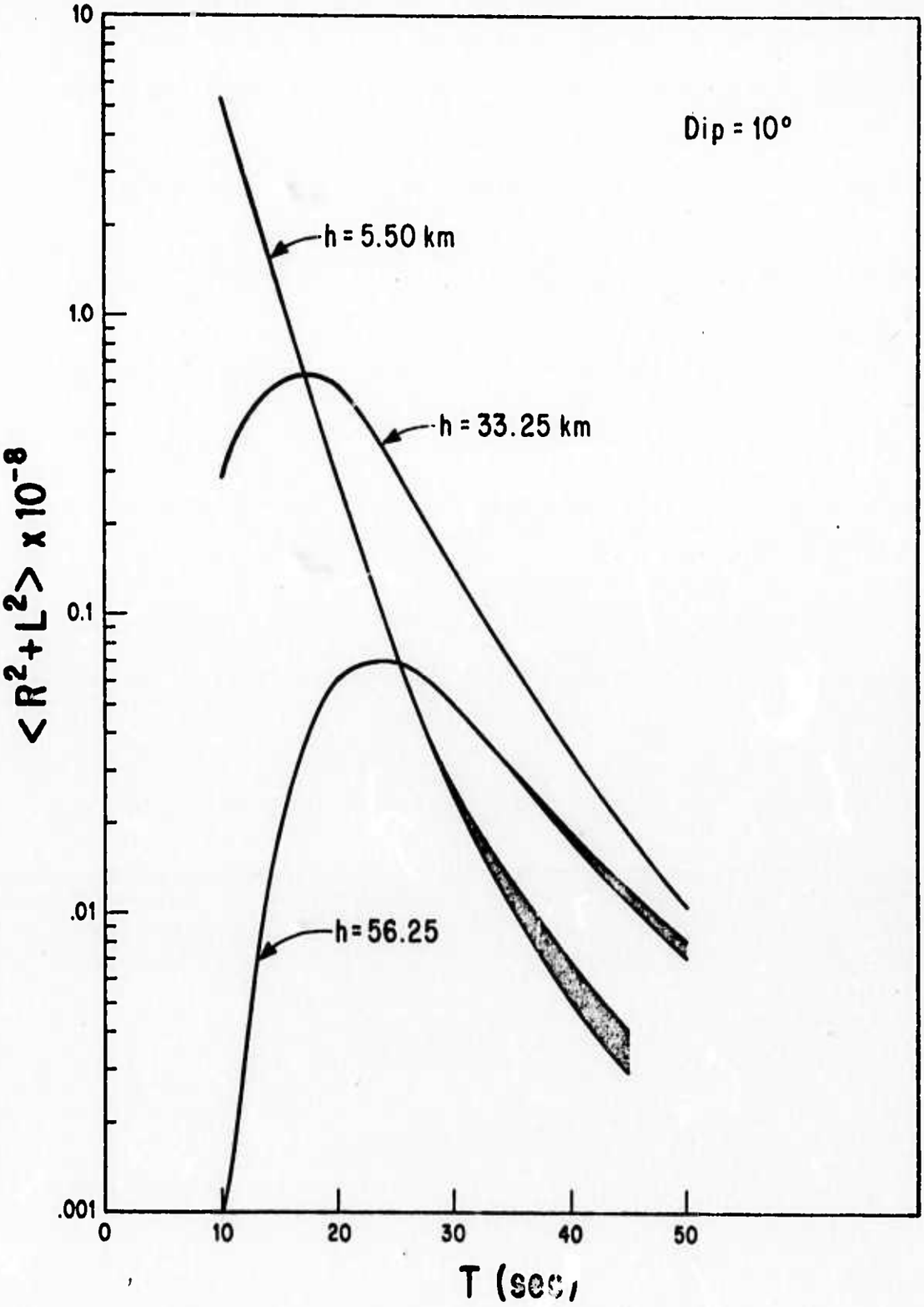
Dip = 10°
h = 5.50 km
h = 33.25 km
h = 56.25
$\langle R^2+L^2 \rangle \times 10^{-8}$
10
1.0
0.1
.01
.001
0
10
20
30
40
50
T (sec)

Figure 3a.

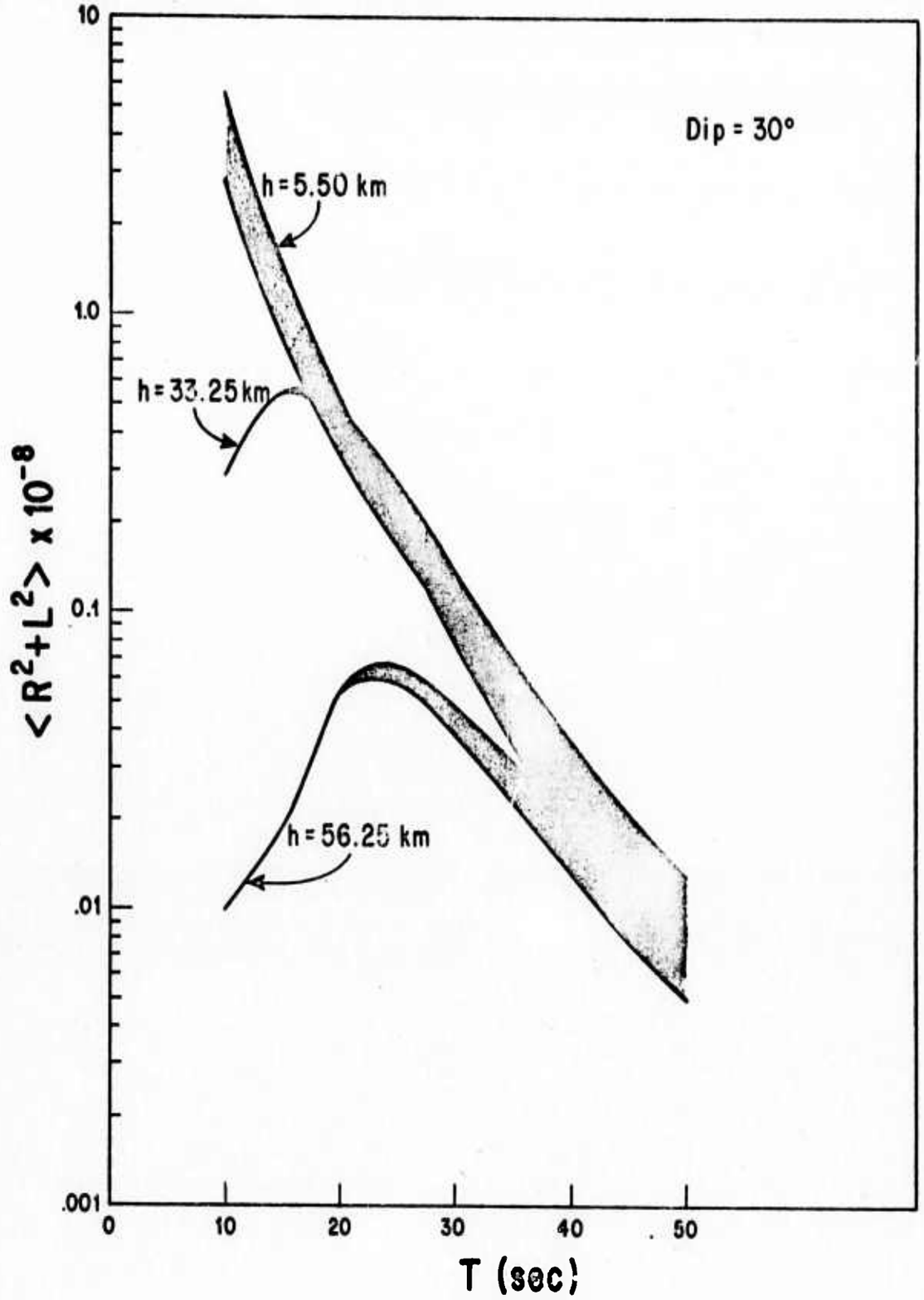
Dip = 30°
h = 5.50 km
h = 33.25 km
h = 56.25 km
$\langle R^2+L^2 \rangle \times 10^{-8}$
10
1.0
0.1
.01
.001
0
10
20
30
40
50
T (sec)

Figure 3b.

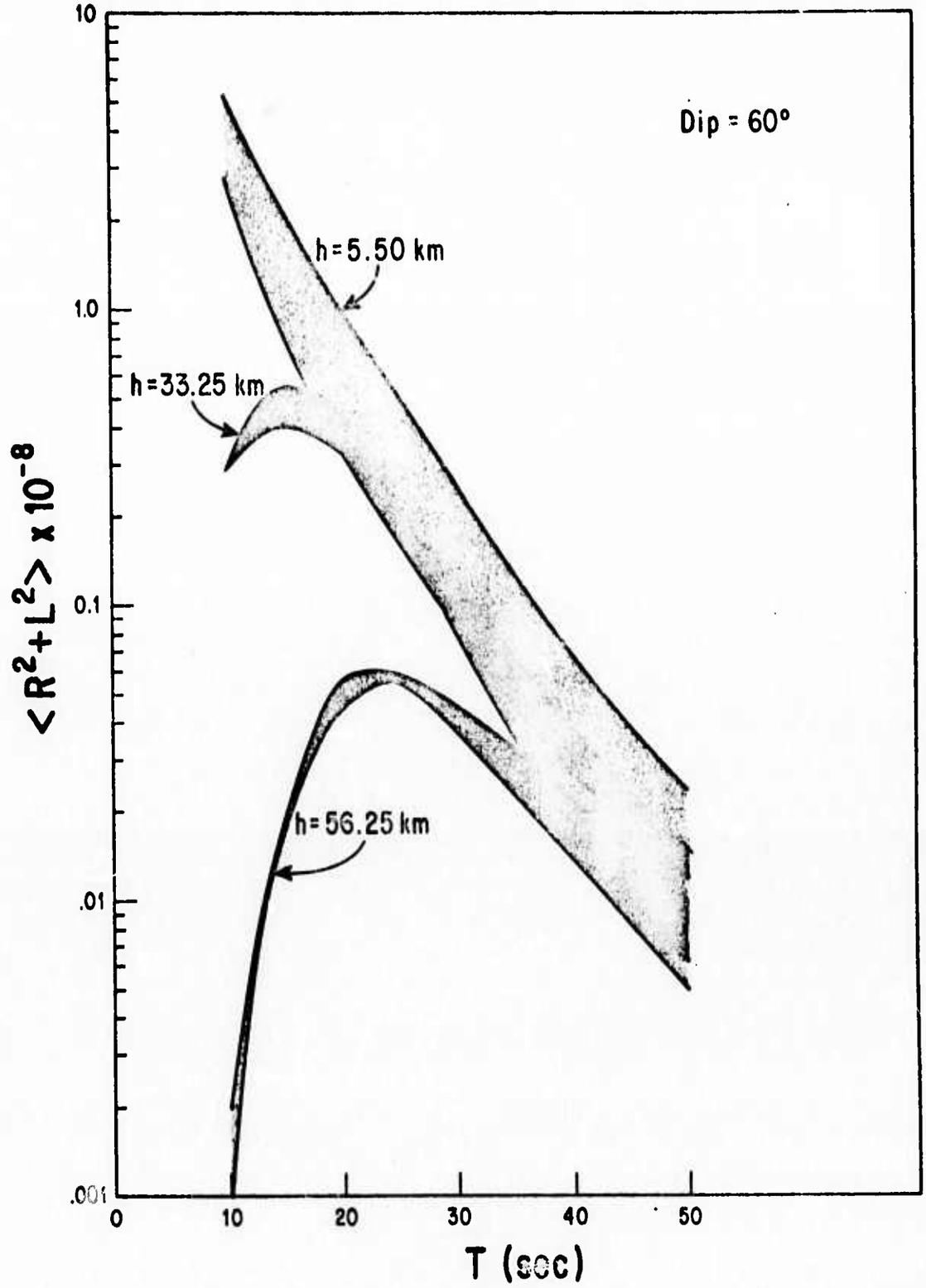
Dip = 60°
h=5.50 km
h=33.25 km
h=56.25 km
$\langle R^2+L^2 \rangle \times 10^{-8}$
10
1.0
0.1
.01
.001
0
10
20
30
40
50
T (sec)

Figure 3c.

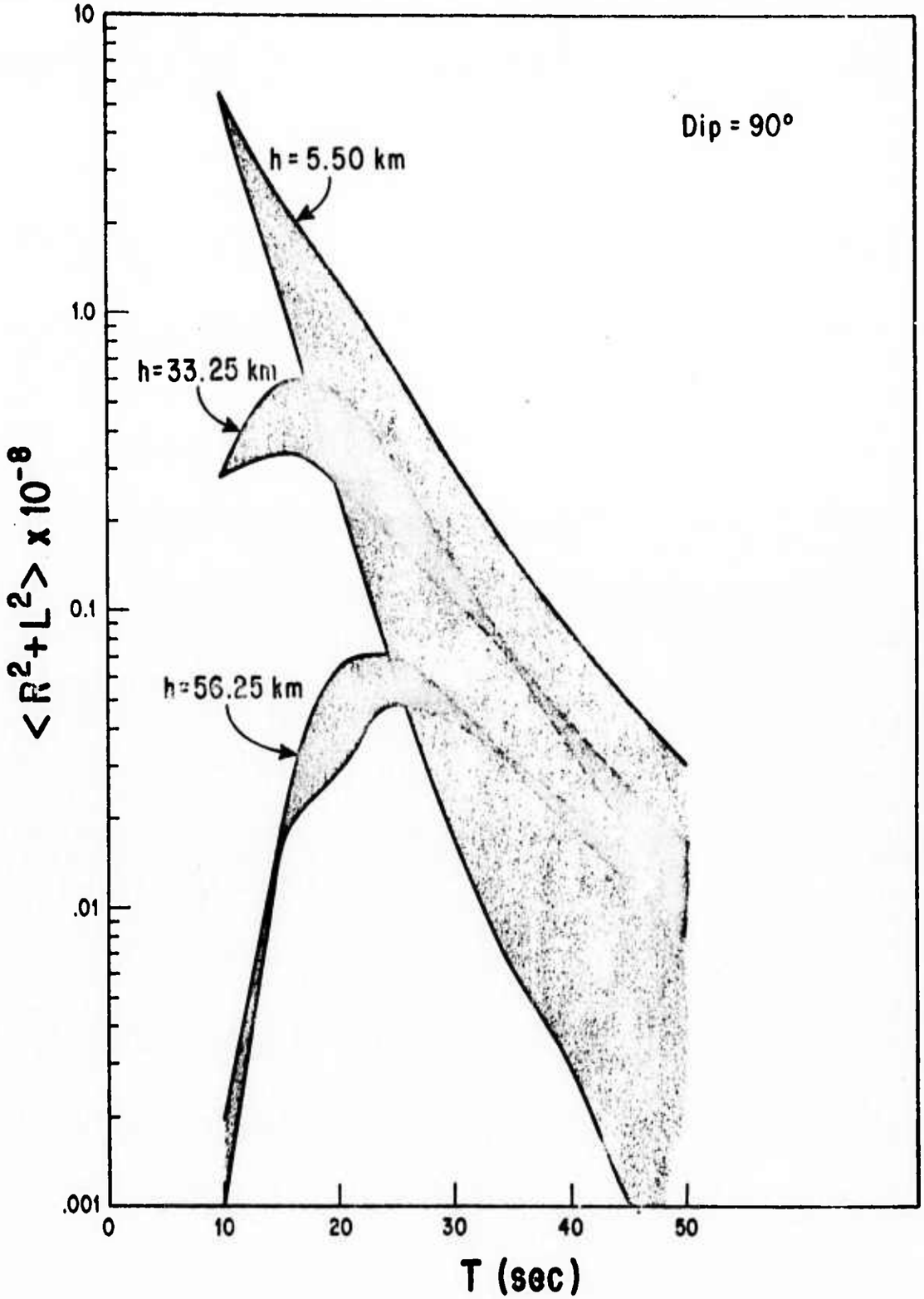
Dip = 90°
h = 5.50 km
h=33.25 km
h=56.25 km
$<R^2+L^2> \times 10^{-8}$
10
1.0
0.1
.01
.001
0
10
20
30
40
50
T (sec)

Figur. 3d.

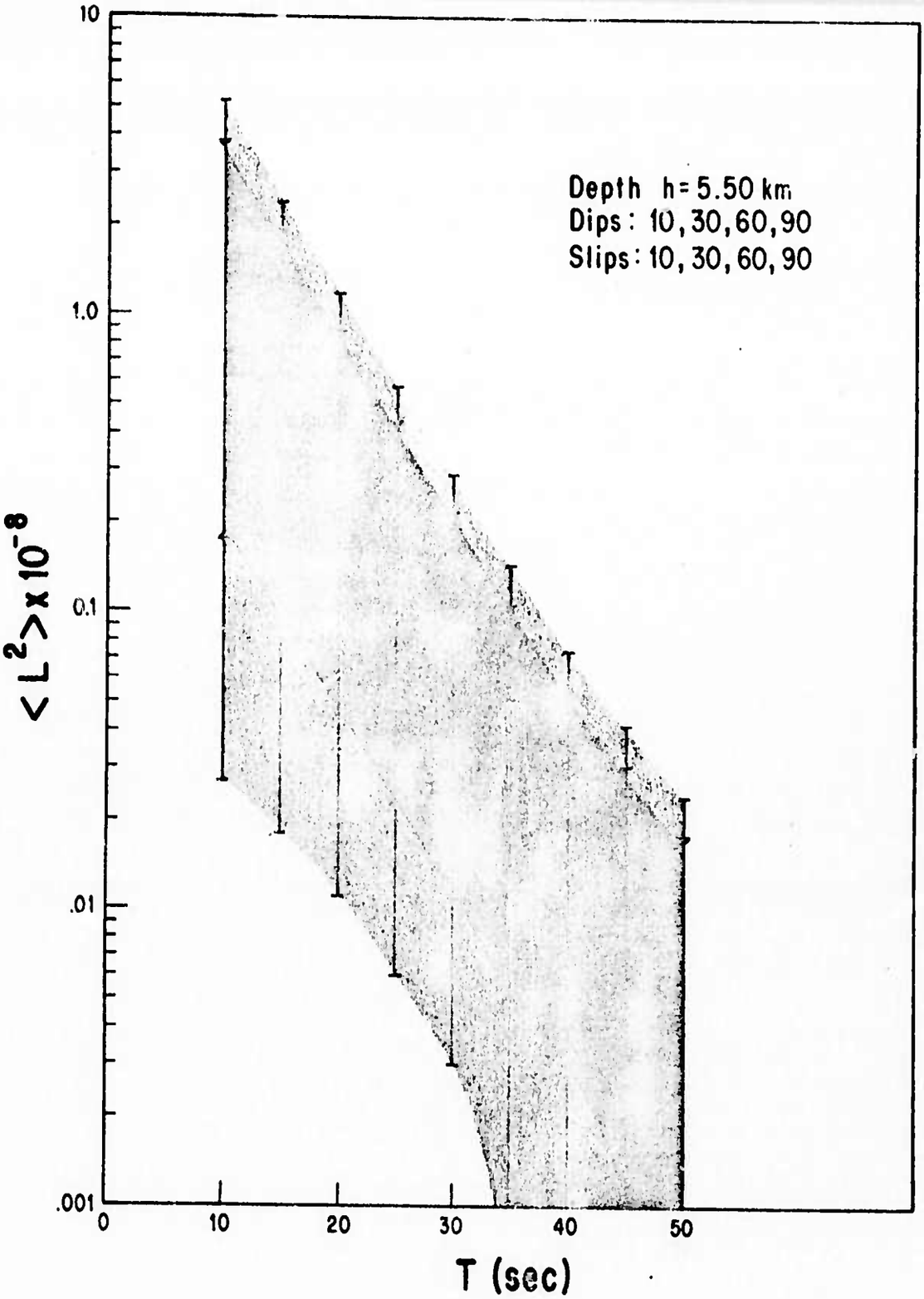
Depth h=5.50 km
Dips: 10,30,60,90
Slips: 10,30,60,90
10
1.0
0.1
.01
.001
$<L^2> \times 10^{-8}$
0
10
20
30
40
50
T (sec)

Figure 4a.

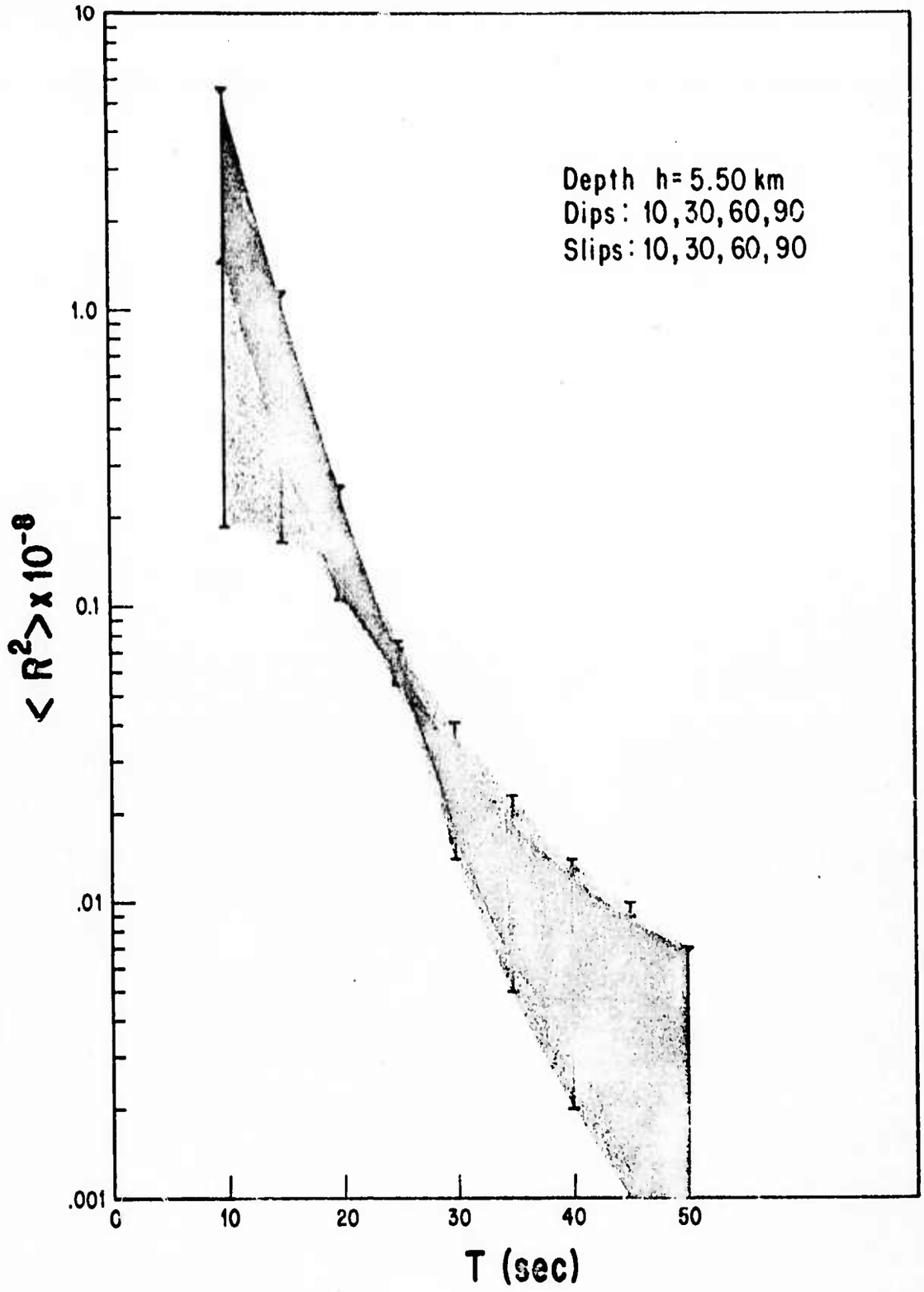
Depth h= 5.50 km
Dips: 10,30,60,90
Slips: 10,30,60,90
10
1.0
0.1
.01
.001
$< R^2 > x 10^{-8}$
0
10
20
30
40
50
T (sec)

Figure 4b.

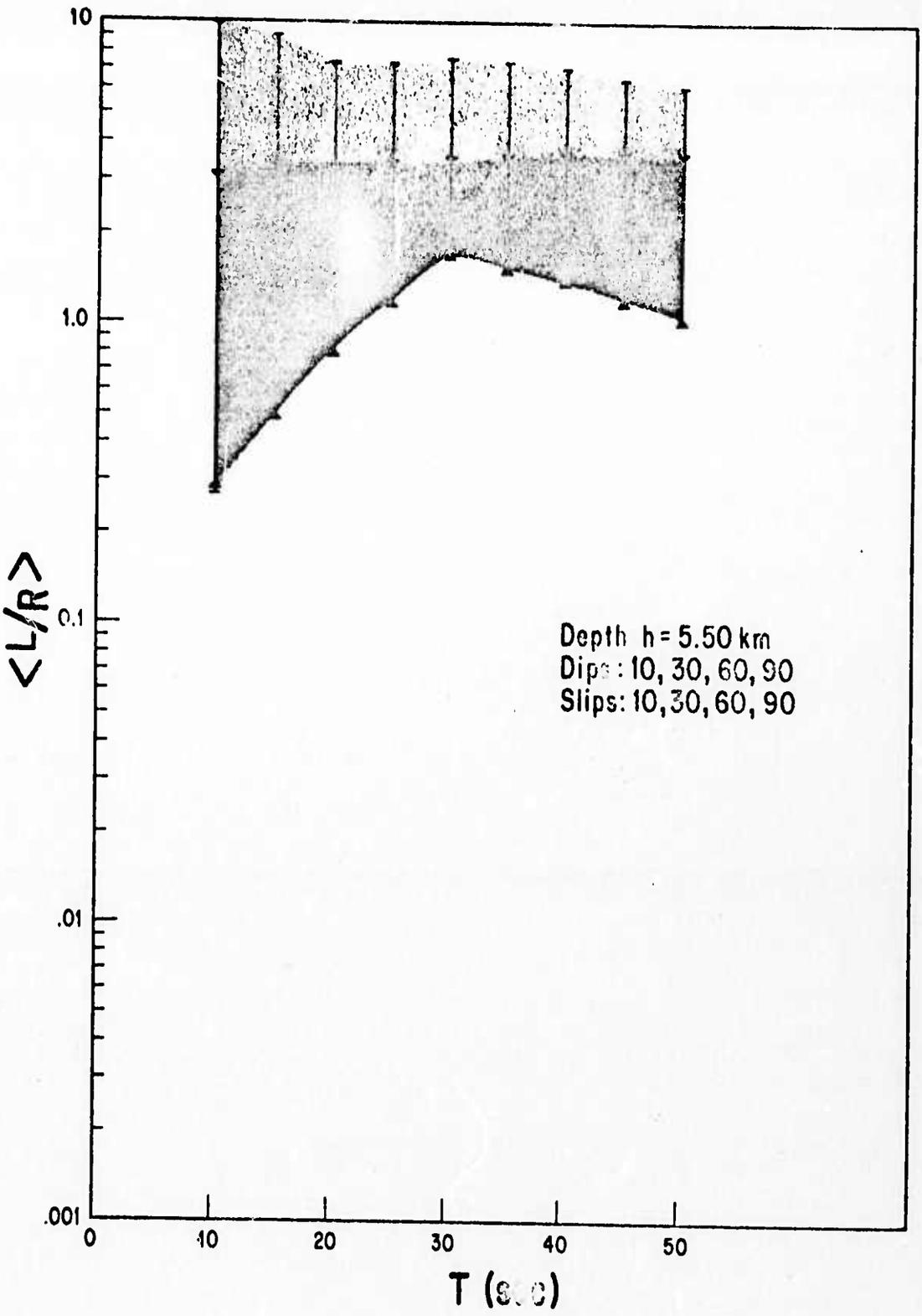
10
1.0
0.1
.01
.001
<L/R>
Depth h = 5.50 km
Dips: 10, 30, 60, 90
Slips: 10, 30, 60, 90
0
10
20
30
40
50
T (sec)

Figure 4c.

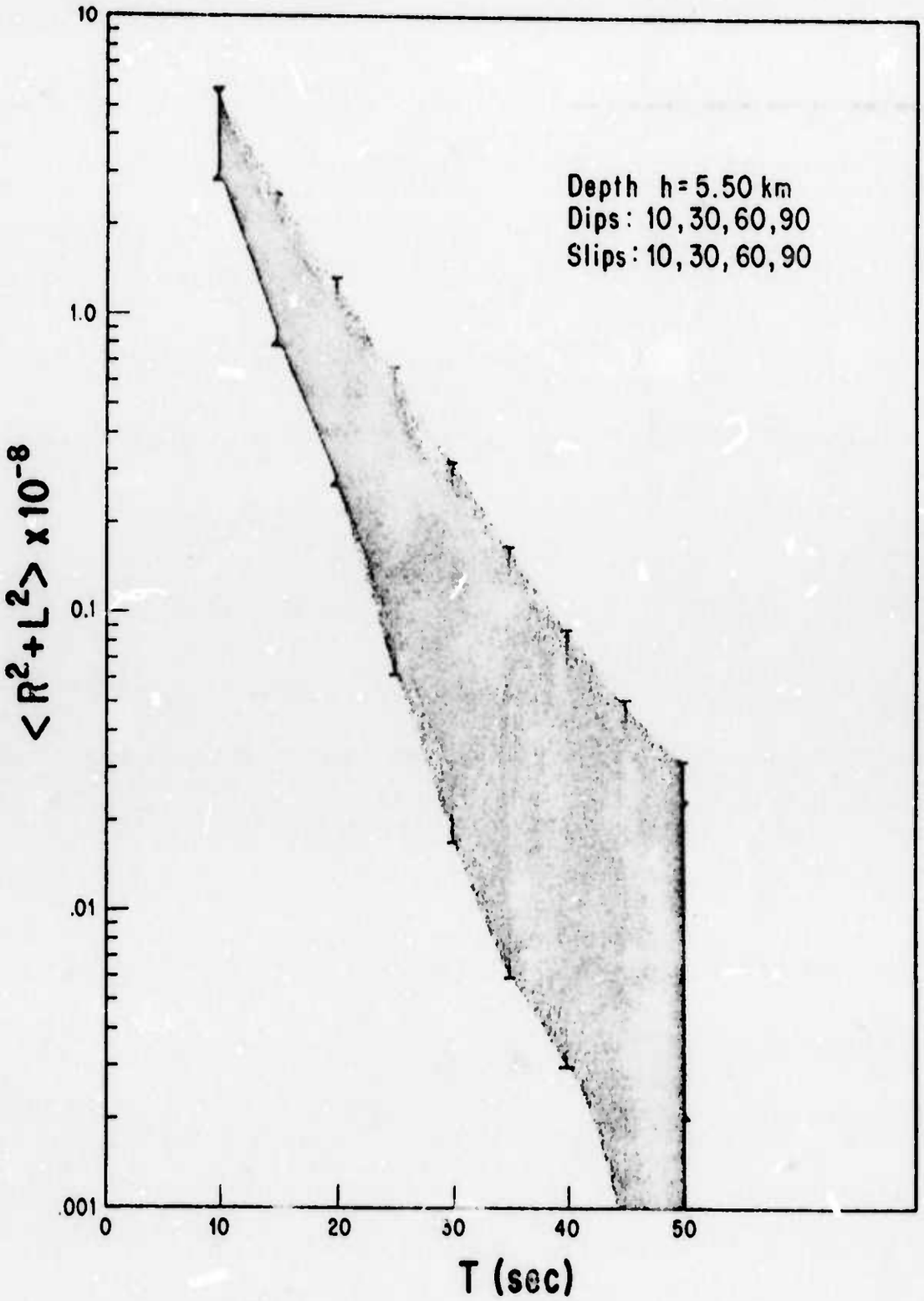
Depth h=5.50 km
Dips: 10,30,60,90
Slips: 10,30,60,90
$\langle R^2+L^2 \rangle \times 10^{-8}$
10
1.0
0.1
.01
.001
0
10
20
30
40
50
T (sec)

Figure 4d.

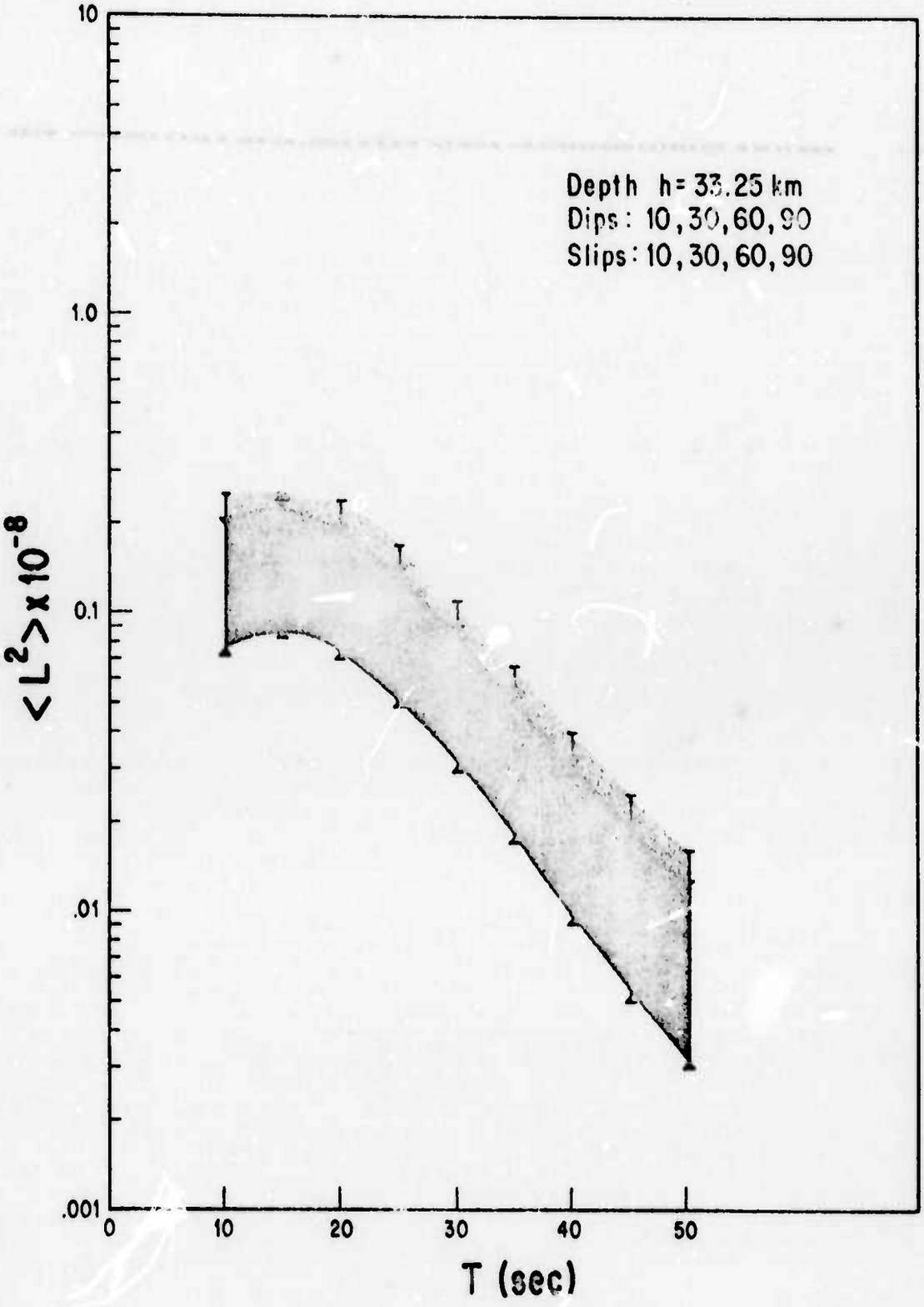
Depth h= 33.25 km
Dips: 10,30,60,90
Slips: 10,30,60,90
10
1.0
0.1
.01
.001
$<L^2>x10^{-8}$
0
10
20
30
40
50
T (sec)

Figure 5a.

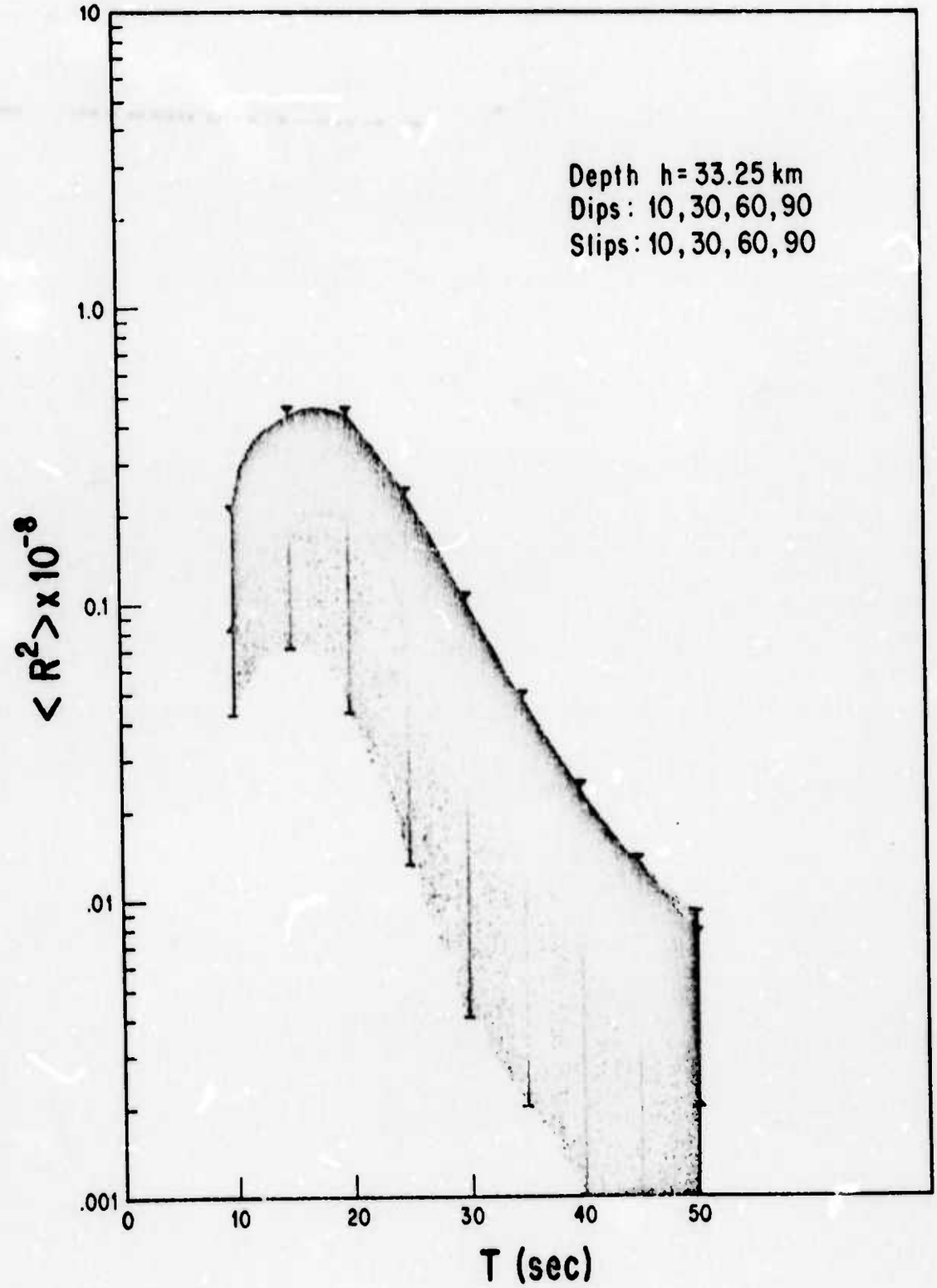
Depth h = 33.25 km
Dips: 10, 30, 60, 90
Slips: 10, 30, 60, 90
$< R^2 > x 10^{-8}$
10
1.0
0.1
.01
.001
0
10
20
30
40
50
T (sec)

Figure 5b.

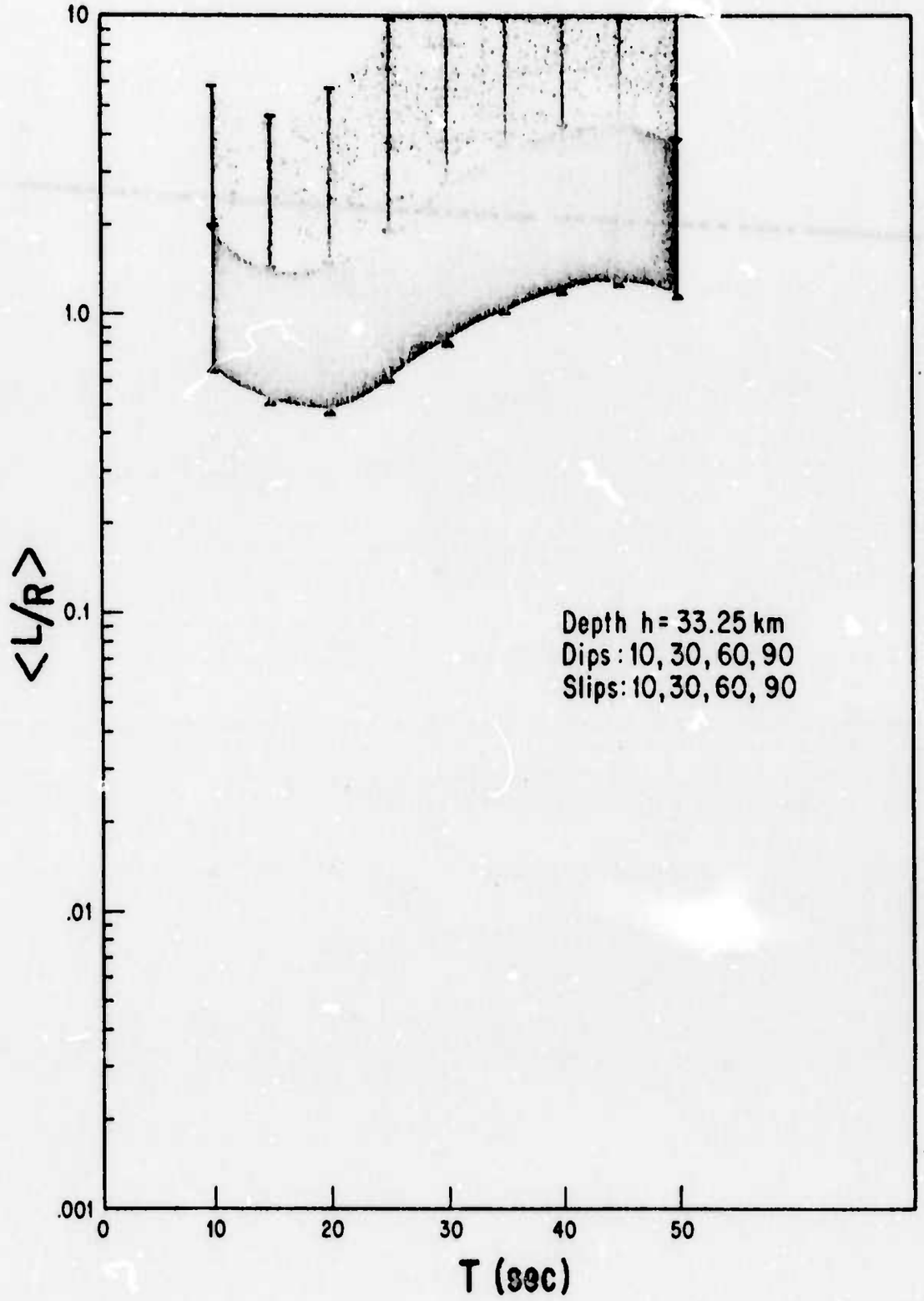
10
1.0
0.1
.01
.001
<L/R>
Depth h = 33.25 km
Dips: 10, 30, 60, 90
Slips: 10, 30, 60, 90
0
10
20
30
40
50
T (sec)

Figure 5c.

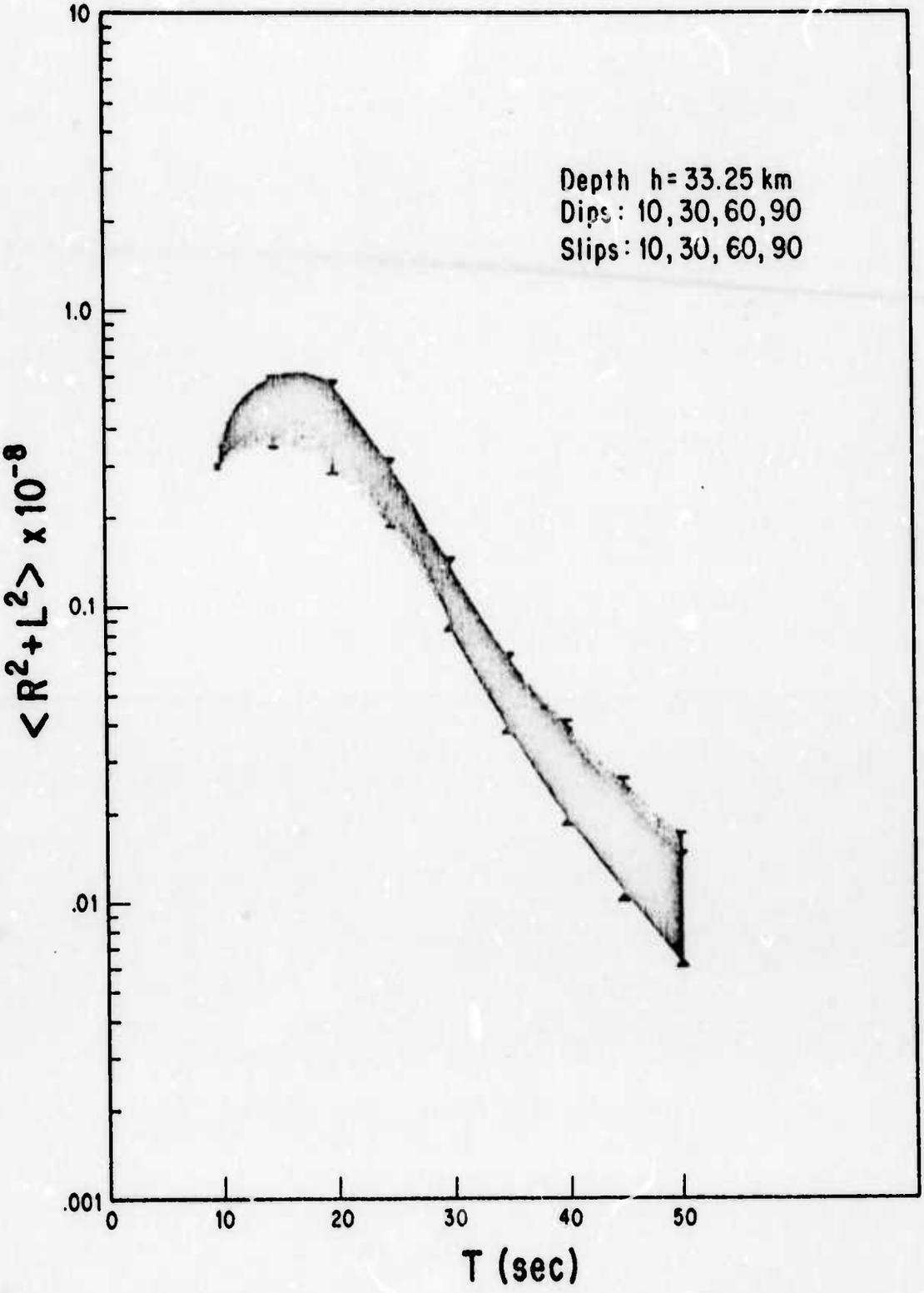
Depth h = 33.25 km
Dips: 10, 30, 60, 90
Slips: 10, 30, 60, 90
10
1.0
0.1
.01
.001
$\langle R^2+L^2 \rangle \times 10^{-8}$
0
10
20
30
40
50
T (sec)

Figure 5d.

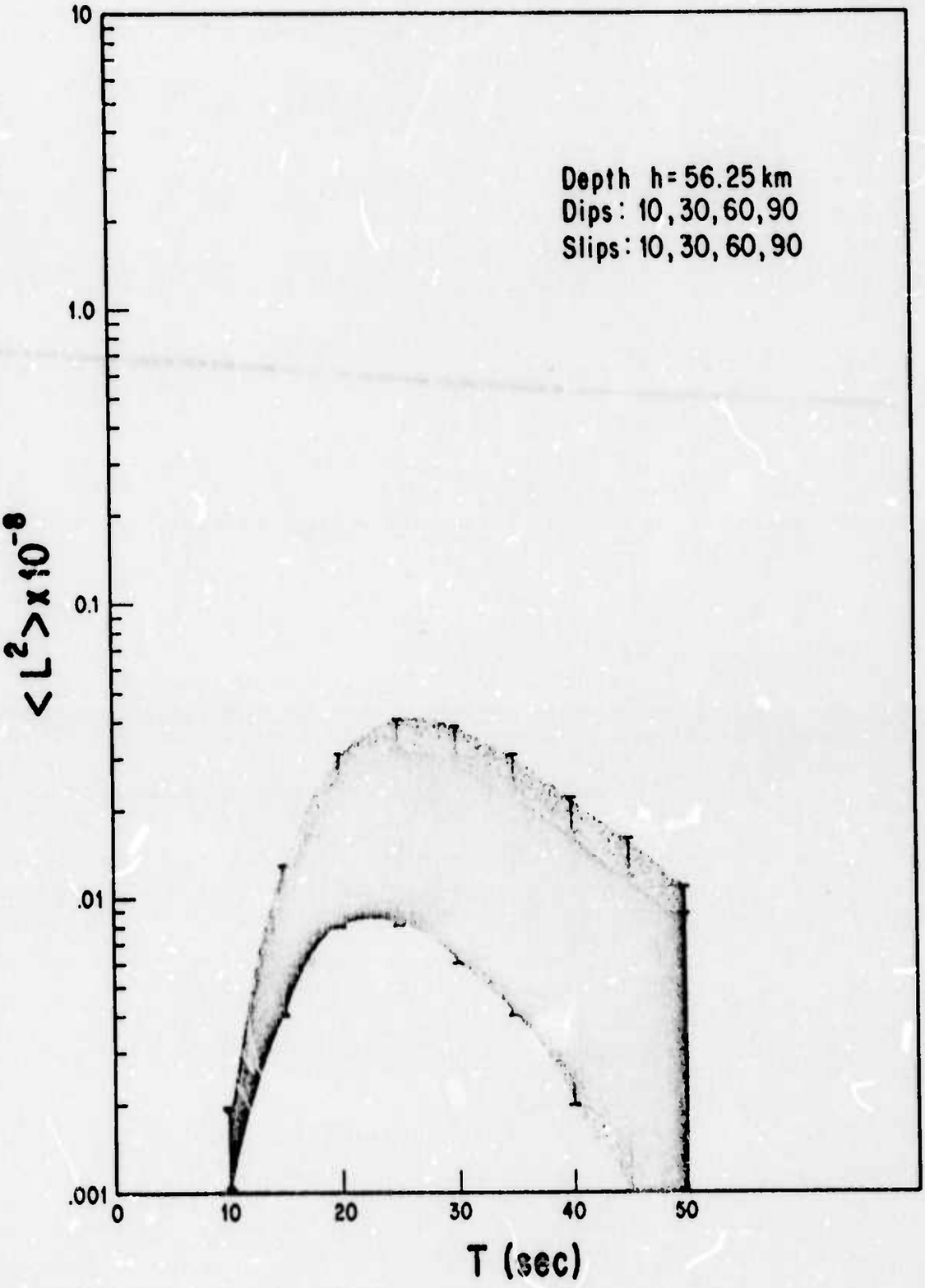
Depth h=56.25 km
Dips: 10, 30, 60, 90
Slips: 10, 30, 60, 90
$<L^2> \times 10^{-8}$
10
1.0
0.1
.01
.001
0
10
20
30
40
50
T (sec)

Figure 6a.

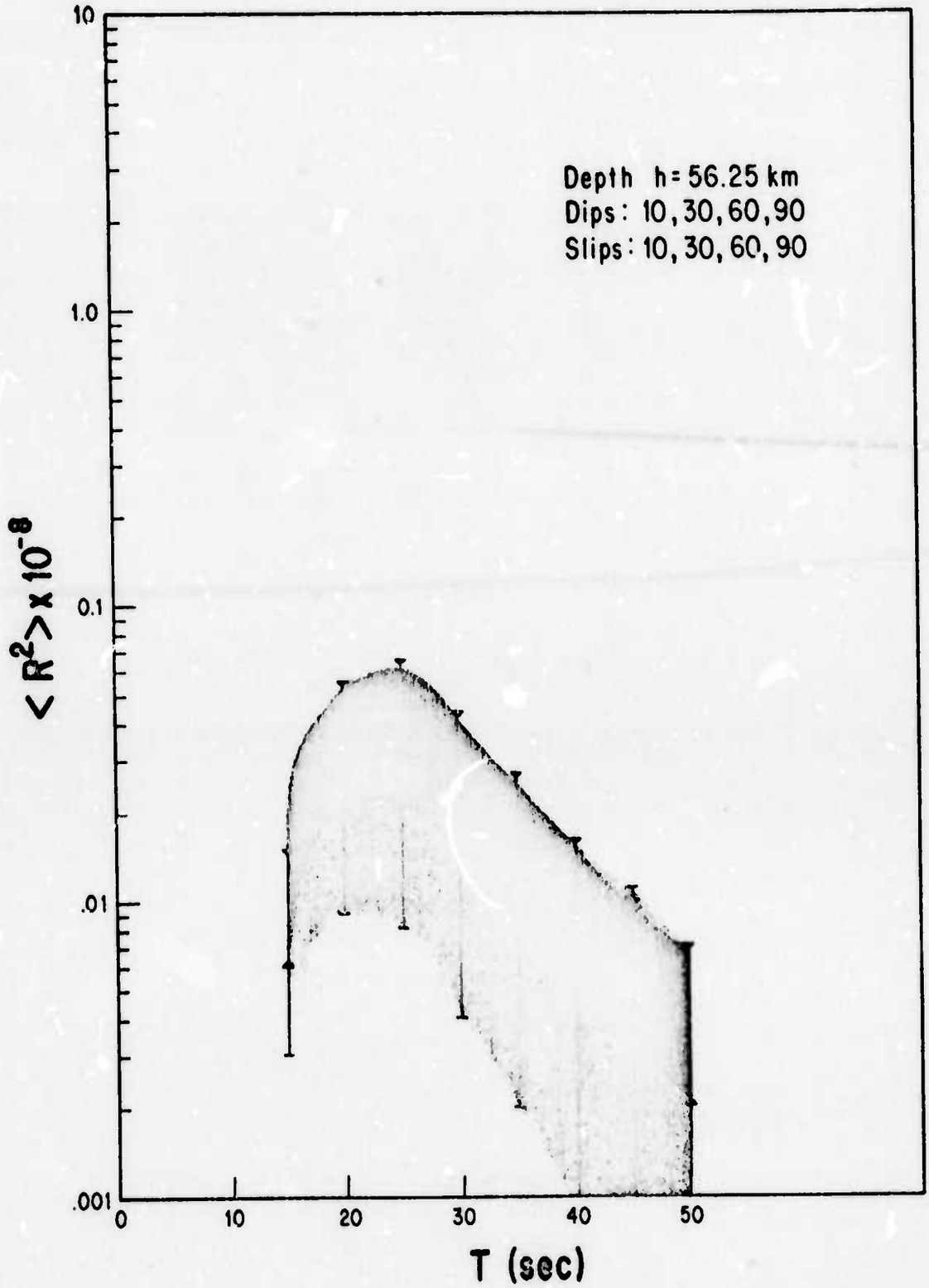
Depth h = 56.25 km
Dips: 10, 30, 60, 90
Slips: 10, 30, 60, 90
$\langle R^2 \rangle \times 10^{-8}$
10
1.0
0.1
.01
.001
0
10
20
30
40
50
T (sec)

Figure 6b.

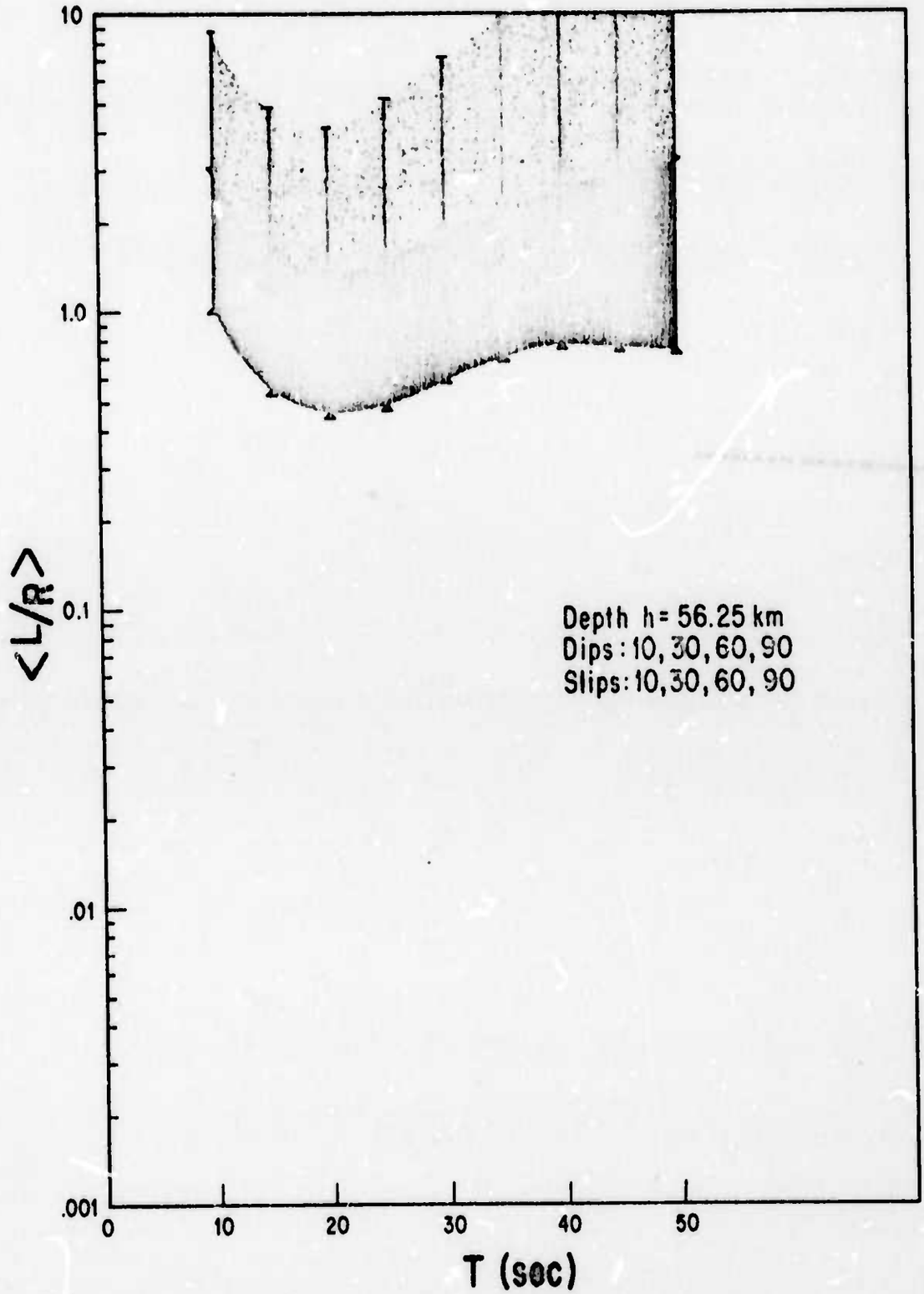
10
1.0
0.1
.01
.001
<L/R>
Depth h = 56.25 km
Dips: 10, 30, 60, 90
Slips: 10, 30, 60, 90
0
10
20
30
40
50
T (sec)

Figure 6c.

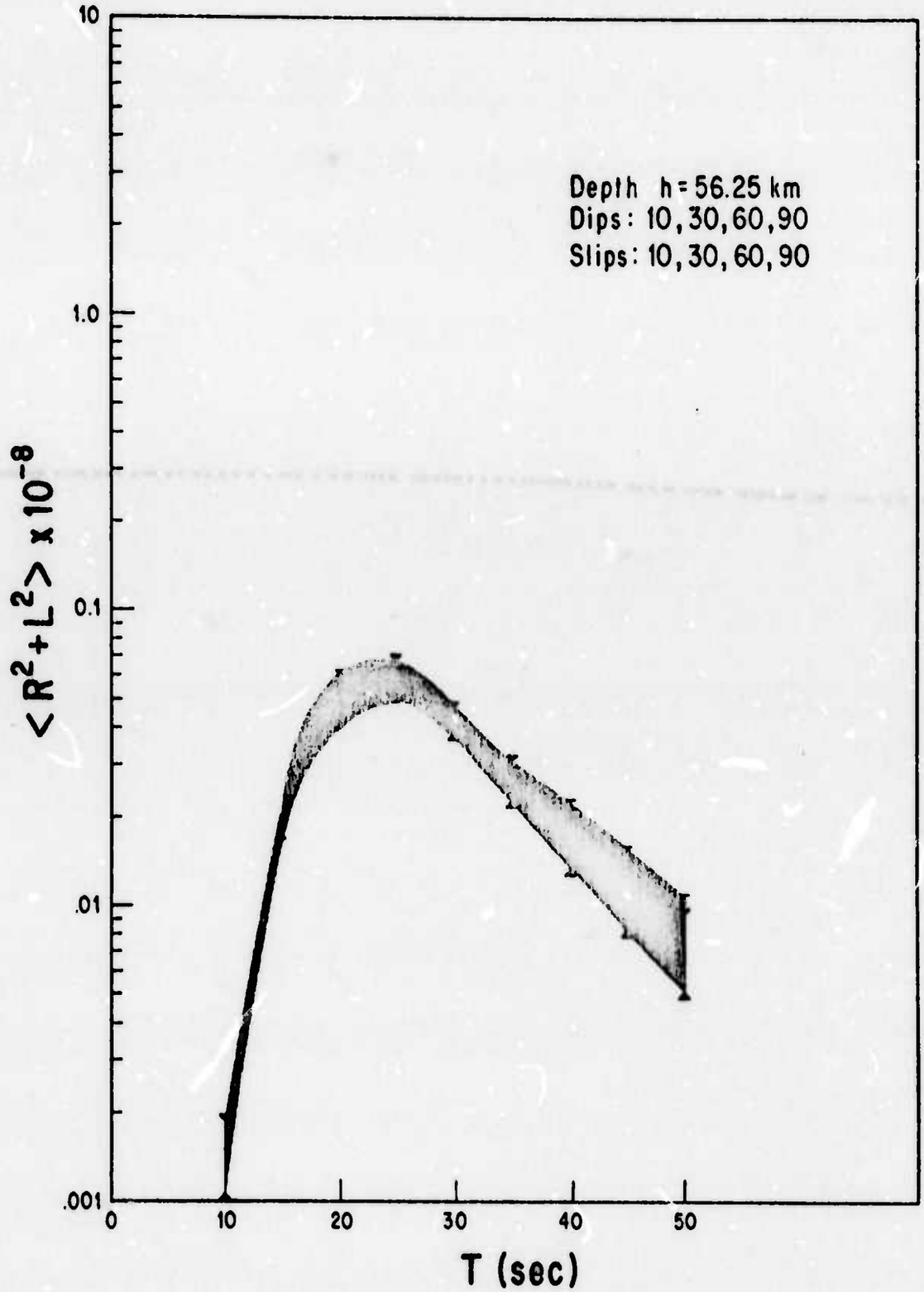
Depth h = 56.25 km
Dips: 10, 30, 60, 90
Slips: 10, 30, 60, 90
$\langle R^2+L^2 \rangle \times 10^{-8}$
10
1.0
0.1
.01
.001
0
10
20
30
40
50
T (sec)

Figure 6d.

APPENDIX II

DIFFERENTIAL SURFACE WAVE ANALYSIS AS A MEANS FOR THE SEISMIC INVESTIGATION OF INACCESSIBLE AREAS

by

R. Taylor and S. Alexander

ABSTRACT

A method of differential surface wave analysis using common-path, multiple-station recordings is developed which extends the potential of conventional surface wave studies to inaccessible areas. The method is developed theoretically and verified through a two-dimensional ultrasonic model experiment. Remote recordings of selected seismic events are used to determine group or phase velocity dispersion and amplitude of the transfer function associated with propagation between the events. The group or phase velocity determined using this approach is shown theoretically and from the results of model experiments to be independent of the source time functions, the origin time of the events, the propagation characteristics of the recording instruments. The amplitude of the tranfer function is shown in addition to be independent of source geometry for arbitrarily selected earthquake sources, except for very large events. The importance of the method is that it provides a means of utilizing the differential amplitude and phase information of remotely recorded surface waves in the investigation of instrumentally inaccessible geologic regions while assuring source effects are eliminated or reduced to an inconsequential level.

INTRODUCTION

Surface wave dispersion studies have proven highly successful in delineating the general features of the crust and upper mantle. Although individual contributions are too numerous to mention, summary articles are provided by Oliver and Dorman (1963), Kovach (1965), Nuttli (1963), Anderson (1965), Brune (1969) and Dorman (1969). While proving highly successful, the available means of analysis (Alexander, 1963; Dziewonski and Hales, 1972) limit the application of surface wave studies to instrumentally bracketed regions and are not suited to the investigation of inaccessible geologic features. Exceptions to this general rule are provided by the one-station method (Knopoff and Schwab, 1968), the path-crossing procedure (Santo, 1960a,b; 1961a,b) and the ray-path network technique (Tarr, 1969). The one-station method, however, is limited to the determination of average group velocity over long propagation paths and is not suited to the study of totally inaccessible regions of limited extent. The path-crossing and ray-path network methods are statistical in nature and require extensive instrumentation outside the region of interest. In addition, neither method provides a means of statistically determining the significance of the results.

To achieve the full potential of surface wave studies in the investigation of instrumentally inaccessible regions, additional methods of analysis are necesssary. The theoretical studies of surface wave excitation (Ben-Menahem and Harkrider, 1964, 1970; and Haskell, 1963, 1964) provide a basis for the establishment of the method developed in the present study. The resulting procedure, initially proposed by Alexander and Taylor (1969), while similar in some general respects to the methods of

phase equalization (Aki, 1960), amplitude equalization (Toksöz et al, 1964) and common-path (Marshall and Burton, 1971; Alexander and Taylor, 1968) is directed at determining the propagation characteristics of the path separating selected events rather than the excitation characteristics of the events.

Theory

The frequency transformed surface wave displacement field, recorded at point i and resulting from an event ℓ at distance $r_{i\ell}$ is given by

$$R_{i\ell}(\omega) = |I(\omega)||S_\ell(\omega)||G(\omega, r_{i\ell})|\, e^{j(k(\omega) r_{i\ell} + s_\ell(\omega) + P_i(\omega))} \tag{1}$$

where $|I_i(\omega)|e^{jP_i(\omega)}$ is the instrumental response of the recording system, $|S_\ell(\omega)|e^{js_\ell(\omega)}$ is the source excitation function appropriate to the particular mode of propagation and component of motion, and $G(\omega, r_{i2})\, e^{jk(\omega)r_{i\ell}}$ is the transfer function of the earch characteristic of the path and mode of propagation. The constant phase terms necessary in equation (1) are arbitrarily incorporated with the instrument response. Theoretical source excitation functions for a point double couple in a layered medium have been determined by Harkrider (1964), Ben-Menahem and Harkrider (1964) and Harkrider (1970) among others. Utilizing the results of these publications and including the effects of finite fault size and rupture velocity (Haskell, 1963), the excitation function in functional form with the involved dependencies indicates is

$$S(\omega) = F\ k(\omega)\, N(\omega, h)\, |L(\omega)||D(\omega, \theta, \lambda, \delta, h)||X(\omega, \theta, \lambda, \delta, h)| \times \exp\{j[\eta(\omega) - \nu(\omega, \theta, \lambda, \delta, h) + \varepsilon(\omega, \theta, \lambda, \delta, h)]\} \tag{2}$$

where

F = a constant characteristic of the evert

k(ω) = Rayleigh or Love wavenumber

θ = angle measured counterclockwise from strike of fault to station azimuth

δ = dip of fault plane

λ = rake of displacement vector measured counterclockwise from horizontal

h = source depth

$N(\omega,h)$ is the medium amplitude response as defined by Ben-Menahem and Harkrider (1964) and may be related to the medium amplitude response defined by Harkrider (1964) or the Thomson-Haskell layer matrices defined by Haskell (1953). For the purposes required here it is sufficient to note that $N(\omega,h)$ is dependent on frequency, layer thicknesses, elastic parameters of the layers and source depth but is independent of source type and geometry. $|L(\omega)|e^{j\eta(\omega)}$ is the source temporal factor or Fourier transform of the source time function and has been investigated by Haskell (1964b, 1966), Aki (1960a), Ben-Menahem and Toksöz (1962, 1963) and Tsai (1969). $|D(\omega,\Theta,\lambda,\delta,h)|e^{j(\nu(\omega,\Theta,\lambda,\delta,h))}$ is the source directivity resulting from finite fault size and rupture velocity (Ben-Menahem, 1961; Haskell, 1963; Harkrider, 1964). $|X(\omega,\Theta,\lambda,\delta,h)|e^{j(\varepsilon(\omega,\theta,\lambda,\delta,h))}$ is the source spatial term (Ben-Menahem and Toksöz, 1962, 1963; Ben-Menahem and Harkrider, 1964). In addition to the indicated dependencies this latter term is in general an inseparable function of the medium amplitude response functions and their derivatives with respect to source depth.

The functional form of the displacement field including the source excitation function is for the ℓth event at the ith station

$$R_{i\ell}(\omega) = F_\ell\, k(\omega) N(\omega,h_\ell) |L_\ell(\omega)| |D(\omega,\theta_\ell,\lambda_\ell,\delta_\ell,h_\ell)| \times |X(\omega,\theta_\ell,\lambda_\ell,\delta_\ell,h_\ell)| |I_i(\omega)| |G(\omega,r_{i\ell})| \times \exp\left\{j\left[k(\omega)r_{i\ell} + P_i(\omega) + \eta_\ell(\omega) - \nu(\omega,\theta_\ell,\lambda_\ell,\delta_\ell,h_\ell) + \varepsilon(\omega,\theta_\ell,\lambda_\ell,\delta_\ell,h_\ell)\right]\right\} \quad (3)$$

Considering the geometry of Figure 1 and temporarily suppressing the dependence on dip, rake and depth define

$$Z(\omega) = |Z(\omega)| e^{j\phi(\omega)} = \frac{R_{12}(\omega)\, R_{21}(\omega)}{R_{11}(\omega)\, R_{22}(\omega)} \tag{4}$$

$$= |D(\omega,\theta_2)|\,|X(\omega,\theta_2)|\,|D(\omega,\theta_1+\pi)|\,|X(\omega,\theta_1+\pi)|\,|G(\omega,r_{12})|\,|G(\omega,r_{21})|$$

$$\times \exp\Big\{ j\big[\varepsilon(\omega,\theta_2) - \nu(\omega,\theta_2) - \nu(\omega,\theta_1+\pi) + \varepsilon(\omega,\theta_1+\pi) + \nu(\omega,\theta_1)$$

$$- \varepsilon(\omega,\theta_1) + \nu(\omega,\theta_2+\pi) - \varepsilon(\omega,\theta_2+\pi) + k(\omega) r_{12} + k(\omega) r_{21}$$

$$- k(\omega) r_{11} - k(\omega) r_{22}\big]\Big\}$$

From the results of Ben-Menahem and Harkrider (1964)

$$|X(\omega,\theta)| = |X(\omega,\theta+\pi)| \tag{6}$$

from Aki (1964)

$$\varepsilon(\omega,\theta) - \varepsilon(\omega,\theta+\pi) = 2\varepsilon(\omega,\theta) - \pi/2 \tag{7}$$

and from Figure 1

$$r_{12} = r_0 + r_{11} \tag{8}$$

$$r_{21} = r_0 + r_{22} \tag{9}$$

Utilizing these relations and equating amplitude and phase terms in equation (5) we find

$$|Z(\omega)| = \frac{|D_2(\omega)|}{|D_1(\omega)|} |G(\omega, r_0)|^2 \tag{10}$$

$$\phi(\omega) = 2k(\omega)r_0 + \Delta\nu(\omega,\theta_1) - \Delta\nu(\omega,\theta_2) + 2\varepsilon(\omega,\theta_2) - 2\varepsilon(\omega,\theta_1) \tag{11}$$

where

$$|D_i(\omega)| e^{j\Delta\nu(\omega,\theta_i)} = \frac{|D(\omega,\theta_i)|}{|D(\omega,\theta_i+\pi)|} e^{j[\nu(\omega,\theta_i)-\nu(\omega,\theta_i+\pi)]} \tag{12}$$

Thus, the quantity $Z(\omega)$, calculated from records obtained at points remote from the source area, yields an amplitude which is independent of propagation effects outside the source area, the response of the recording instruments, the source temporal factors, the source spatial factors and the medium amplitude response. The magnitude is completely determined by the ratio of directivities resulting from finite size and rupture velocity and the amplitude of the transfer function characteristic of the source area. The phase of $Z(\omega)$ is independent of propagation effects outside the source region, instrumental phase corrections and the source temporal factors. While it is not obvious from the preceding development, the phase (equation 11) is also independent of origin time errors as the linear phase terms resulting from these effects cancels when the ratios in equation (4) are formed.

$|D(\omega,\theta_i)|$ is the amplitude directivity defined by Ben-Menahem (1961)

and is identically unity for vertical dip-slip faulting and all forms of bilateral faulting. The quantity deviates most severely from unity for strike slip faulting observed parallel to the fault strike. For this case Table 1 indicates the period range over which the directivity will contribute less than 10 percent to variations in the amplitude spectra of the event. The fault length-magnitude relation necessary to establish these

Table 1. Criteria for Neglecting the Effects of Finite Size and Rupture Velocity on Source Amplitude Spectra

Magnitude m_b	Period range over which the amplitudes will vary by less than 10 percent
5	T>10 sec
6	T>25 sec
7	T>100 sec

criterion was taken from Tocher (1958) and Schick (1968). If the fault length-magnitude relation suggested by Brune and Allen (1967) and Liebermann and Pomeroy (1970) were accepted, it would be necessary to revise the criteria of Table 1 to somewhat higher periods for a given magnitude. (See Taylor (1972) for a more detailed discussion of the construction of this table.) Assuming the directivity is determined primarily by the component of rupture toward or away from the observer the criteria of Table 1 may be considered applicable to arbitrary fault geometries. Subject to the limitations of this Table

$$|G(\omega, r_o)| = [|Z(\omega)|]^{1/2} \qquad (13)$$

or the amplitude of the transfer function characteristic of the path r_o is determined by the magnitude of $Z(\omega)$ and the results are independent of the instrumental, propagation and source effects as previously noted.

For a laterally homogeneous, spherical earth

$$|G(\omega, r_{il})| = \frac{A}{\sqrt{\sin \Delta_{il}}} e^{-\gamma(\omega) r_{il}} \tag{14}$$

where A is a constant, Δ_{il} the angular source receiver distance and $\gamma(\omega)$ the spatial decay factor. Relating $\gamma(\omega)$ to the more familiar quantity Q (Brune, 1962; Knopoff, et al. 1964; Knopoff, 1964) and using equations (5), (13) and (14)

$$Q = \frac{-2\pi r_o}{T U(\omega) \ln \left\{ \frac{\sqrt{\sin \Delta_{12} \sin \Delta_{21}}}{\sqrt{\sin \Delta_{11} \sin \Delta_{22}}} |Z(\omega)| \right\}} \tag{15}$$

where $U(\omega)$ is the group velocity. This expression gives the value of Q appropriate to the source region (r_o in Figure 1).

Returning to the phase of $Z(\omega)$, if the term

$$\Delta\phi = \Delta\nu(\omega, \theta_1) - \Delta\nu(\omega, \theta_2) + 2\varepsilon(\omega, \theta_2) - 2\varepsilon(\omega, \theta_1) \tag{16}$$

can be reduced to an acceptably small level, then the phase velocity characteristic of the path r_o is

$$C(\omega) = \frac{2\omega r_o}{\phi(\omega) \pm 2n\pi} \tag{17}$$

Conventional methods for the measurement of phase velocity are expected to yield results with an accuracy of 1% and this is considered sufficient

for the determination of useful structural information (Press, Ben-Menahem and Toksöz, 1961). Therefore, the phase velocity characteristic of the source area may be reliably calculated from the phase of $Z(\omega)$ if $\Delta\phi$ is less than 1% of ϕ. Assuming the phase terms resulting from finite size and rupture velocity, $\Delta v(\omega,\Theta_i)$, are determined primarily by the component of rupture towards or away from an observer, the maximum effect is expected from a strike slip fault observed parallel to the fault strike. Using the fault length studies of Tocher (1958) and Schick (1968) and the expression of Ben-Menahem (1961) for strike-slip faulting, the criteria of Table 2 were established. These criteria indicate the degree of fault alignment required to ensure the difference in phase directivity for Rayleigh waves is less than 0.5 percent of the total phase for a source separation of 200 km. As in the case of amplitudes, use of the fault

Table 2. Criteria for Neglecting the Differences in Phase Resulting from Finite Fault Size and Rupture Velocity.

Magnitude m_b	Required Conditions
5	Strikes aligned within 30° at Θ = 90° strikes aligned within 60° at Θ = 0° fault lengths differing by less than 50%
6	Strikes aligned within 5° at Θ = 90° strikes aligned within 35° at Θ = 0° fault lengths differing by less than 10%
7	No reasonable conditions for Θ = 90° strikes aligned within 10° at Θ = 0° fault lengths differing by less than 1%

length studies of Brune and Allen (1967) and Liebermann and Pomeroy (1970) would require a revision in the criteria of this Table or an increase in the considered source separation. (See Taylor (1972) for a more detailed discussing of these criteria.) In any case, the criteria are sufficiently relaxed for moderate magnitude events to ensure the existence in most seismic areas of numerous event pairs for which the effect of finite size and rupture velocity may be neglected.

If the influence of finite size and rupture velocity on the phase spectra is considered negligible, then a sufficient condition to ensure the validity of equation (17) is

$$\mathcal{E}(\omega,\theta_2) - \mathcal{E}(\omega,\theta_1) \leq 0.01\, k(\omega) r_o \qquad (18)$$

Confining attention to double couple source types, this condition is automatically satisfied for vertical strike-slip faulting, vertical faulting with equal components of strike and dip and any surface source since in these cases the individual terms are zero. For arbitrary fault geometries the required inequality implies a degree of similarity in the selected events. The numerical evaluation (Turnbull, 1970) of the expression for initial phase (Ben-Menahem and Harkrider, 1964) for a number of fault geometries in an oceanic-type structure indicates that at points removed from an amplitude null, alignment of about 25° in the fault strikes, 15° in the fault dips and 15° in the rake of the slip vector is sufficient to ensure the validity of the above inequality for a source separation of 200 km. However, the number of parameters involved, ω, Θ, λ, δ and h makes it extremely difficult to establish unequivocal conditions of fault similarity and the above conditions are intended only as a guide. However, using

these requirements as a guide, the source mechanisms studies of Syed and Nuttli (1971), Wu (1970), Sylvester, et al. (1970), Fitch (1970) and Sykes (1967, 1970a,b) indicate that selected event subsets within a seismic area commonly can be found that satisfy the inequality of equation (18) for source separations on the order of 200 km.

Because it is not reasonable to establish rigid similarity requirements or to demonstrate the desired conditions could be satisfied in arbitrary regions an alternate procedure was developed that uses both the consistency of results from a number of independent measurements within a seismic area and an expression that requires no further information than the $R_{i\ell}$ determination used above. Thus, if consistent results are obtained from a number of events at differing source separations within a given region, it is reasonable to assume that the fault geometries are sufficiently similar to make the difference in the spatial phase terms negligible. Since any area satisfying the geometry requirements of Figure 1 will usually be characterized by a number of events, the use of numerous sources poses no problems. The ability of the method proposed here to provide independent velocity measurements is a feature not available from the statistical methods of Santo (1960a,b; 196la,b) or Tarr (1969).

In addition to the consistency of results, an indication of fault similarity for any two events can be inferred from the calculated quantity

$$|V(\omega)|^{1/2} = \left[\frac{|R_{11}(\omega)||R_{21}(\omega)|}{|R_{12}(\omega)||R_{22}(\omega)|}\right]^{1/2} = \frac{F_1|L_1(\omega)||\chi(\omega,\theta_1,\lambda_1,\delta_1,h_1)|\,N(\omega,h_1)}{F_2|L_2(\omega)||\chi(\omega,\theta_2,\lambda_2,\delta_2,h_2)|N(\omega,h_2)} \qquad (19)$$

From the mathematical form of the functions L, χ and N, and physical

considerations, if $[|V(\omega)|]^{1/2}$ is independent of frequency, it is expected that

$$|L_1(\omega)| = |L_2(\omega)| \tag{20}$$

$$|\mathcal{X}(\omega,\theta_1,\lambda_1,\delta_1,h_1)| = |\mathcal{X}(\omega,\theta_2,\lambda_2,\delta_2,h_2)| \tag{21}$$

$$N(\omega,h_1) = N(\omega,h_2) \tag{22}$$

The equivalence of the temporal factors is expected for small events (Tsai, 1969) and the terms could have been neglected in equation 19. The equivalence of the medium amplitude response implies the events were at similar depths in geologic setting with similar vertical structure profiles. The independence of $[|V(\omega)|]^{1/2}$ as a function of frequency is particularly significant in terms of the medium responses, $N(\omega,h_1)$ and $N(\omega,h_2)$, as these functions are highly dependent on frequency and source depth for shallow events (Tsai and Aki, 1970). In view of the linear independence of the frequency dependent terms comprising the source spatial factors, the amplitude equivalence of these terms is a necessary condition for equivalence of the fault geometries. From general considerations it may be assumed the equivalence is also a sufficient condition. This is particularly true, if for all combinations of events within a seismic area, taken two at a time, the quantity $[|V(\omega)|]^{1/2}$ is independent of frequency. Hence if $[|V(\omega)|]^{1/2}$ is found to be independent of frequency for selected event subsets within a seismic area and the phase velocities calculated

from these events are self-consistent, it is reasonable to infer that the fault geometries are sufficiently similar to ensure the difference in spatial phase terms is negligible. Under these conditions the phase velocities, calculated from observations remote to the source area, will provide a reliable measure of surface wave dispersion within the source area.

Lateral heterogeneity in structure can also cause $[V(\omega)]^{1/2}$ to be frequency dependent even though the fault geometries may be identical because the medium response $N(\omega,h)$ will be different. Thus, invariance of $[V(\omega)]^{1/2}$ with frequency is a strong constraint assuring similarity of spatial phase terms. If the fault geometry and depth are known to be identical from independent data, then $[V(\omega)]^{1/2}$ is a direct measure of the relative medium response (structure) at the two source locations; an experimental example verifying this assertion will be presented in a later section.

Group velocities appropriate to the source area may be calculated from the phase velocity or from the quantity $\frac{d\phi(\omega)}{d\omega}$. From calculations for different fault geometries it appears that the fault similarity criteria required for the reliable determination of group velocity from $\frac{d\phi(\omega)}{d\omega}$, are less stringent than the fault similarity criteria required for the reliable determination of phase velocity from $\phi(\omega)$.

The advantages of this approach are that: (1) only fixed remote stations are required to investigate the structure of inaccessible source areas; (2) origin time errors are eliminated; (3) no corrections for path effects to distant receivers are needed; and (4) a test is provided to assure that source phase terms do not affect the calculated dispersion curves.

ULTRASONIC MODEL STUDY

In the preceding development it was implicitly assumed that the geologic structures in the selected source regions were characterized by plane parallel layering. Actual structure in tectonic areas may change rapidly over short distances and cannot in general be characterized by plane parallel layering. Since theoretical treatments of initial surface wave phase and amplitude spectra in laterally inhomogeneous regions do not exist, a two-dimensional ultrasonic model study was employed to determine the effect of source area inhomogeneities on the results of the proposed method.

Conventional two-dimensional modeling techniques were employed (Oliver, et al., 1954; Abe and Suzuki, 1970). The models employed (Figure 2) were fabricated from polystyrene and plexiglas. The layer over a half space was used for calibration purposes in keeping with the suggestion of Faizullin (1966) that all model studies should incorporate the results from standard models for which established theoretical results are available.

The Rayleigh wave phase and group velocities determined for the simply layered half space in the conventional two-station manner are compared with theoretically expected results in Figure 3. The amplitude decay associated with propagation between the recording sites is shown in Figure 4a. These figures provide the results from standard models as proposed by Faizullin (1966) and demonstrate that consistent transducer coupling and rigid material bounding was achieved an important consideration as pointed out by Toksöz and Schwab and Burridge (1968).

Substituting sources (transmitters) at the receiver sites, the previously defined quantity $[|V(\omega)|]^{1/2}$ was calculated from the waveforms recorded at points remote from the source area. The calculated values of $[|V(\omega)|]^{1/2}$

are shown in Figure 4b and they are seen to be clearly frequency independent. The independence is expected since the source temporal factors, spatial factors and source layering are identical. The phase and group velocity and amplitude decay, calculated from the previously defined quantity $Z(\omega)$, are shown in Figures 3 and 4a where the equivalence of the conventional two-station method and common path procedure is evident.

Source area geometries investigated for which theoretical results are not available consist of models of topographic relief and a lateral discontinuity. The source and receiver positions and the recorded waveforms are shown in Figures 5 and 6 for each model. The quantity $[|V(\omega)|]^{1/2}$ calculated from these waveforms and shown in Figure 7 for each case is strongly frequency dependent. While the medium amplitude responses for these geometries are not known, they may be empirically determined from the P-wave excitation below each source. The ratio of the medium responses determined in this manner is also plotted in Figure 7. The similarity of the functions defined by the data of Figure 7 indicates the common path procedure has reliably determined the ratio of medium amplitude responses associated with each source.

When applied to natural events the frequency dependence of the data of Figure 7 would cause the calculation of phase velocity for that particular event pair to be suspect. Under the known conditions of the model study, however, it is possible to determine to what extent the directionally dependent medium responses has affected the calculated phase velocities. The phase velocity for the model of topographic relief, calculated by the differential analysis of the waveforms of Figure 5, is compared with the conventional two station determination for propagation across the

transition region in Figure 8a. The theoretical dispersion curves appropriate to the two constant sections of the model are also indicated for reference. While the difference in up-dip and down-dip velocity noted by Alexander (1963) and Abe and Suzuki (1970) is evident in Figure 8a, the phase velocities determined from differential analysis defines an average dispersion curve, within the accuracy of the system, appropriate to the transition region. The phase velocity for the laterally discontinuous model (Figure 2a), determined by differential analysis from the waveforms of Figure 6, is compared with the conventional two station determination for propagation across the discontinuous region in Figure 8b. It is again evident that the dispersion curve defined by differential dispersion is identical, within the accuracy of the system, to the curve defined by the conventional two station measurements. Thus, the model results suggest that lateral inhomogeneities within the source area will not significantly affect the phase velocities calculated and the quantity $[|V(\omega)|]^{1/2}$ is a reliable measure of changes in the geologic structure associated with each event.

The amplitude decay determined by differential analysis, for propagation across the inhomogeneous region of Figures 5 and 6 is plotted in Figures 9a and b. The amplitude decay determined in the conventional two station manner by interchanging the transmitter and sources of Figures 5 and 6 and averaging the measured decay for each direction of propagation, is plotted in the same Figure. The theoretical amplitude decay expected to result from the material Q is also shown for reference. While for each model the two station and differentially determined decays are identical, within the accuracy of the system, they are both significantly in excess of the decay expected to result from material Q. This is a result of reflection, conversion and vertical redistribution of energy

within the transition region and suggests the use of differentially determined decay as an indication and possible measure of inhomogeneity within the source region. A comparison of Figures 8 and 9 also suggests that while appreciable amplitude distortion may result from propagation through the inhomogeneous region, the phase is essentially determined by the dispersion characteristics of an average section.

In general the model results demonstrate the utility of the quantity $[|V(\omega)|]^{1/2}$ as a means of determining similar geologic structure in the immediate vicinity of the selected sources and the validity of the phase velocity calculated from the differential analysis. The results also demonstrate that the amplitude decay resulting from propagation in the source region may be reliably determined by the procedure. However, the resulting decay is strongly dependent upon the geometry of the transversed region and may be related to material Q only if the region is known to be laterally homogeneous.

CONCLUSIONS

Present methods for utilizing surface wave observations in the investigation of inaccessible areas rely upon the statistical treatment of large data sets and are limited to the determination of group velocity (Tarr, 1969; Santo, 1960a,b; 1961a,b). The differential analysis procedure proposed here is an alternative to these methods and relies directly upon the mechanics of surface wave generation and propagation to determine amplitudes and phase effects associated with the propagation path. Thus, the method provides a means for the investigation of tectonic regions through surface wave observations without requiring instrumentation in the region. It is equally applicable to all modes of Rayleigh and Love wave propagation.

Amplitude effects are in general related to attenuation or magnification along the propagation path, source parameters and instrumental factors. The amplitude determined in the proposed manner is independent of all source parameters (except for large magnitude events), propagation effects outside the source region and all instrumental factors. Therefore the results are completely determined by the attenuation and geometrical factors characteristic of the source area; for a laterally homogeneous region the observed amplitude ratios can be directly related to the material Q.

The phase or group velocities determined using differential analysis are independent of origin time errors, source time functions, propagation effects outside the source region and instrumental factors. While the velocities are dependent to some extent on source geometries, the dependence may be reduced to a negligible level through careful selection of the events. In addition, an independent indication of the degree of similarity among events can be obtained from the same data necessary for application of the

method. Finally, because most seismic areas are characterized by a distribution of many events, independent pair-wise determinations of velocities or amplitude effects may be statistically tested for significance or combined for increased precision.

The results of the ultrasonic model study indicate the general validity of the method. In particular, the results from the models containing lateral changes within the source region demonstrate the relation of measured phase velocity to average structural properties. However, the measured amplitude decay while equivalent to that determined in the conventional manner, is unrelated to the decay expected to result from material attenuation. This suggests that the observed amplitude decay can be used as a measure of source area inhomogeneity. Applications of this nature require greater theoretical knowledge of amplitudes expected in laterally changing regions than is presently available. However, very soon the use of dynamic finite element codes should provide suitable numerical solutions for complicated structure and allow better interpretation of observed amplitudes.

The method presented here has also been applied successfully to an area on the mid-Atlantic Ridge. The results of that study are presented in the companion paper that follows (Taylor and Alexander, 1973).

REFERENCES

Abe, M. and Z. Suzuki, A Model-Seismological Study on the Propagation of Rayleigh Waves in a Medium with a Dipping Boundary Between Superficial Layer and Basement, Science Reports on the Tohoku University, Geophysics Series, 20, 1-25, 1970.

Aki, K., The Interpretation of Source Functions of Circum-Pacific Earthquakes Obtained From Long Period Rayleigh Waves, Jour. Geophys. Res., 65, 2405-2419, 1960a.

Aki, K., The Use of Love Waves for the Study of Earthquake Mechanism, Jour. Geophys. Res., 65, 323-337, 1960b.

Aki, K., Study of Earthquake Mechanisms by a Method of Phase Equalization Applied to Rayleigh and Love Waves, Jour. Geophys. Res., 65, 729-740, 1960c.

Alexander, S. S., Surface Wave Propagation in the Western United States, Ph.D. Thesis, Cal. Inst. Tech., Pasadena, Calif., 1963.

Alexander, S. S., and R. Taylor, Spectral Estimates for Weak Teleseismic Surface Waves, Trans. Am. Geophys. Union, 49, 718, 1968.

Alexander, S. S., and R. W. Taylor, Source Parameters and Crustal Structure in Active Seismic Areas from Relative Event Analysis, Trans. Am. Geophys. Union, 59, 240, 1969.

Anderson, D., Recent Evidence Concerning the Structure and Composition of the Earth's Mantle, Phys. and Chem. of the Earth, 6, 1-132, 1965.

Ben-Menahem, A., Radiation of Seismic Surface Waves from Finite Moving Sources, Bull. Seis. Soc. Am., 51, 401-435, 1961.

Ben-Menahem, A., and M. N. Toksoz, Source Mechanism from Spectra of Long-Period Seismic Surface Waves, 1. The Mongolia Earthquake of December 4, 1957, Jn. Geophys. Res., 67, 1943-1955, 1962.

Ben-Menahem, A , and M. N. Toksoz, Source Mechanism from Spectrums of Long Period Surface WAves, 2. The Kamchatka Earthquake of November 4, 1962, Jn. Geophys. Res., 68, 5207-5222, 1963.

Ben-Menahem, A., and D. G. Harkrider, Radiation Patterns of Seismic Surface Waves from Dipolar Point Sources in a Flat Stratified Earth, Jn. Geophys. Res., 69, 2605-2620, 1964.

Ben-Menahem, A., Observed Attenuation and Q Values of Seismic Surface Waves in the Upper Mantle, Jn. Geophys. Res., 70, 4641-4651, 1965.

Brune, J. N., Attenuation of Dispersed Wave Trains, Bull. Seis. Soc. Am., 52, 109-112, 1962.

Brune, J. N., and C. R. Allen, A Low Stress Drop, Low-Magnitude Earthquake with Surface Faulting: The Imperial, California Earthquake of March 4, 1966, Bull. Seis. Soc. Am., 57, 501-514, 1967.

Brune, J. N., Surface Waves and Crustal Structure, The Earth's Crust and Upper Mantle, ed. P. J. Hart, Monograph 13, Am. Geophys. Union, 230-242, 1969.

Dorman, J., Seismic Surface-Wave Data on the Upper Mantle, The Earth's Crust and Upper Mantle, ed. P. J. Hart, Monograph 13, Am. Geophys. Union, 257-265, 1969.

Dziewonski, A. M. and A. L. Hales, Methods in Computational Physics, Vol 11, ed. B. A. Bolt, B. Alder, S. Fernbach, M. Ratenberg, Academic Press, 1972.

Faizullin, I. S., On Estimating the Accuracy of Seismic Modeling, Akad. Nauk SSSSR, Izvestiya, Physics of the Solid Earth, 665-666, 1966.

Fitch, T. J., Earthquake Mechanisms and Island Arc Tectonics in the Indonesian-Philippine Region, Bull. Seis. Soc. Am., 60, 565-591, 1970.

Harkrider, D. G., Surface Waves in Multilayered Elastic Media, I. Rayleigh and Love Waves from Buried Sources in a Multilayered Elastic Half Space, Bull. Seis. Soc. Am., 54, 627-680, 1964.

Harkrider, D. B., Surface Waves in Multilayered Elastic Media, Part II Higher Mode Spectra and Spectral Ratios from Point Sources in Plane Layered Models, Bull. Seis. Soc. Am., 60, 1937-1987, 1970.

Haskell, N. A., The Dispersion of Surface Waves on a Multi-layered Media, Bull. Seis. Soc. Am., 43, 17-34, 1953.

Haskell, N. A., Radiation Pattern of Rayleigh Waves from a Fault of Arbitrary Dip and Direction of Motion in a Homogeneous Medium, Bull. Seis. Soc. Am., 53, 619-642, 1963.

Haskell, N. A., Total Energy and Energy Spectral Density of Elastic Wave Radiation from Propagating Faults, Bull. Seis. Soc. Am., 54, 1811-1841, 1964.

Knopoff, L., Q, Reviews of Geophysics, 2, 625-660, 1964.

Knopoff, L., K. Aki, C. B. Archambeau, A. Ben-Menahem and J. A. Hudson, Attenuation of Dispersed Waves, Jour. Geophys. Res., 69, 1655-1657 1964.

Knopoff, L., and F. A. Schwab, Apparent Initial Phase of a Source of Rayleigh Waves, Jour. Geophys. Res., 73, 755-760, 1968.

Kovach, R., Seismic Surface Waves: Some Observations and Recent Developments, Phys. and Chem. of the Earth, 6, 251-314, 1965.

Liebermann, R. C., and P. W. Pomeroy, Source Dimensions of Small Earthquakes as Determined from the Size of the Aftershock Zone, Bull. Seis. Soc. Am., 60, 879-890, 1970.

Marshall, P. D., and P. W. Burton, The Source Layering Function of Underground Explosions and Earthquakes - An Application of a "Common Path" Method, Geophys. J. R. Astr. Soc., 24, 533-537, 1971.

Nuttli, O., Seismic Evidence Pertaining to the Structure of the Earth's Upper Mantle, Rev. Geophys., 1, 351-400, 1963.

Oliver, J., F. Press and M. Ewing, Two-Dimensional Model Seismology, Geophysics, 19, 202-219, 1954.

Oliver, J. F., and J. Dorman, Exploration of Sub-Oceanic Structure by the Use of Seismic Surface Waves, The Sea, M. N. Hill, ed., 3, 110-133, 1963.

Press, F., A. Ben-Menahem and M. N. Toksoz, Experimental Determination of Earthquake Fault Length and Rupture Velocity, Jn. Geophys. Res., 66, 3471-3485, 1961.

Santo, T. A., Observations of Surface Waves by Columbia-Type Seismograph Installed at Tsukula Station, Japan, Part I, Rayleigh Wave Dispersion Across the Oceanic Basin, Bull. Earthquake Res. Inst., 38, 219-240, 1960a.

Santo, T. A., Part II, Rayleigh Wave Dispersion Across the Oceanic Basin Around Japan. Bull. Earthquake Res. Inst., 38, 385-401, 1960b.

Santo, T. A., Rayleigh Wave Dispersion Across the Oceanic Basin Around Japan, (Part III) - On the Crust of the Southwestern Pacific Ocean, Bull. Earthquake Res. Inst., 39, 1-22, 1961a.

Santo, T. A., Division of the Southwestern Pacific Into Several Regions in Each of Which Rayleigh Waves Have the Same Dispersive Character, Bull. Earthquake Res. Inst., 39, 603-620, 1961b.

Schick, V. R., Untersuchungen Uber die Bruchausdehnung und Bruchgeschwindigkeit bie Erdbeden mit Kleinen Magnituden (M4)., Zeitschr. Geophysik, 34, 267-286, 1968.

Schwab, F., Accuracy in Model Seismology, Geophysics, 32, 819-826, 1968.

Schwab, F., and R. Burridge, The Interface Problem in Model Seismology, Geophysics, 33, 473-480, 1968.

Syed, A. A., and O. W. Nuttli, A Method of Connecting P-Wave Magnitudes for the Effect of Earthquake Focal Mechanism, Bull. Seis. Soc. Am., 61, 1811-1826, 1971.

Sykes, L. R., Mechanism of Earthquakes and Nature of Faulting on the Mid-Oceanic Ridges, Jn. Geophys. Res., 72, 2131-2147, 1967.

Sykes, L. R., Earthquake Swarms, Jn. Geophys. Res., 75, 6598-6611, 1970a.

Sykes, L. R., Focal Mechanism Solutions for Earthquakes Along the World Rift System, Bull. Seis. Soc. Am., 1749-1752, 1970b.

Sylvester, A. G., S. W. Smith and C. H. Scholz, Earthquake Swarm in the Santa Barbara Channel, California, 1968, Jour. Geophys. Res., 60, 1047-1060, 1970.

Tarr, A. C., Rayleigh Wave Dispersion in the North Atlantic Ocean, Caribbean Sea and Gulf of Mexico, Jn. Geophys. Res., 74, 1591-1607, 1969.

Taylor, R. W., Relative Event Analysis with Application to the Mid-Atlantic Ridge, Ph.D. Thesis, The Penna. State Univ., Univ. Park, Pa., 1972.

Tocher, D., Earthquake Energy and Ground Breakage, Bull. Seis. Soc. Am., 48, 147-153, 1958.

Toksöz, M. N., A. Ben-Menahem and D. G. Harkrider, Determination of Source Parameters of Explosions and Earthquakes by Amplitude Equalization of Seismic Surface Waves, Jn. Geophys. Res., 69, 4355-4366, 1964.

Toksöz, M. N., and F. Schwab, Bonding of Layers in Two-Dimensional Seismic Modeling, Geophysics, 29, 405-413, 1964.

Tsai, Y. B., Determination of Focal Depths of Earthquakes in the Mid-Oceanic Ridges from Amplitude Spectra of Surface Waves, Ph.D. thesis, Mass. Inst. of Tech., Cambridge, Mass., 1969.

Tsai, Y., and K. Aki, Precise Focal Depth Determination From Amplitude Spectra of Surface Waves, Jn. Geophys. Res., 75, 5729-5743, 1970.

Turnbull, L. S., Personal Communication, The Pennsylvania State University, Dept. Geosciences, University Park, Pa., 1970.

Wu, F. T., Focal Mechanisms and Tectonics in the Vicinity of Taiwan, Bull. Seis. Soc. Am., 2045-2056, 1970.

CAPTIONS

Figure 1 Plan view and vertical cross-section of assumed source-receiver geometry.

Figure 2 The models employed in this study.

Figure 3 Phase velocity, C, and group velocity, U, determined by the conventional two-station method and by differential dispersion analysis compared to the theoretically expected results, for a layer over a half-space model.

Figure 4 a. Amplitude decay, $|V(\omega)|^{1/2}$, for a layer over a half-space model.
b. Predicted source amplitude ratios, solid lines are theoretically expected results.

Figure 5 Recorded waveforms obtained at distance X for the model of topographic relief using the indicated source-receiver geometry.

Figure 6 Recorded waveforms obtained at distance X for the model containing a lateral discontinuity using the indicated source-receiver geometry; origin times are arbitrary.

Figure 7 Source amplitude ratios for a. model of topographic relief, b. model containing a lateral discontinuity; origin times are arbitrary.

Figure 8 Phase velocity determined by differential dispersion, compared with the velocity determined in the conventional two-station method for a. model of topographic relief; solid lines indicate theoretical velocities for each section, b. model containing a lateral discontinuity; solid line indicates theoretical velocity for an average section.

Figure 9 Amplitude decay, $|V(\omega)|^{1/2}$, determined by differential dispersion analysis and the conventional two-station method for a. model of topographic relief, b. model containing a lateral discontinuity; solid lines indicate decay expected to result from material Q for average section.

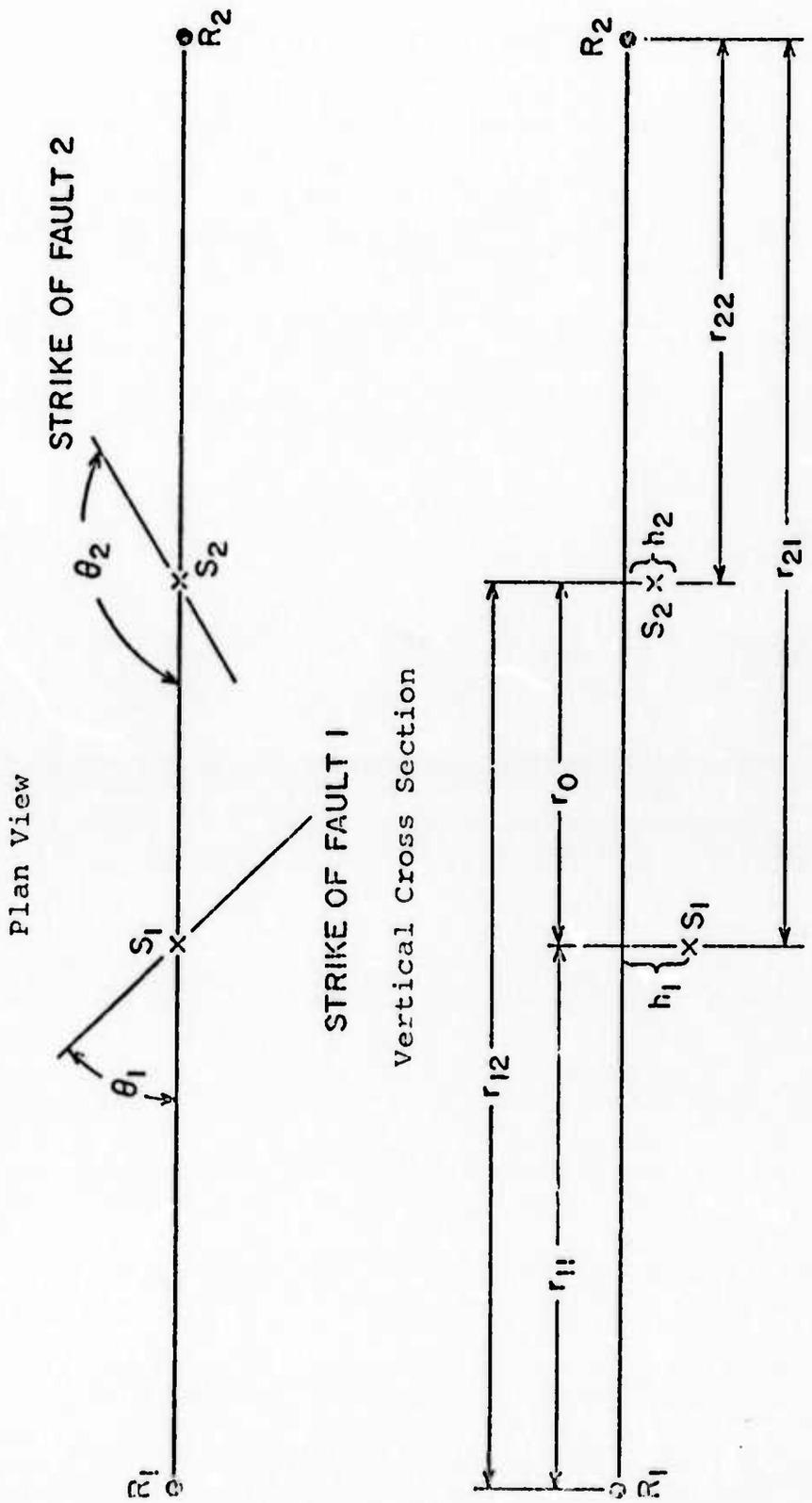

Figure 1. Plan view and vertical cross-section of assumed source-receiver geometry.

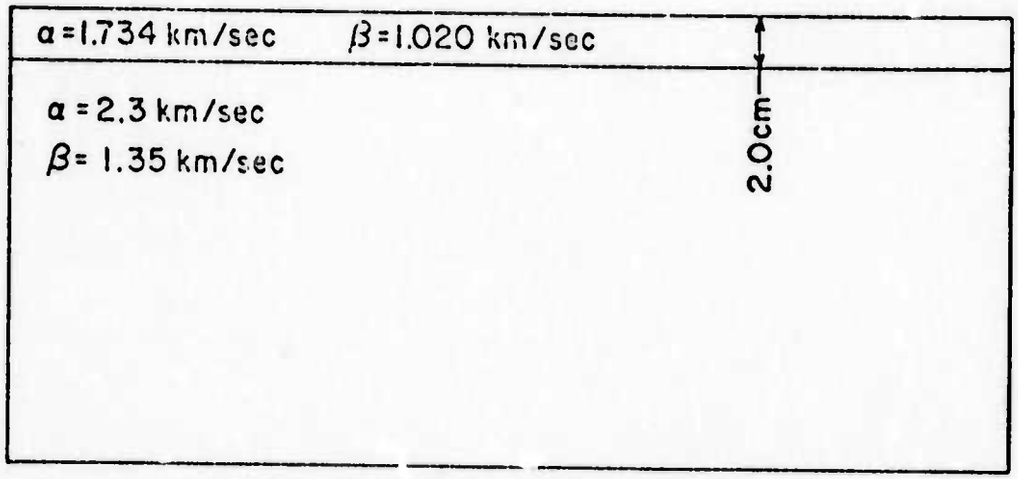

LAYER OVER A HALF SPACE

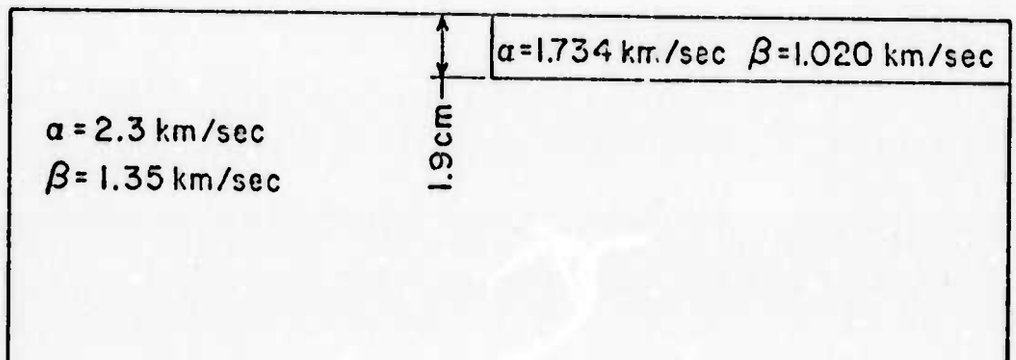

LATERAL DISCONTINUITY

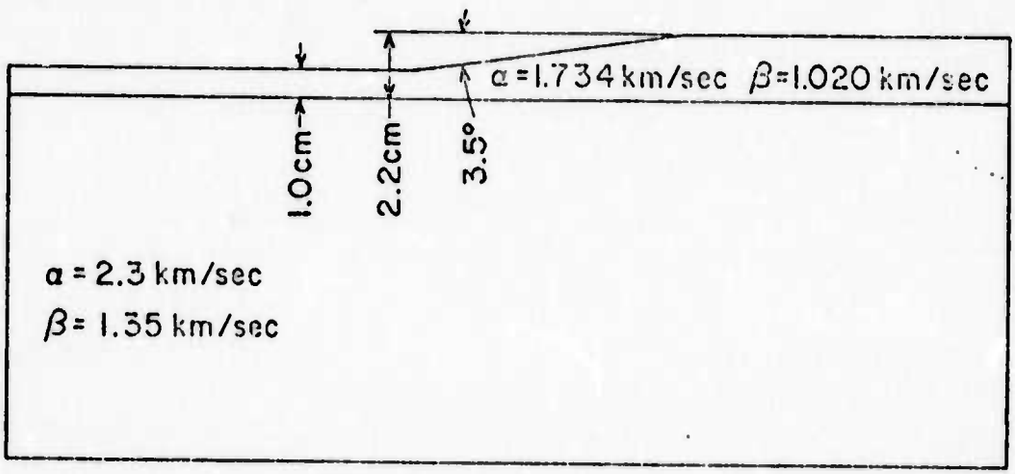

TOPOGRAPHIC RELIEF

Figure 2. The models employed in this study.

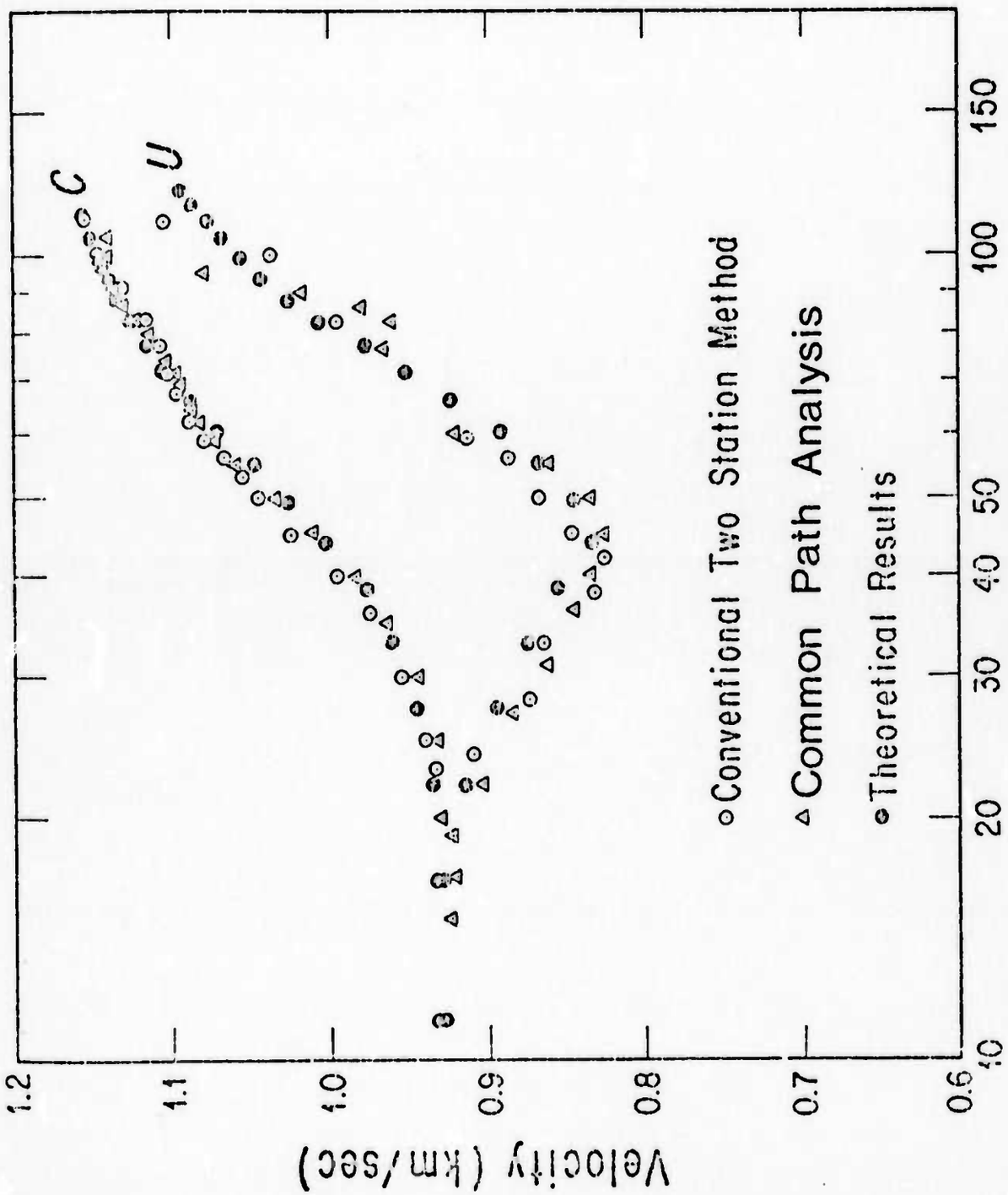

Figure 3. Phase velocity, C, and group velocity, U, determined by the conventional two-station method and by differential dispersion analysis compared to the theoretically expected results, for a layer over a half-space model.

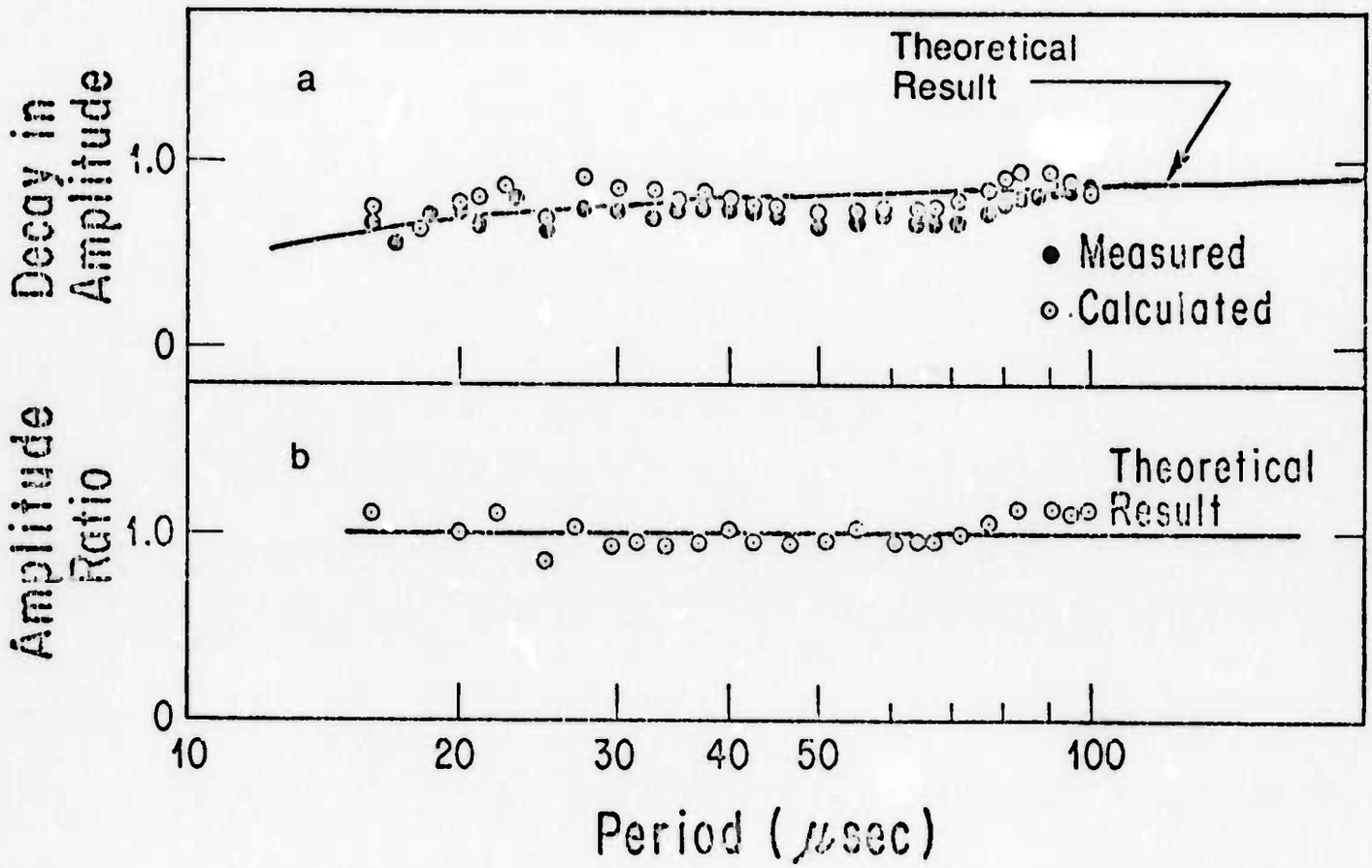

Figure 4. a. Amplitude decay, $|V(\omega)|^{1/2}$, for a layer over a half-space model.
b. Predicted source amplitude ratios, solid lines are theoretically expected results.

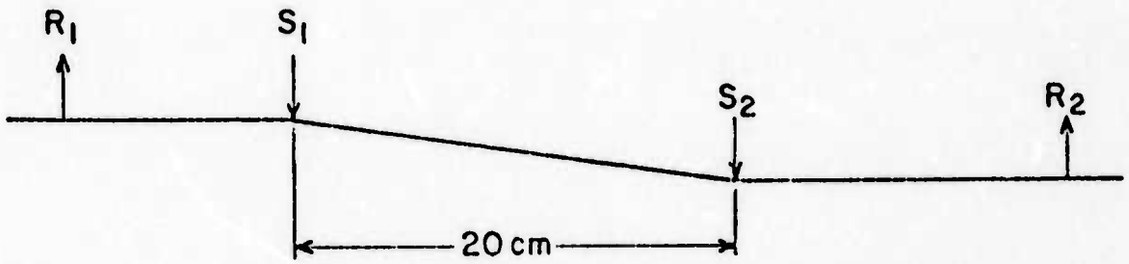

MODEL GEOMETRY

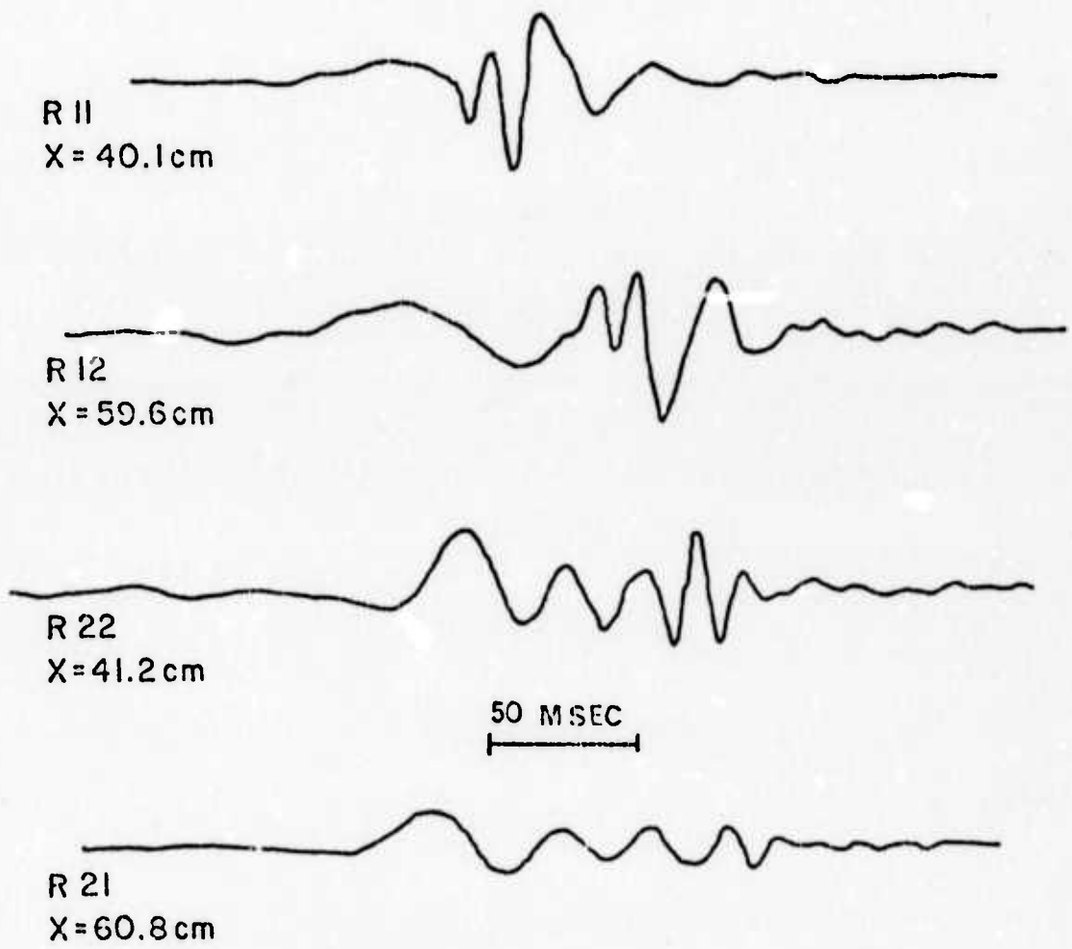

RECORDED SIGNALS

Figure 5. Recorded waveforms obtained at distance X for the model of topographic relief using the indicated source-receiver geometry.

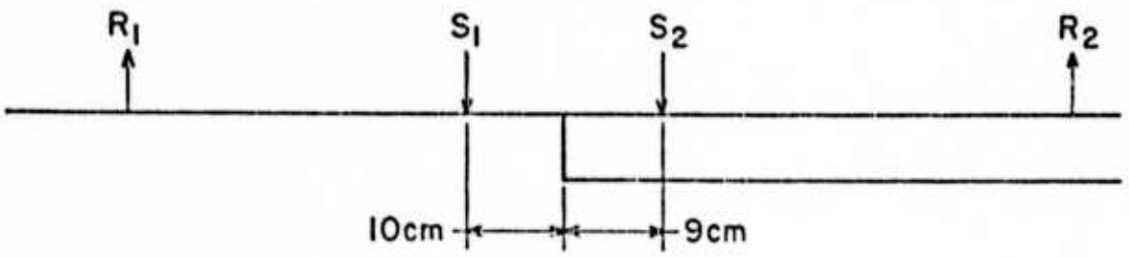

MODEL GEOMETRY

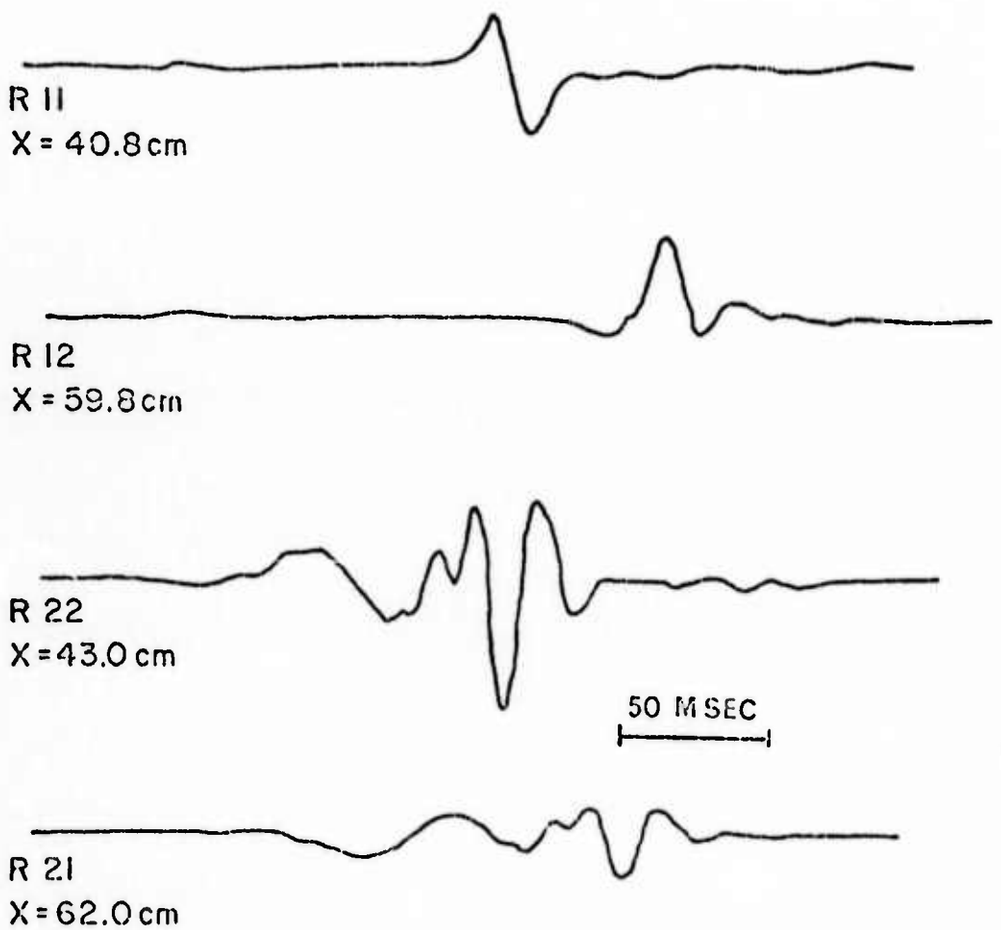

RECORDED SIGNALS

Figure 6. Recorded waveforms obtained at distance X for the model containing a lateral discontinuity using the indicated source-receiver geometry; origin times are arbitrary.

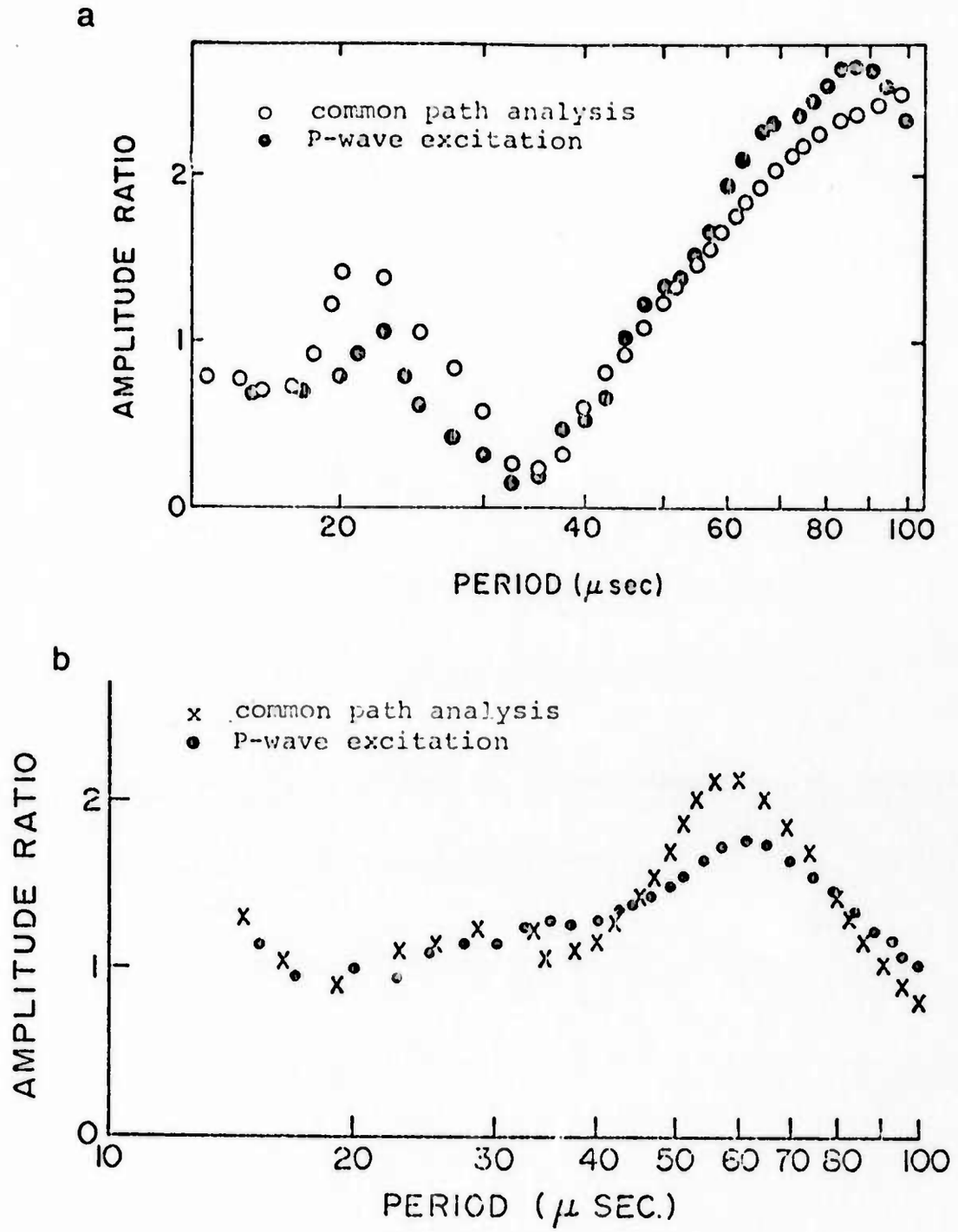

Figure 7. Source amplitude ratios for a. model of topographic relief, b. model containing a lateral discontinuity; origin times are arbitrary.

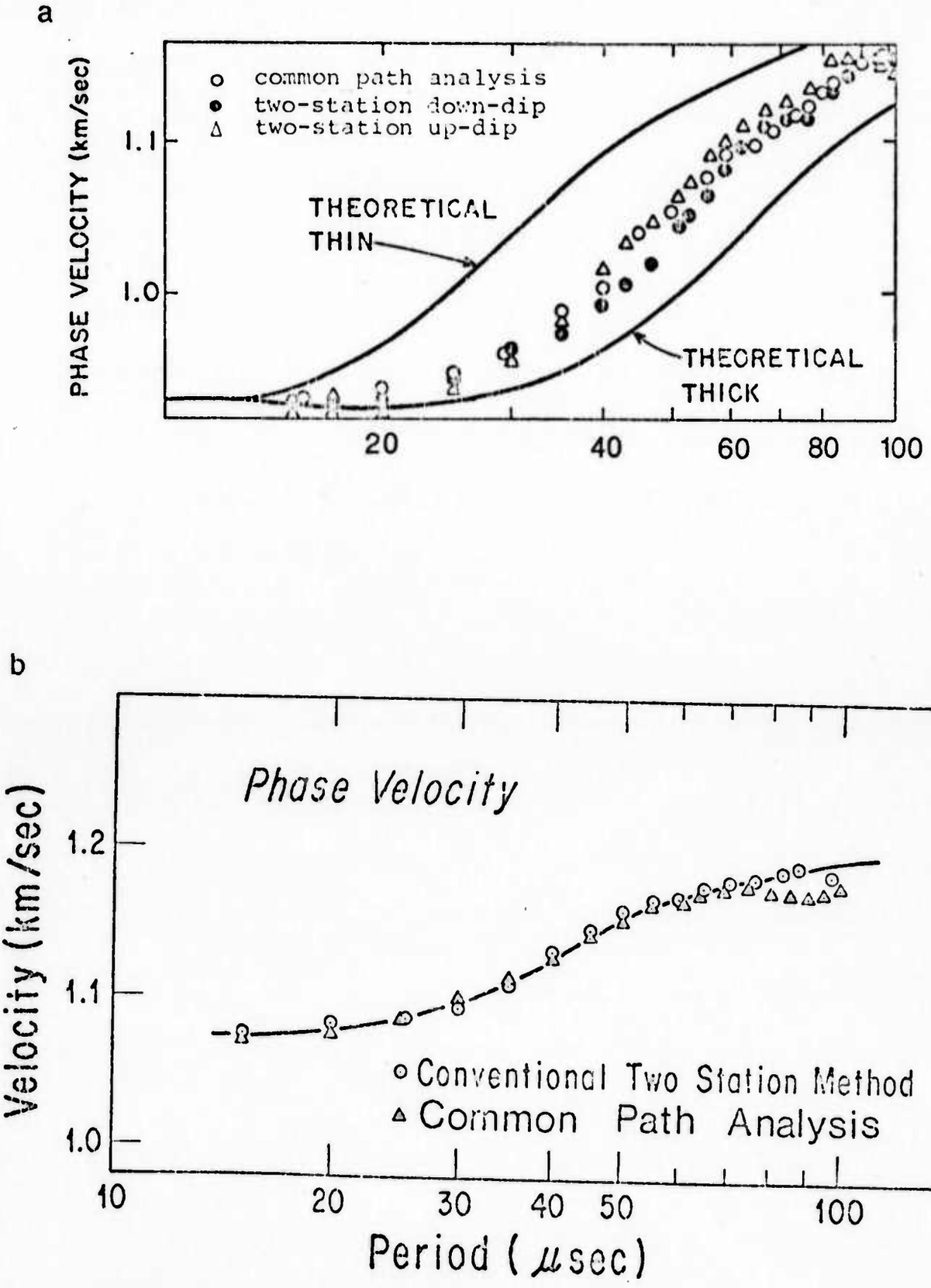

Figure 8. Phase velocity determined by differential dispersion, compared with the velocity determined in the conventional two-station method for a. model of topographic relief; solid lines indicate theoretical velocities for each section, b. model containing a lateral discontinuity; solid line indicates theoretical velocity for an average section.

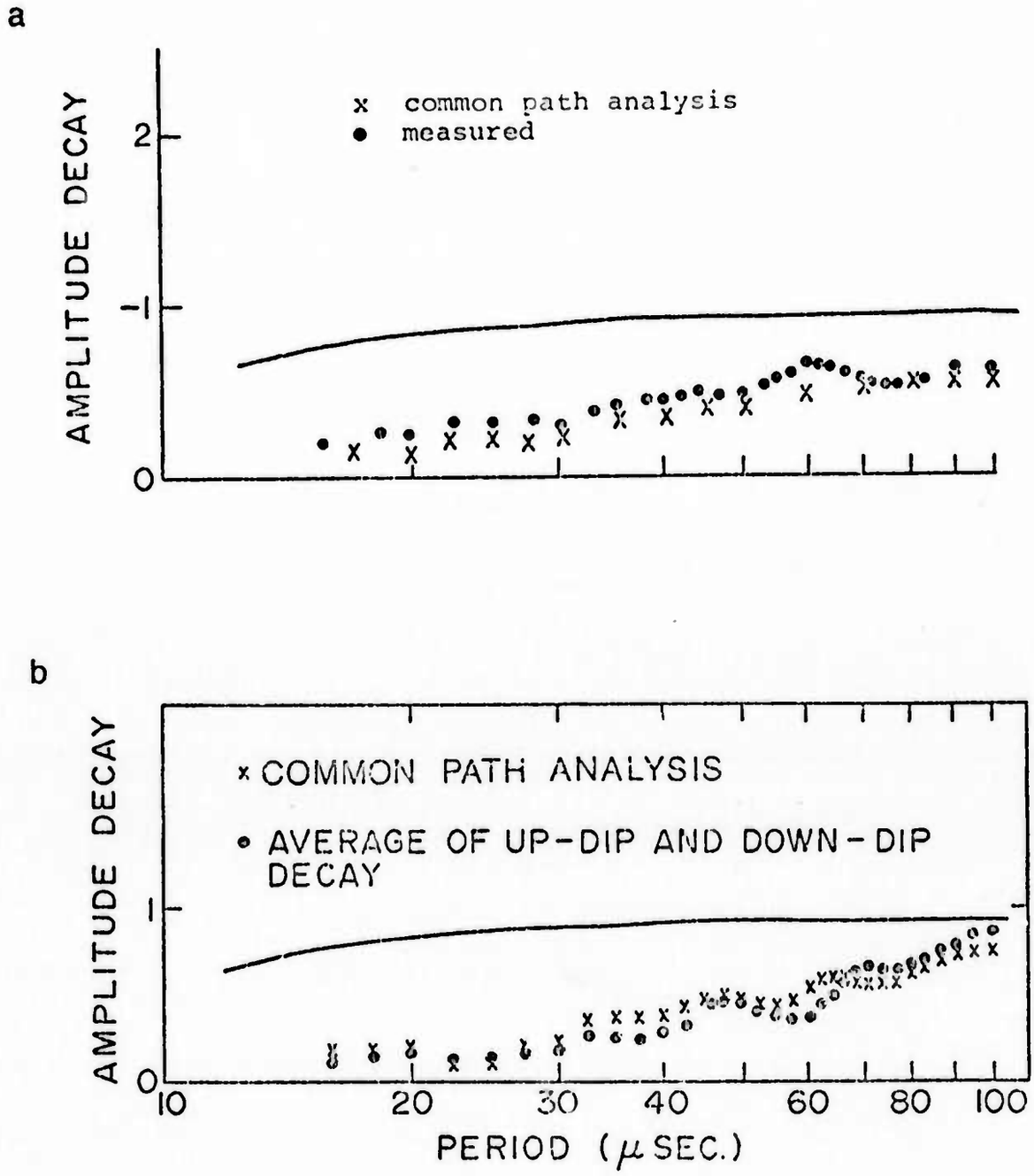

Figure 9. Amplitude decay, $|V(\omega)|^{-1/2}$, determined by differential dispersion analysis and the conventional two-station method for a. model of topographic relief, b. model containing a lateral discontinuity; solid lines indicate decay expected to result from material Q for average section.

APPENDIX III

RAYLEIGH WAVE DISPERSION AND AMPLITUDE MEASUREMENTS FOR A SECTION OF THE MID-ATLANTIC RIDGE

BY

R. W. Taylor and S. S. Alexander

ABSTRACT

Multiple Rayleigh wave phase and amplitude spectra were used to determine phase velocity dispersion and amplitude effects associated with propagation along a section of the mid-Atlantic ridge. Source factors and external path effects were eliminated by a common path method of differential analysis described in Part I.* From 21 independent measurements, phase velocities were determined for a period range from 10 sec. to 60 sec. with a variance in calculated velocities at any particular period on the order of 0.01 km^2/sec^2. First order inversion of the phase velocity data suggest a base for the low P-velocity material (known from refraction studies to immediately underlay the ridge crest) in the vicinity of 50 km. A phase velocity minimum at a period of 32 seconds, somewhat more pronounced than the minimum associated with standard oceanic phase velocities, is suggestive of increased partial melting below the ridge crest. The amplitude data indicate strong inhomogeneity within the ridge crest region and cannot be interpreted in terms of material attenuation.

*Taylor, R. W. and S. S. Alexander; Differential Surface Wave Analysis as a Means for the Seismic Investigation of Inaccessible Areas

INTRODUCTION

The mid-ocean ridges are a major feature of oceanic regions and are of considerable importance in theories of sea floor spreading and global tectonics. The upper features associated with sections of these ridge systems have been investigated through conventional seismic refraction methods by Ewing and Ewing (1959), Keen and Tramontini (1970), Le Pichon, et.al. (1965) and Talwani, et.al. (1971) among others. A summary of the features associated with the ocean ridges as inferred from various geophysical studies is provided by Vogt, et.al. (1969).

Surface wave studies with this potential for information from greater depths than available from other seismic methods are limited in number. More over, the dispersion data which are available for the ridges are either contaminated by propagation outside the ridge area (Ossing, 1968) or do not contain the period range of primary interest (Tarr, 1968; Tryggvason, 1962). The method developed in Part I provides a possible means for extending the available surface wave data appropriate to propagation along the ridge crest.

THE AREA INVESTIGATED

The section of the mid-Atlantic ridge selected for investigation and the WWSSN stations employed are shown in Figure 1. An enlarged view of the event epicenter and ridge flanks is given in Figure 2 with the position of the flanks taken from Heeyen and Thorp (1965). The hypocenters, magnitudes and origin times for each event are given in Table 1. Event No. 5 appearing in Figure 2 and Table 1 was not employed in this study as the necessary records for this event were not available. A fault-plane solution for one event within this area, which due to a lack of the necessary records was not included in this study, indicated equal components of slip along a steeply dipping fault surface (Sykes, 1967, 1970). On the basis of this solution, the location of the epicenters near the ridge crest, and lack of known transform faults within the region, the selected events were assumed to represent ridge crest faulting.

The receiving stations, events and great circle propagation paths closely approximate the conditions required: collinearity to within 10° and in general less than 5°. Phase velocities were calculated from

$$C(w) = \frac{2 w r_o}{\phi(w) \pm 2N\pi}$$

TABLE 1. Origin Time, Hypocenter and Body Wave Magnitude for Each Event.

EVENT	ORIGIN DATE			ORIGIN TIME (GMT)			LOCATION		DEPTH	MAGNITUDE
NO.	DAY	MONTH	YEAR	HOUR	MIN	SEC	LAT (N)	LONG (W)	(KM)	m_b
1	14	3	70	07	33	42.2	28.3	43.8	----	5.2
2	18	7	69	00	00	47.4	29.7	42.9	----	5.0
3	27	1	68	00	48	35.6	29.9	42.8	34	5.0
4	2	1	69	00	36	11.7	30.5	41.9	----	4.7
5	2	12	64	08	20	45.6	30.6	42.0	33	5.2
6	2	1	69	01	05	07.0	30.8	42.0	33	4.9
7	19	9	68	11	13	07.4	30.8	41.9	33	4.9
8	10	6	66	22	14	37.3	32.9	39.8	18	5.2

subject to the constraint

$$[|V(w)|]^{1/2}$$

where all quantities are defined in Part I and r_o is corrected to account for the deviation of the events from a collinear condition. The amplitude of the transfer function associated with the path r_o was determined from $[|Z(w)|]^{1/2}$

RESULTS

The available records from the six stations and seven events yielded 21 independent station-pair, event-pair combinations. The event separations varied from 180 km to 640 km with the majority of separations centered around 300 km.

Typical examples of the quantity $[|V(w)|]^{1/2}$ are shown in Figures 3 and 4 for various station-pair, event-pair combinations. A careful examination of these Figures indicates no systematic changes for the same station-pair as various event-pairs are employed, nor are any systematic changes evident for the same event-pair as viewed from various station-pairs. The Figures indicate the quantity $[|V(w)|]^{1/2}$ is essentially independent of frequency and, the faulting geometries of the various events are similar in nature. In addition the independence of the quantity $[|V(w)|]^{1/2}$ and of the frequency indicates the vertical

structure does not change significantly along the length of the ridge under investigation.

The phase velocity dispersion calculated from 21 analyses showed little, if any, dependence upon the station-pair, event-pair combination. Without attempting to distinguish between the individual event-pair, station-pair combinations, the results are shown in Figure 5. Calculating the mean and standard deviation of the data from the 21 analyses at a period interval of 2.5 seconds yielded the average dispersion curve of Figure 6. It is evident from Figure 6 that the standard deviation associated with each data set varies from about 0.1 km/sec at 35 seconds to about 0.05 km/sec in the neighborhood of 50 seconds.

For a laterally homogeneous earth, the amplitude of transfer function associated with propagation is determined by the attenuation coefficients of the earth and the distance of propagation. In this ideal case the transfer function is everywhere less than 1 and may be related to a single quantity Q (Brune, 1962; Knopoff, 1964; Knopoff, et.al., 1964). In the actual practice the effect of attenuation is often obscured by differential scattering resulting from propagation along slightly different paths or interference effects within the wave trains. The net effect may yield an amplitude function in excess of 1.

While the common path method employed in this investigation effectively doubles the propagation distance it is still not expected that source separations of approximately 300 km would produce significant amplitude decay. The only event-pair for which measurable decay might be expected involved events 1 and 8 of Figure 2 with a separation of 638 km. Although it was not expected that reliable determinations of Q could be achieved, the amplitude of the transfer function, $|Z(w)|^{1/2}$ of Part I equation 13, yielded interesting results. The quantity $[|Z(w)|]^{1/2}$ is shown in Figures 7 and 8 for various event-pair separations (r_o). It is immediately evident from these Figures that the measured amplitude function is greater than 1 for the majority of the period range considered. While the measured results are not physically possible for a homogeneous space, the data are consistent and appear independent of station-pair or event-pair effects. For example, the nearly identical curves for a source separation of 300 km, shown in Figure 7, represent differing event-pairs and propagation over different sections of the selected area. For any given separation (with the exception of r_o = 638 km) the data represent several event-pairs as viewed by several station-pairs.

While the results do not appear to depend on the particular events or stations, there does appear to be a dependence upon the source separation r_o. Thus, with a

separation of 20 km, a distance sufficiently small to preclude any propagation effects, the data are frequency independent and nearly equal to 1. For separations of 200 km and greater, the data deviates from 1 and is characterized by pronounced peaks. The curves for source separations of 20 km and 100 km were included for the purpose of indicating the dependence on source separation and were not included in the velocity calculations. That the data represents amplitude effects resulting from propagation along the ridge crest is supported by Figures 3 and 4. These Figures, which theoretically do not contain propagation effects but do contain source effects, indicate little if any frequency dependence. While no unequivocal explanation of the amplitude results of Figure 7 and 8 is possible, it is reasonable to assume the results are reflecting the effects of inhomogeneity within the propagation region. If this is accepted as true, the data for Figures 7 and 8 contain information concerning the nature and extent of the inhomogeneity.

COMPARISON WITH OTHER STUDIES

The phase velocities obtained here are compared with the standard oceanic phase velocities of Brune (1969) and Oliver (1962) in Figure 9. In the same Figure are shown the oceanic phase velocities expected if the average ocean water depth were 3 km. For the period range from 40 sec to

60 sec the velocities obtained here are essentially equivalent to average oceanic velocities. For periods from 10 sec to 40 sec the velocities obtained here are lower than standard ocean velocities with the exception of periods around 25 sec where the two velocities are equal. The difference suggests S velocities for an approximate 200 km section below the ridge crest which are somewhat lower than S velocities for standard oceanic sections of the same depth.

Group velocities appropriate to the ridge crest have been indirectly determined by Santo (1966), Tarr (1969), and Ossing (1964) while Tryggvason (1962) directly determined Rayleigh wave dispersion from measurements in Iceland. The results of these studies are compared with the results obtained here in Figure 10. (The data of Tryggvason (1962) has been adjusted to account for the differences in water depth near Iceland and that over the area investigated here). It is evident from this Figure that the data obtained here and that from Iceland are in complete accord. This indicates the upper structure of Iceland is identical to the upper structure of that part of the ridge investigated here. Since the area considered here is a typical ridge section, these results suggest that the structure of Iceland is identical to other parts of the mid-Atlantic ridge.

While the results presented here are in excellent accord with the results of Tryggvason there is a signifcant disparity, 0.5 km/sec, with the results of Sato (1966), Ossing (1964) and Tarr (1969). This difference may arise from the investigation of different areas or the fact that the above authors employed an indirect method. It is also possible that the variances associated with any method of determining group velocity are sufficiently high to render the difference meaningless.

IMPLIED GEOLOGIC STRUCTURE

A first order indication of implied geologic structure was obtained by calculating theoretical phase velocities for ridge models proposed by Ewing and Ewing (1959) and Keen and Tramontini (1970). The model Ewing and Ewing yielded results more nearly equivalent to the data obtained here and this model was consequently selected for additional consideration. The original model was the perturbed to yield a theoretical dispersion curve in reasonable agreement with the measured data. The resulting model is shown in Figure 11 and the theoretical and measured dispersion data is shown in Figure 12. While the theoretical velocities for the perturbed model of Ewing and Ewing approximate the measured values there are significant differences. The most significant of these differences occurred in the period range from 15 sec to 40 sec. The actual data

indicate a decrease in S velocity somewhere in the vicinity of 50 km in depth. The procedure employed to generate the theoretical velocities was insensitive to S velocity decreases with depth. This is the major reason for the differnces in the theoretical and measured values and as a result of this the implied structure of Figure 10 should be considered as simply a first order approximation to the actual ridge structure. The actual structure must involve a decrease in S velocity at some depth. To improve the structure of Figure 10, methods for calculating theoretical phase velocities in the presence of a decrease in S velocity (Stonely, 1950; Harkrider, et.al., 1963; Thrower and Harkrider, 1965) are presently under investigation.

ACCURACY

The precision of the measured phase velocities is excellent as is evident from Figure 5. The accuracy of the velocities is primarily determined by the accuracy with which the event separations are known and the extent to which the effects of initial source phase have been eliminated. Location errors on the order of 20 km are possible and for the distances involved this would amount to a 5% error in measured velocity. It should be noted, however, that any reasonable systematic location error for events in the selected area will not affect the results.

Only the random errors involved in location are of concern. On the basis of the variance associated with the data of Figure 5 it appears unlikely that the random location errors, in general, exceed 5 km. That the events within the selected region are well located is supported by the work of Evernden (1971) and Weidner and Aki (1973). It, therefore, appears that the random location errors are contributing no more than a $\pm$ 0.02 km/sec error to the mean of the 21 measurements.

The extent to which the effects of source initial phase have been eliminated is more difficult to determine. It is highly unlikely, however, that the initial phases are biasing the results of differing event-pairs and differing station-pairs in a systematic manner. The initial phase is, therefore, expected to bias the mean of the 21 measurements by no more than $\pm$ 0.04 km/sec. On the basis of these arguments the velocity means of Figure 6 are considered reliable to within $\pm$ 0.05 km/sec.

CONCLUSIONS

When applied to the mid-Atlantic ridge the common path method of Part I yielded a consistent phase velocity dispersion curve. Velocities at periods as low as 10 sec appeared reasonable in value and in their relationship to velocities at higher periods despite the very low energy levels available in this period range. While a totally

satisfactory inversion of the dispersion curve was not obtained, the results are in general accord with the ridge model proposed by Ewing and Ewing (1959). In addition to general accord with this model, the results indicate a region from approximately 50 km to 200 km with a lower S velocity than that characterizing standard oceanic sections at equivalent depths.

The amplitude measurements yielded results which were not interpretable in terms of a plane layered earth. The results, however, were consistent for various event-pairs and station-pairs and displayed a dependence on source separation. It is felt that the results of the amplitude measurements are related to the lateral inhomogeneity known to exist within the near surface structure. Thus, the amplitude measurements may provide a means for the investigation of lateral inhomogeneity at the 20 km and 200 km depths the waves are sampling. Utilization of this information, however, will require additional theoretical consideration.

REFERENCES

1. Brune, J.N., Attenuation of Dispersed Wave Trains, Bull. Seis. Soc. Am., 52, 109-112 (1962).

2. Brune, J.N., Surface Waves and Crustal Structure, The Earth's Crust and Upper Mantle, ed. P.J. Hart, Monograph 13, Am. Geophys. Union, 230-242 (1969).

3. Evernden, J.F., Location Capability of Various Seismic Networks, Bull. Seis. Soc. Am., 61, 241-237 (1971).

4. Ewing, J. and M.W. Ewing, Seismic Refraction Measurements in Atlantic, Mediterranean, Mid-Atlantic Ridge and Norwegian Sea, Bull. Geol. Soc. Am., 70, 291-316 (1959).

5. Harkrider, D.G., A.L. Hales and F. Press, On Detecting Soft Layers in the Mantle with Rayleigh Waves, Bull. Seis. Soc. Am., 53, 539-548 (1963).

6. Heezen, B.C. and M. Thorp, Tectonic Fabric of the Atlantic and Indian Oceans and Continental Drift, Phil. Trans. Roy. Soc. Series A, 258, 90-196 (1965).

7. Keen, C.E. and C. Tramontini, A Seismic Refraction Survey on the Mid-Atlantic Ridge, Geophys. Jn., 20, 473-491 (1970).

8. Knopoff, L., Q, Reviews of Geophysics, 2, 625-660 (1964).

9. Knopoff, L., K. Aki, C.B. Archambean, A. Ben-Menahem and J.A. Hudson, Attenuation of Dispersed Waves, Jour. Geophys. Res., 69, 1655-1657 (1964).

10. Le Pichon, X., R.E. Houty, C.L. Drake and J.E. Nafe, Crystal Structure of the Mid-Ocean Ridges, 1, Seismic Refraction Measurements, Jour. Geophys. Res., 70, 319-339 (1965).

11. Oliver, J.F., A Summary of Observed Seismic Surface Wave Dispersion, Bull. Seis. Soc. Am., 52, 81-86 (1962).

12. Ossing, H.A. Dispersion of Rayleigh Waves Originating in the Mid-Atlantic Ridge, Bull. Seis. Soc. Am., 54, 1137-1146 (1964).

13. Santo, T.A., Part III, Atlantic Ocean, Africa and Indian Ocean, Geophys. pura. Appl., 63, 40-59 (1966).

14. Stoneley, R., The Effects of a Low-Velocity Stratum on Surface Elastic Waves, Mon. Nater. Roy. Astrom. Soc. Geophysics Suppl., 6, 28-25 (1950).

15. Sykes, L.R., Mechanism of Earthquakes and Nature of Faulting on the Mid-Oceanic Ridges, Jn. Geophys. Res., 72, 2131-2147 (1967).

16. Sykes, L.R., Focal Mechanism Solutions for Earthquakes Along the World Rift System, Bull. Seis. Soc. Am., 1749-1752 (1970).

17. Talwani, M.C., C. Windisch and M.G. Langseth, Reykjanes Ridge Crest: A Detailed Geophysical Study, Jn. Geophys. Res., 76, 473-517 (1971).

18. Tarr, A.C., Rayleigh Wave Dispersion in the North Atlantic Ocean, Caribbean Sea and Gulf of Mexico, Jn. Geophys. Res., 74, 1591-1607 (1969).

19. Thrower, E.N. and D.G. Harkrider, A Note on the Existence of Relative Maxima and Minima on Phase Velocity Curves, Bull. Seis. Soc. Am., 55, 971-974 (1965).

20. Tryggvason, E., Crustal Structure of Iceland Region From Dispersion of Surface Waves, Bull. Seis. Soc. Am., 52, 359-388.(1962).

21. Vogt, P.R., E.D. Schneider and G.L. Johnson, The Crust and Upper Mantle Beneath the Sea, The Earth's Crust and Upper Mantle, J.P. Hart, ed. Am. Geophys. Union, Monograph 13, 556-617 (1969).

22. Weidner, D.J. and K. Aki, Focal Depth Mechanism of Mid-Ocean Ridge Earthquakes, Jn. Geophys. Res., 1818-1831 (1973).

CAPTIONS

Figure 1 The area of the mid-Atlantic ridge selected for investigation.

Figure 2 Events selected for use in the investigation; arrows indicate initial great circle paths to indicated stations.

Figure 3 The amplitude ratio for typical event-pair, station-pair combinations. From top to bottom the event-pair at each level is 1-3, 1-6, 1-8 and 6-8.

Figure 4 The amplitude ratio for typical event-pair, station-pair combinations. From top to bottom the event-pair at each level is 1-2, 4-8, 1-7, 1-4.

Figure 5 Measured phase velocity.

Figure 6 Mean and standard deviation of measured phase velocities.

Figure 7 The amplitude of the propagation function for event separations of length r_o.

Figure 8 The amplitude of the propagation function for event separations of length r_o.

Figure 9 Phase velocities measured by the common path method for the mid-Atlantic ridge compared with the oceanic phase velocities of other studies.

Figure 10 Group velocities as measured by the common path method for the mid-Atlantic ridge compared to group velocities as determined by other studies.

Figure 11 Approximate plane-layered model of the mid-Atlantic ridge. (Due in part to Ewing and Ewing (1959))

Figure 12 Comparison of theoretical phase velocities for various models with measured data.

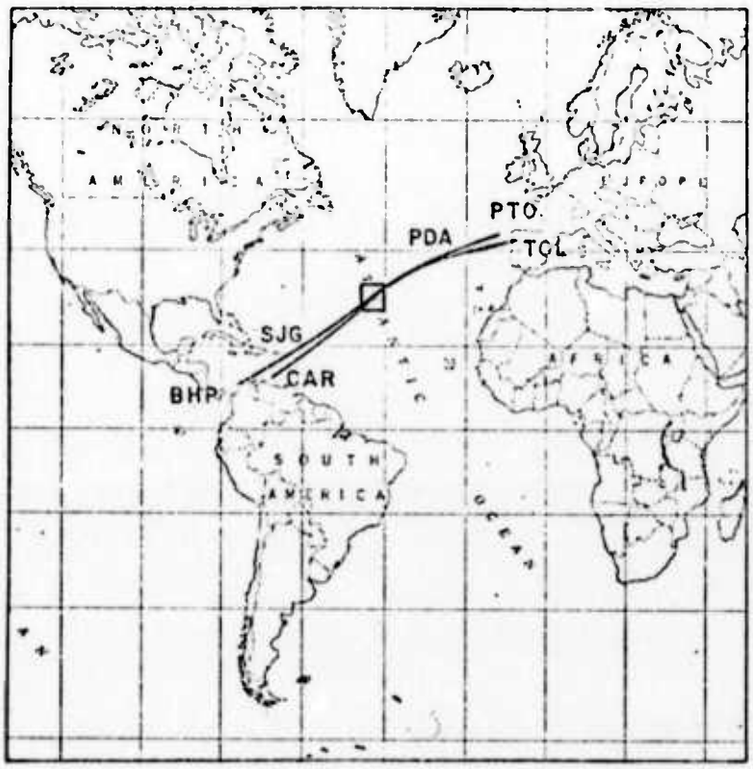

Figure 1. The area of the mid-Atlantic ridge selected for investigation.

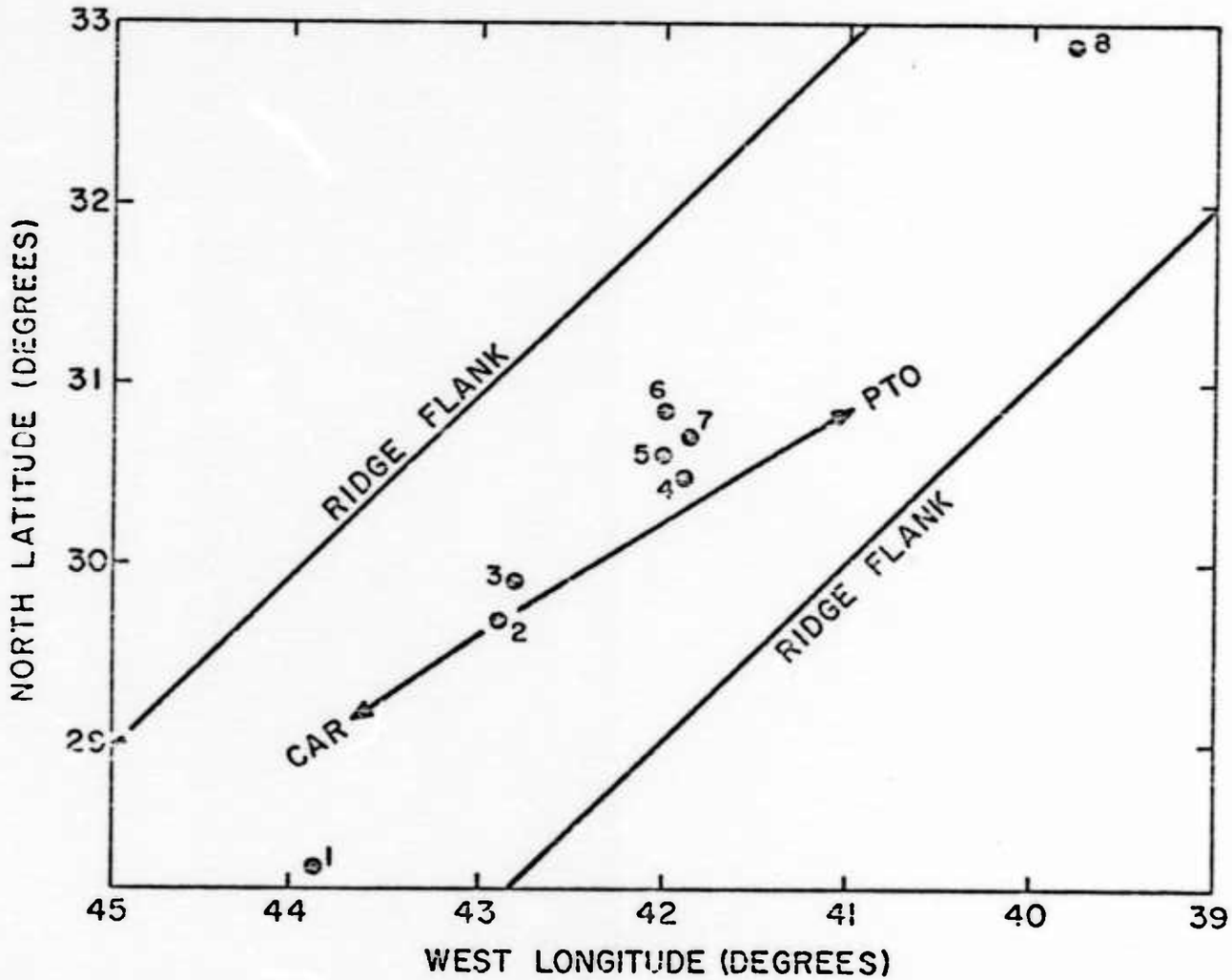

Figure 2. Events selected for use in the investigation; arrows indicate initial great circle paths to indicated stations.

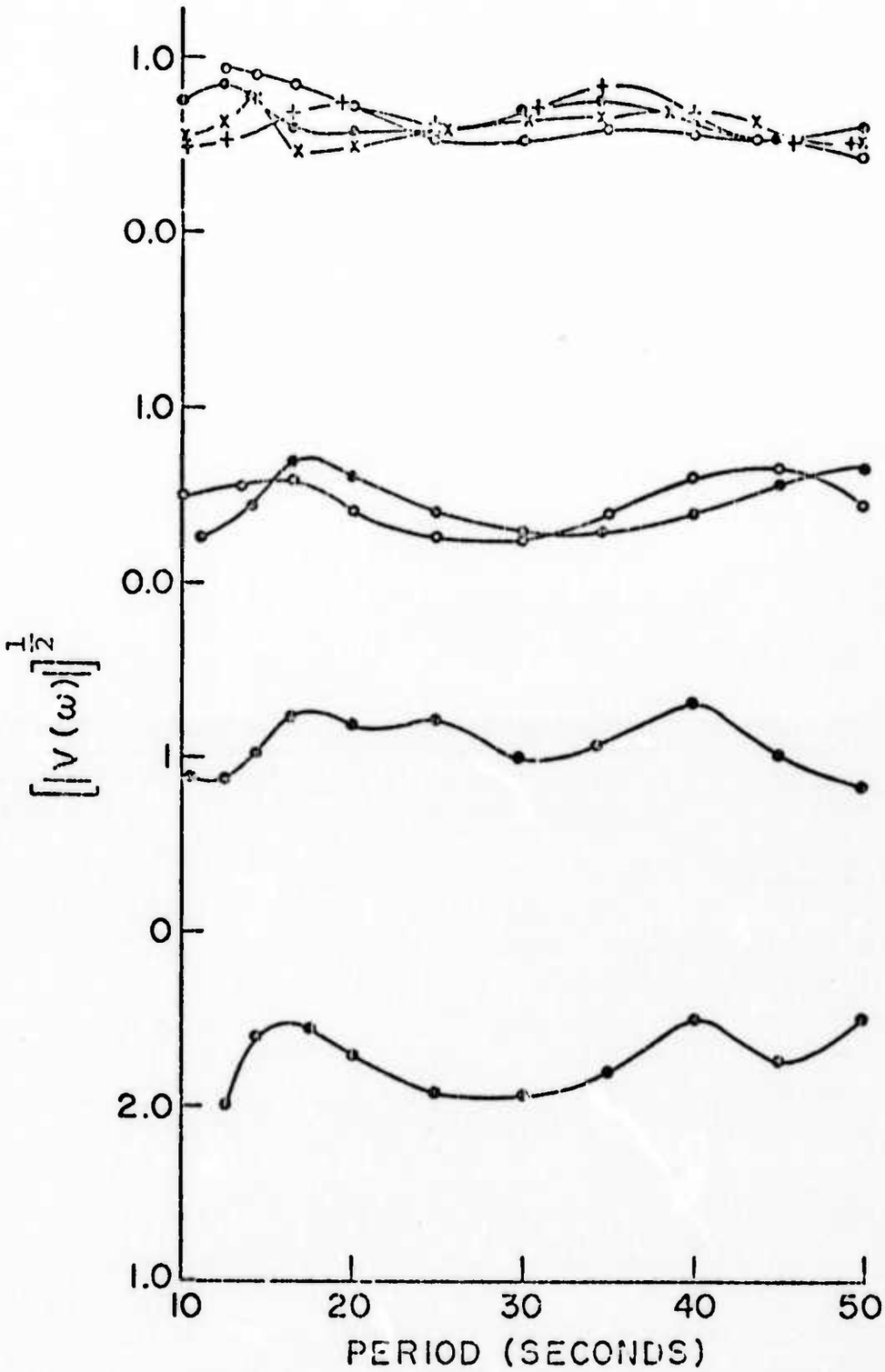

Figure 3. The amplitude ratio for typical event-pair, station-pair combinations. From top to bottom the event-pair at each level is 1-3, 1-6, 1-8 and 6-8.

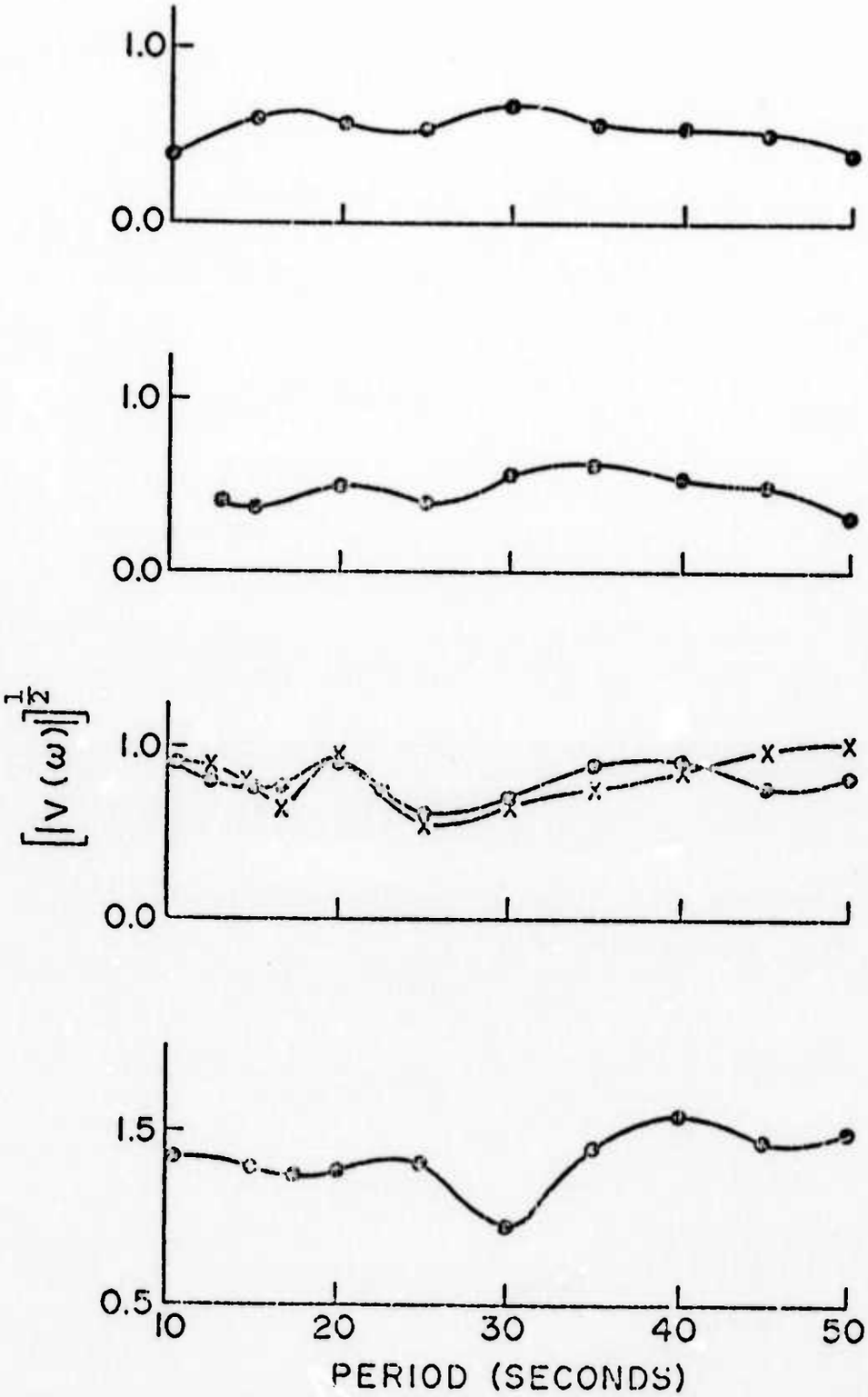

Figure 4. The amplitude ratio for typical event-pair, station-pair combinations. From top to bottom the event-pair at each level is 1-2, 4-8, 1-7, 1-4.

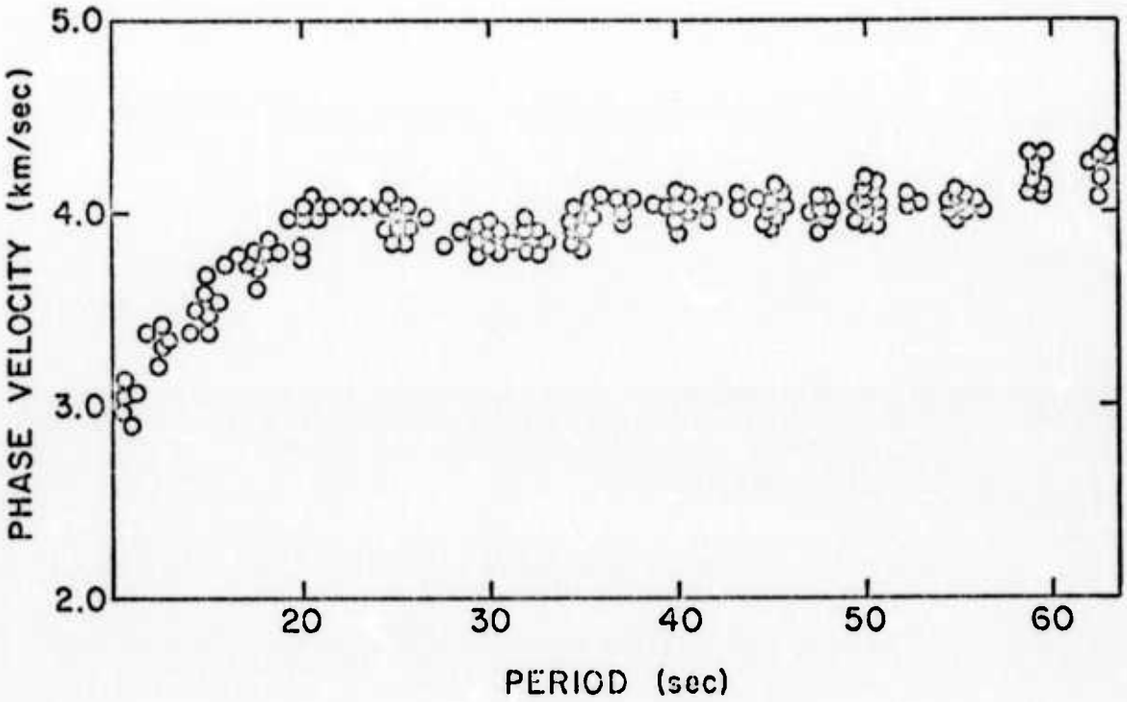

Figure 5. Measured phase velocity.

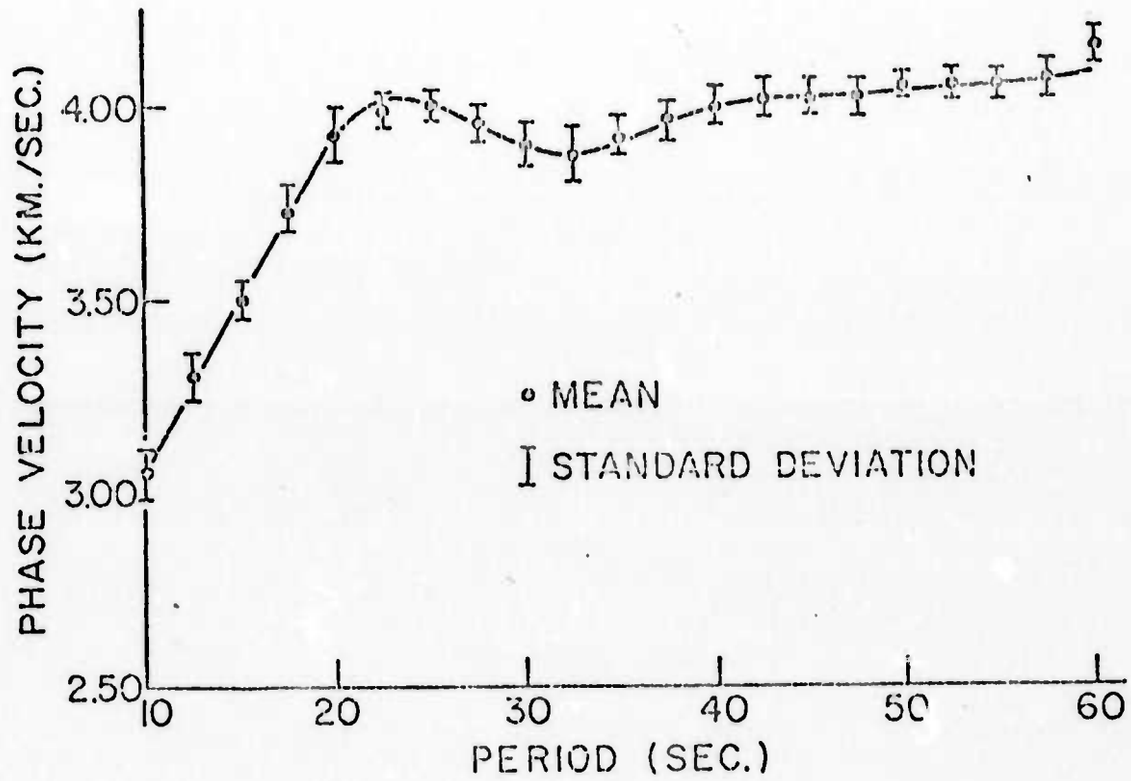

Figure 6. Mean and standard deviation of measured phase velocities.

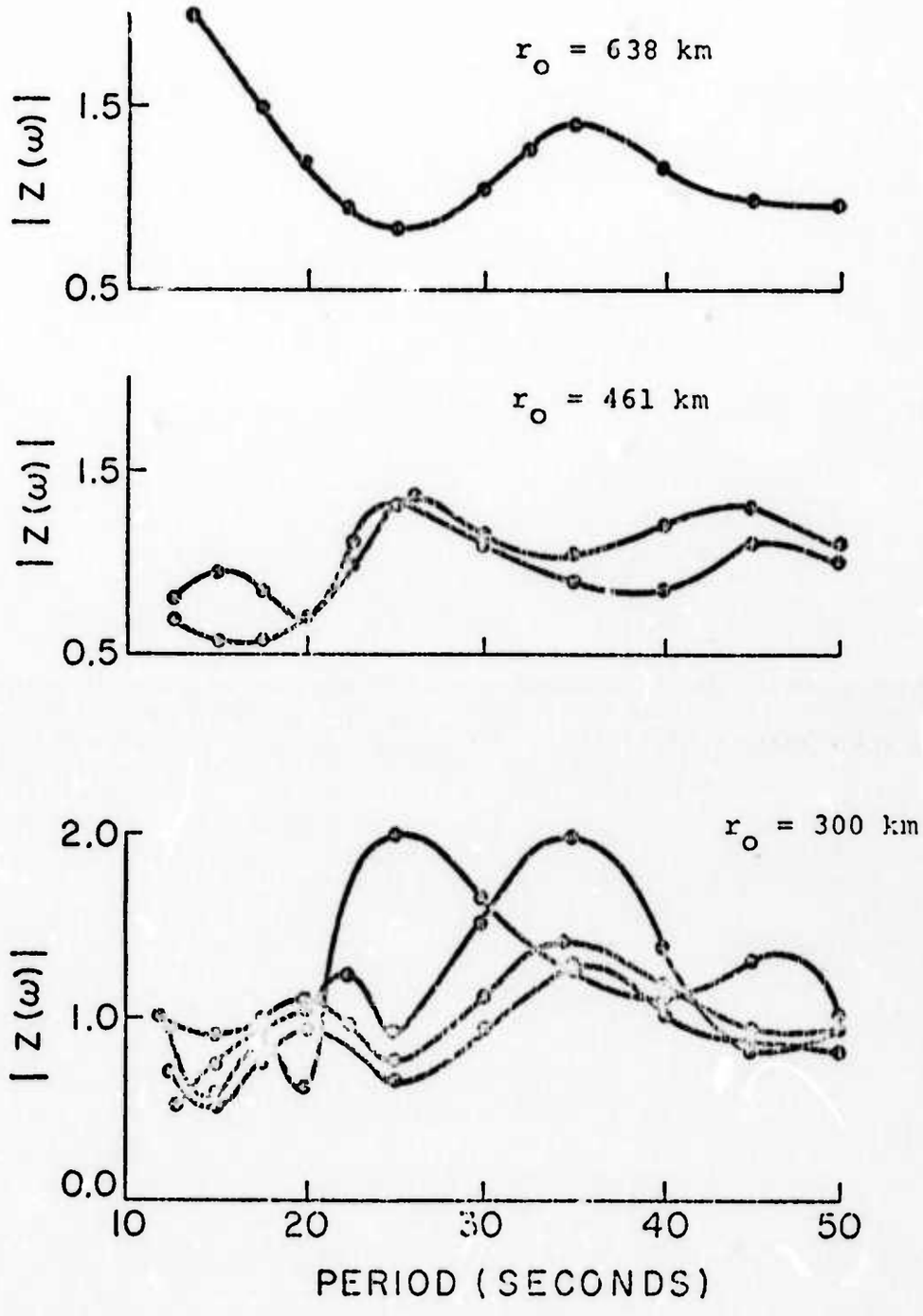

Figure 7. The amplitude of the propagation function for event separations of length r_o.

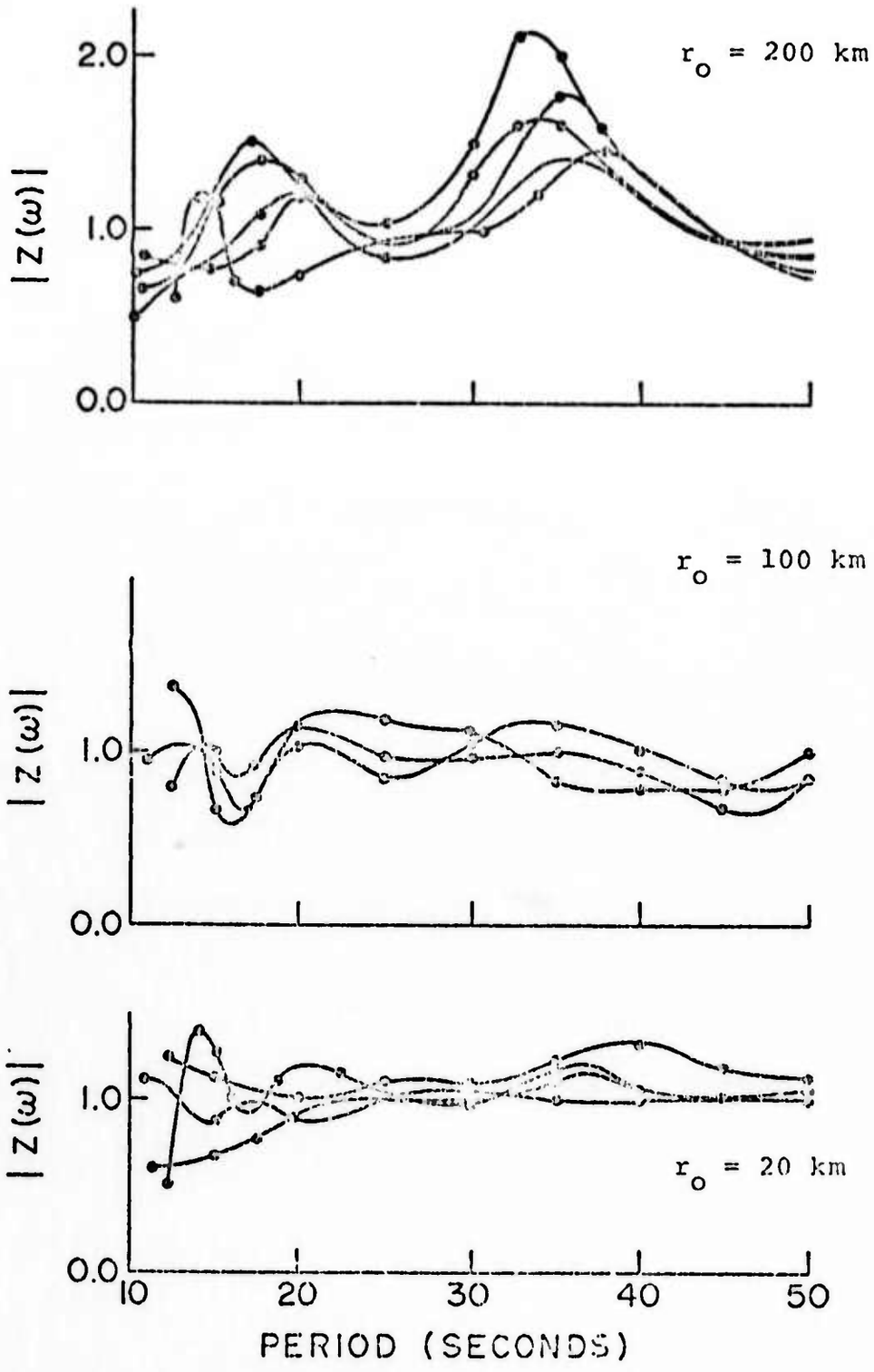

Figure 8. The amplitude of the propagation function for event separations of length r_o.

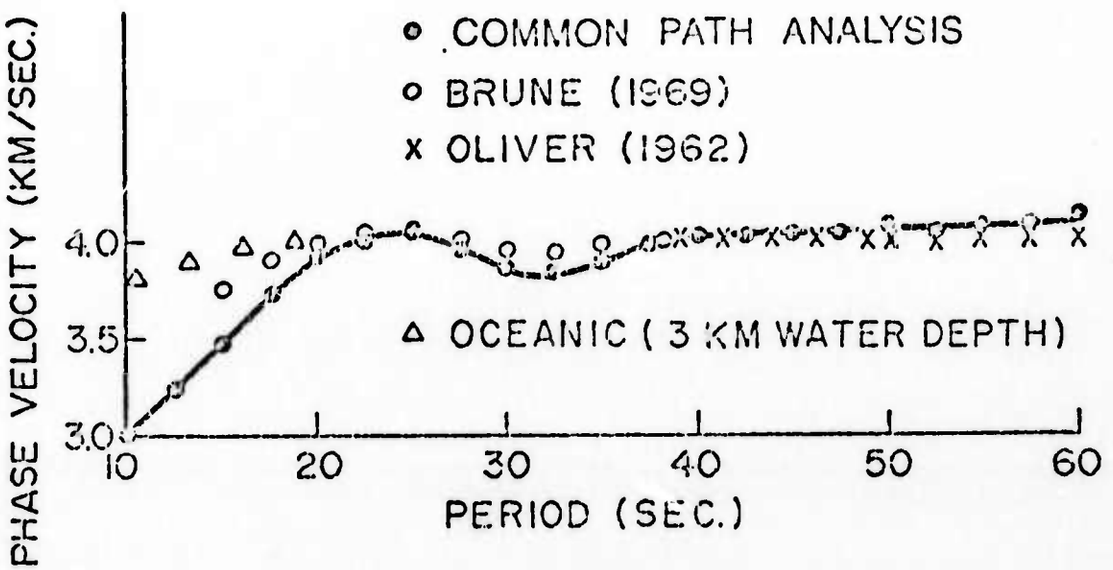

Figure 9. Phase velocities measured by the common path method for the mid-Atlantic ridge compared with the oceanic phase velocities of other studies.

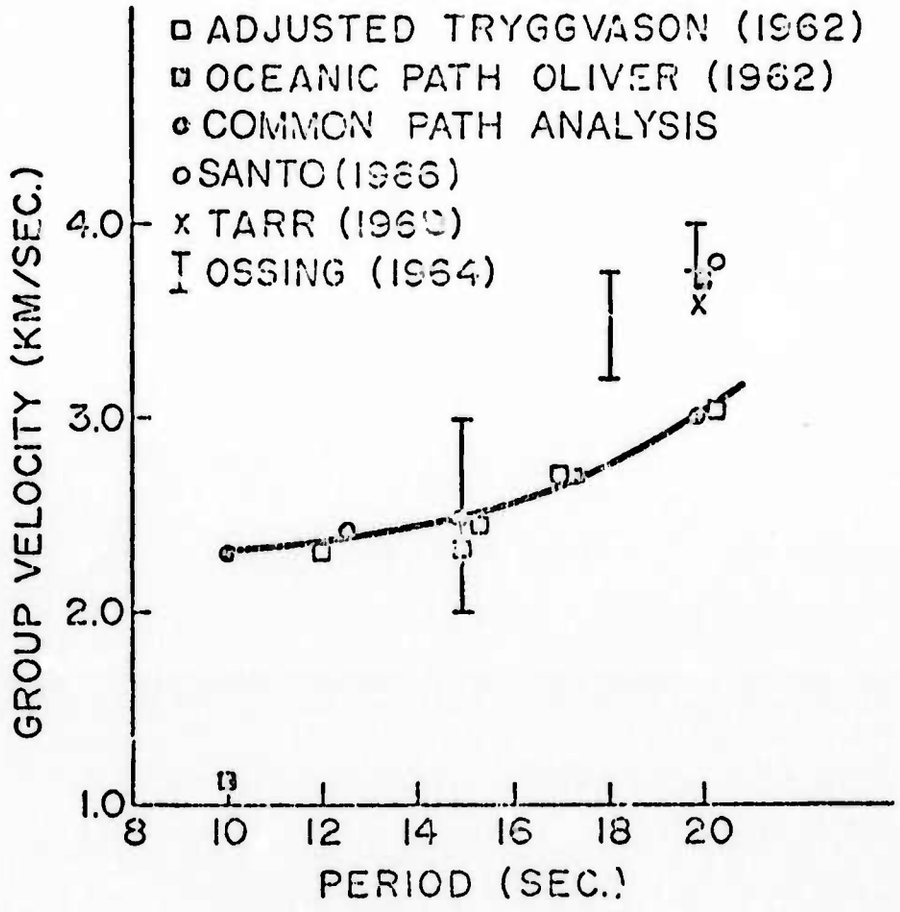

Figure 10. Group velocities as measured by the common path method for the mid-Atlantic ridge compared to group velocities as determined by other studies.

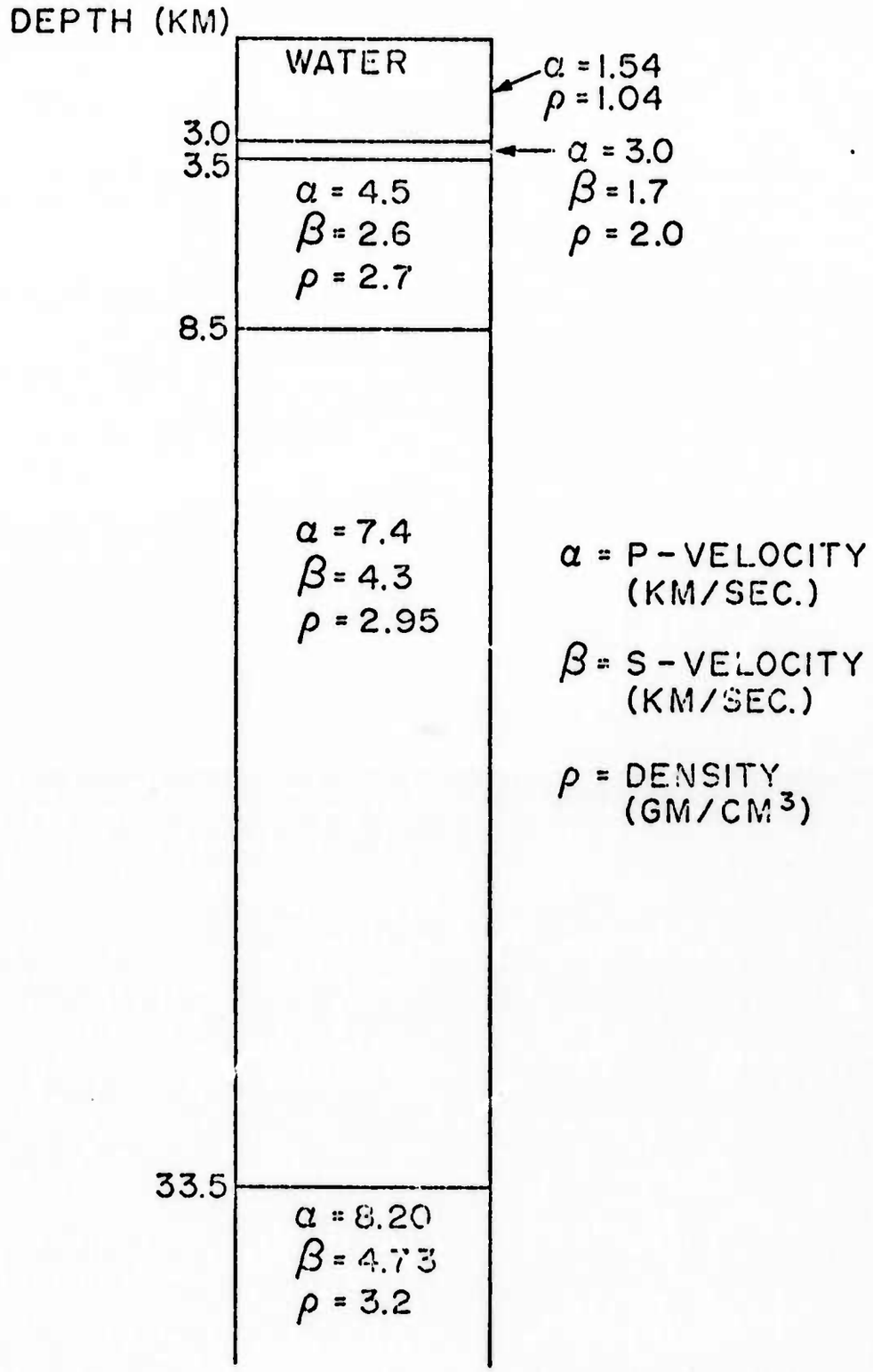

Figure 11. Approximate plane-layered model of the mid-Atlantic ridge. (Due in part to Ewing and Ewing (1959))

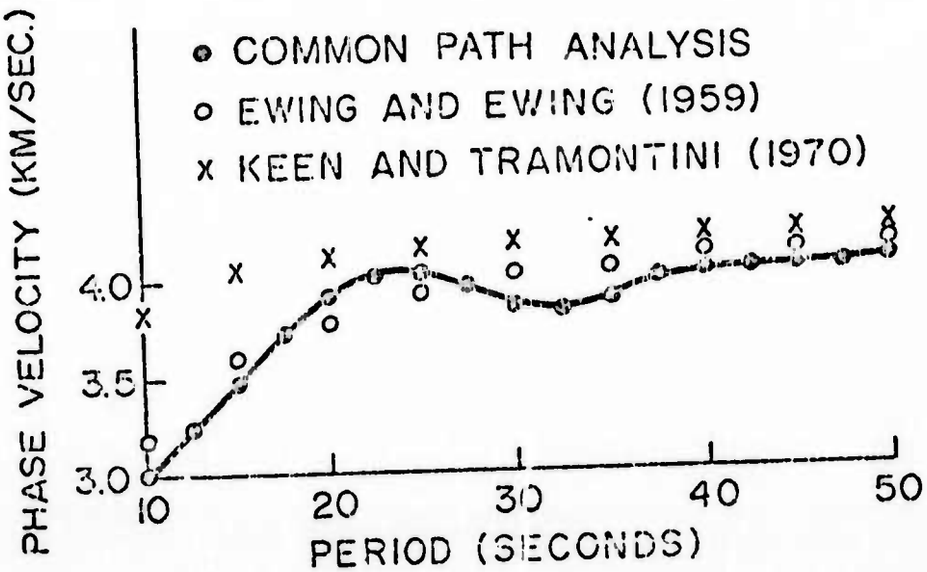

Figure 12. Comparison of theoretical phase velocities for various models with measured data.